INAUGURAL - DISSERTATION

zur

Erlangung der Doktorwürde

der

Naturwissenschaftlich - Mathematischen

Gesamtfakultät

der

Ruprecht - Karls - Universität

Heidelberg

vorgelegt von

Dipl.-Phys. Wouter Roos

aus

Gorinchem, Niederlande

Tag der mündlichen Prüfung: 15. Dezember 2004

Biomimetic cytoskeleton assemblies and living cells on micropillar force sensor arrays

Gutachter: Prof. Dr. Joachim P. Spatz

Prof. Dr. Christoph Cremer

Zur biophysikalischen Analyse mechanischer Eigenschaften der zellulären und intrazellulären Dynamik, sowie zur Untersuchung von Biofilamentnetzwerken wurden Säulenmatrizen entwickelt. Drei Typen von Substraten wurden hergestellt: (1) Mikrosäulen aus Silizium mit einer Goldscheibe auf den Säulenköpfen, (2) Mikrosäulen aus Epoxy-Polymer und (3) Mikrosäulen aus Polydimethylsiloxan (PDMS). Es wurden Säulen mit einem Durchmesser zwischen 1 - 5 µm und einem Aspektverhältnis (Höhe : Durchmesser) von bis zu 20 : 1 produziert. Durch die selektive Funktionalisierung der Säulenköpfe wurde die Kultivierung von Fibroblasten, Epithelialzellen und Herzmuskelzellen auf den Säulenköpfen ermöglicht. Die durch die Zellen auf die Spitzen der Mikrosäulen ausgeübten Kräfte führen zu deren Biegung. Daraus konnten die ausgeübten Kräfte quantifiziert werden. Auf den Säulensubstraten wurden durch Filamin vernetzte zweidimensionale Netzwerke aus Aktinfilamenten hergestellt. Diese künstlichen Netzwerke dienen als Modellsystem für biophysikalische Untersuchungen des Aktinkortexes von Zellen. Experimente zur Vernetzung von Aktinfilamenten wurden auch mit divalenten Kationen und fluoreszenzmarkierten Myosin II-Motoren durchgeführt. Mittels Fourieranalyse der Fluktuation von Einzelfilamenten, die zwischen zwei Säulenspitzen eingespannt waren, konnten die mechanischen Eigenschaften von Aktin bestimmt werden. Die Transporteigenschaften von Myosin V auf den Netzwerken wurden quantifiziert. Durch die Beschichtung der Säulenköpfe mit Kinesinmotoren wurde das aktive Gleiten von Mikrotubuli auf diesen neuen Oberflächen untersucht.

Micropillar force sensor arrays are produced for biophysical studies of cellular and intracellular mechanics and for the assembly of suspended biofilament networks. Three types of pillars are made: (1) gold capped silicon pillars, (2) epoxy pillars and (3) polydimethylsiloxane (PDMS) pillars. Pillars with diameters of 1 - 5 µm and with a maximum aspect ratio (height : diameter) of 20 : 1 are produced. The pillar heads are selectively functionalised to allow the cultivation of fibroblasts, epithelial cells and heart muscle cells on their tops. Cellular traction forces are determined by measuring the bending of the pillar tops during cell movement. A model system for the actin cortex is produced by crosslinking actin filaments on the pillar heads, with the actin binding protein filamin. Crosslinking experiments are also conducted with divalent cations and with fluorescently labelled myosin II motors. The mechanical properties of single filaments are determined by Fourier analysis of their fluctuations. Transport properties of myosin V motors on the networks are quantified. Microtubule gliding assays in a three dimensional environment are conducted on the pillar tops by coating these with kinesin motors.

Table of contents

Chapter 1

Introduction

Cell motility is an essential mechanism for the proper functioning of many biological organisms. Significant progress has been made in enhancing the existing knowledge of the biology and biochemistry of motile cells [Evans, 1993]. However, there is still a lack in the description of the physical dynamics of such movements. Despite a better understanding of the biophysics and the mechanics of cells [Fung, 1993], there are still many open questions remaining [Ingber, 2004]. The purpose of this study is to gain more insight in the mechanics of whole cells and of the intracellular cytoskeleton. This is done with the help of novel surface preparations, the so-called microfabricated pillar arrays. These substrates are used as force sensor arrays and as a templates with reduced boundary conditions. The pillar arrays are employed for several types of experiments. Contractile forces of cells plated on the pillar tops are measured and suspended networks of protein filaments are assembled on the pillar heads. Both types of experiments are closely related as will be discussed in this chapter.

To describe the mechanical properties of cells, it is necessary to consider their cytoskeleton. Three types of protein filaments build up the cellular cytoskeleton. These polymers are called actin, microtubules and intermediate filaments. The flexibility of all these polymers differs from each other. Microtubules have the highest stiffness, actin is more flexible and as last intermediate filaments are the most flexible protein filaments in cells. All these different filaments have their special tasks in cells. Actin is responsible for cellular shape and rigidity. Microtubules are responsible for pulling the chromosomes apart during cellular division and for intracellular transport of vesicles. Intermediate filaments belong to a heterogeneous family, whose diversity is used for different purposes in different cells. For example, in epethelial cells they are present in the entire cytoplasm and give strength to the entire epithelium [Alberts *et al*., 2002], while in hair cells they are also abundant. The study presented here mainly considers actin and microtubules; the next section will briefly describe these polymers and the associated molecular motor proteins.

1.1 Introduction to actin, microtubuli and molecular motors

In the early 1940s actin and myosin was identified by Banga, Szent-Györgyi and Straub in extracts of rabbit skeletal muscle [Pardee and Spudich, 1982]. Straub isolated actin

by separating the viscous protein from an actomyosin preparation. Further research revealed that actin could be obtained in a non-viscous, i.e. monomeric, state by extracting the actin in a buffer with low inonic strenght. Subsequent addition of salt induced a conversion into the viscous, i.e. filamentous, state.

Filamentous actin (F-actin) is a polymer build up from the monomer globular actin (G-actin). G-actin is a 42 kDa protein with a binding site for adenosine triphosphate (ATP) in its centre. Polymerisation starts with the relatively slow process of nucleation. For actin, the binding of two monomers is rather unstable, but the binding of three monomers is stable. The actin filament needs to be stabilised by divalent cations, like Mg^{2+}, for this process to occur. The relatively slow process of nucleation is followed by a much faster process of further elongation (fig. 1.1 A). Finally an equilibrium state is achieved where the rate of association of new monomers is equal to the rate of dissociation of monomers. For the initiation process of nucleation and polymerisation to take place, a critical monomer concentration is necessary. It occurs under optimal conditions in the presence of ATP, event though polymerisation also takes place without ATP present [Lodish *et al.*, 1999]. When ATP is present, the ATP molecule in the monomer hydrolyses to adenosine diphosphate (ADP), shortly after addition of a monomer to the polymer-chain. Hydrolysis of the ATP means that the monomer in the F-actin becomes less favourable for the addition of new monomers. Furthermore it can dissociate more easily from the polymer [Alberts *et al.*, 2002].

Actin filaments underlie a dynamic treadmilling process (fig. 1.1 C) where at one side (barbed or plus end) the monomers predominantly assemble and at the other side (pointed or minus end) the monomers predominantly disassemble. The terms barbed and pointed end originate from experiments to identify the polarity of actin. The ATP in G-actin is at the bottom of a cleft in the monomer [Lodish *et al*., 1999]. At the F-actin minus end this cleft is exposed to the environment, at the plus end this cleft is next to a neighbouring monomer. The resolution of electron micrographs is not good enough to resolve these clefts and to distinguish between the minus and the plus end of actin filaments. However, when the filament is decorated with S1 myosin heads (see later in this introduction) a specific arrow structure is observed, because the S1 domains bind with a preferred orientation. The arrows point to the so-called pointed end and the other end is then called the barbed end.

Even when the resolution of electron microscopy is not good enough to resolve the polarity of actin, it is sufficient to observe the helical structure actin possesses. Figure 1.1 C shows a schematic image of the helical structure of F-actin. The periodicity of the helix is approximately 36 nm and the diameter of the filaments is around 7 nm.

Microtubules normally consist of 13 protofilaments, which are arranged parallel to each other to form a tube-like polymer. There are however examples of microtubules with a different amount of protofilaments. The number of protofilaments found in microtubules ranges form 11 to 16 [Eichenlaub-Ritter and Tucker, 1984]. For all microtubules the protofilaments are formed from the tubulin dimer, which is a 100 kDa dimer consisting of a pair of very tightly bound α- and β-tubulin monomers. Both the monomers have a binding pocket for GTP [Alberts *et al.*, 2002]. In β-tubulin this GTP hydrolyses to GDP shortly after addition of the dimer to the polymer. Microtubules have a so-called plus and minus end. From both sides association and dissociation of dimers takes place, but at the plus-end this process is much faster (fig. 1.1 D). The polymerisation of microtubules is characterised by a process called dynamic instability, which is an alternation of continuous addition of dimers and rapid shrinkage of the polymer (fig. 1.1 B). This sudden change between growth and disassembly is probably triggered by a change in rate of dimer assembly and GTP hydrolysis [Howard, 2001]. When the addition of dimers is slower than the hydrolysis of GTP, dimers with bound GDP are exposed to the outside of the polymer. GDP-tubulin on the polymer end makes it

unstable and depolymerisation is promoted. Microtubules have a bigger diameter than actin and whereas actin can not be imaged by contrast microscopy, microtubules can be imaged by differential interference contrast microscopy. The outer and inner diameters of microtubules are around 25 nm and 18 nm respectively.

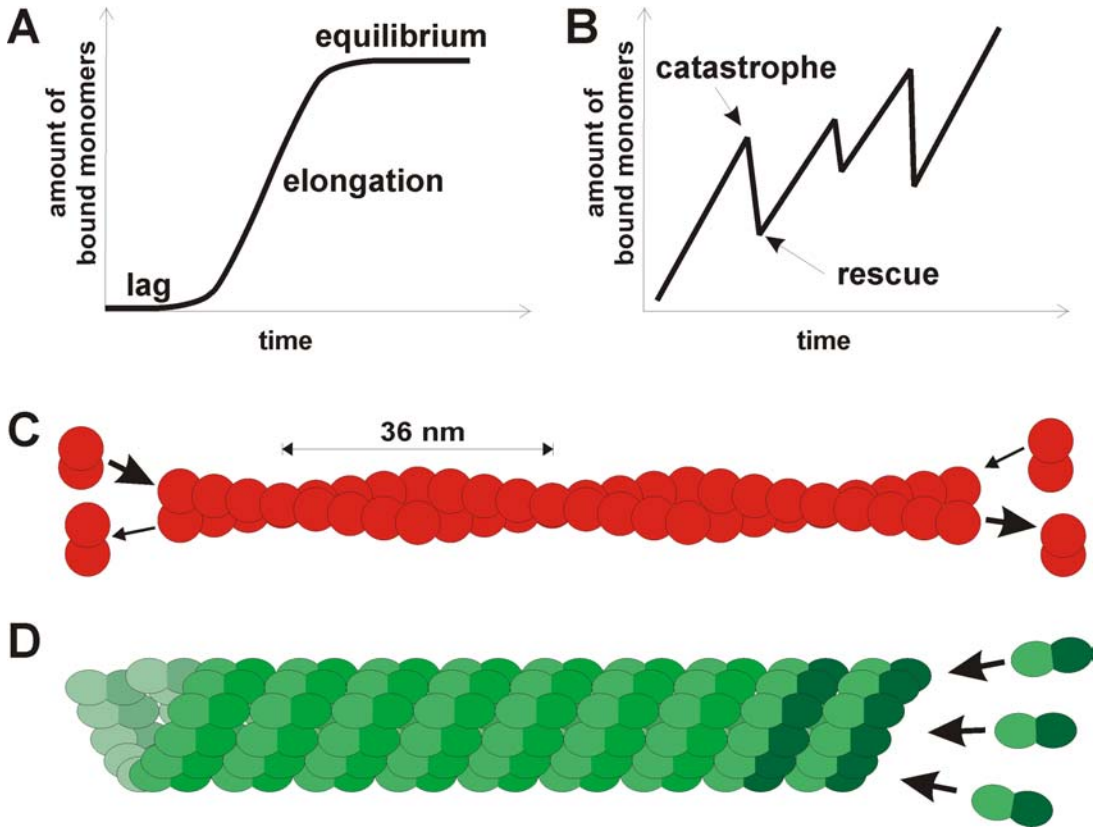

Fig. 1.1 Actin and microtubule models. (A) Polymerisation starts with nucleation, which takes a relatively long time (lag phase). There is a big increase in bound monomers after the lag phase, when the filaments rapidly elongate (elongation phase). Finally F-actin gets to the equilibrium phase where the average length does not change anymore and steady treadmilling takes place. (B) Microtubules do not have this equilibrium phase, but exhibit dynamic instability. Periods of growth are alternated with periods of rapid depolymerisation. (C) Treadmilling model of actin; on the left side (barbed end) more monomers attach than dissociate, on the right side (pointed end) it is the opposite. (D) Model of microtubule growth; on the right side (microtubule plus-end) dimers with GTP-β-tubulin (dark) associate to the filament and the GTP hydrolyses to GDP (lighter colour). In this example a GTP-tubulin cap is present, which means that GTP-β-tubulin is everywhere at the end and elongation continues. When elongation slows down and GDP-β-tubulin is exposed at the end, a catastrophe occurs and rapid shrinkage takes place until a rescue happens where polymerisation continues again. At the minus-end both growth and shrinkage is slower than at the plus-end. Images after Alberts *et al*. [2002] and Verde *et al.* [1992].

Actin and microtubules have many proteins that associate to them. Next to passive binding proteins there exists a class of active binding proteins, the motor proteins. Motor proteins can move over protein filaments, either as a transporter of cargo, or to transport filaments. Myosin motors bind to actin, whereas kinesin motors bind to microtubules. The

motions these motors generate are associated with muscle contraction, intracellular organelle transport and cell division. Both types of motors have many variants, each optimised for its specific function. Recent studies give evidence that myosin and kinesin share a common core structure and that they convert energy from ATP to directed motion using a similar conformational change strategy [Vale and Milligan, 2000].

There are several types of myosin motors, being myosin II the first one to be discovered. Myosin II is abundant in muscle tissue in which it forms thick bundles. In muscles these thick bundles are alternated with thin bundles, the F-actin. Together they make muscle contraction possible where the energy comes from the hydrolysis of ATP by the myosin motor. Myosin II is a dimer consisting of two heavy chains and four light chains. The two α-helices of the heavy chains wrap around each other to form a stalk. The light chains are near the catalytic domain (Fig. 1.2). The latter, also called the head, binds the nucleotide and actin. At physiological salt concentrations myosin is insoluble, because the stalk region is not soluble in [KCl] < 0.3 M. The head region, with the catalytic domain, resides in water under all conditions [Margossian and Lowey, 1982]. Even though myosin II is a dimer it seems that the two heads do never simultaneously bind to the same actin filament. Active myosin-actin cross-bridges attach and dissociate at least 50 times per second. The cross-bridges act asynchronously, this ensures that, in muscles, at any time a fraction of the cross-bridges produces work strokes [Vale and Milligan, 2000; Pollard, 1987]. The work or force stroke of a single myosin II head advances the molecule about 10 - 15 nm and the force it exerts during the work stroke is about 1 pN [Ishijima *et al.*, 1991].

Myosin II can be cleaved in several domains by proteases, these are enzymes that cleave proteins at certain peptide bounds. This process is called protein digestion or proteolysis. Trypsin and chymotrypsin are proteases found in the stomach of mammals. They are closely related in structure, but they target different peptide bounds. Papain is a protease derived form papaya. Chymotrypsin and papain can cleave myosin II (fig. 1.2). One of the end products of this cleavage is S1, the head domain of the myosin heavy chain. Gliding assays show that S1 alone can move actin filaments forward [Lodish *et al*., 1999]. This means that the catalytic domain and the actin binding domain of myosin II are present in the head.

Whereas myosin II is non-processive, myosin V is a processive motor. Processivity means that a motor undergoes multiple catalytic events which results in directed motion along the filament. This property allows for being involved in organelle and mRNA transport. The structure of myosin V shows similarities to that of myosin II. Instead of essential and regulatory light chains there are calmodulin light chains present in the neck region of myosin V. The stall force for myosin V movement is about 3 pN, which is roughly half the stall force for kinesin, a microtubule based processive motor [Mehta *et al.*, 1999]. Myosin II and V both move towards the barbed end of F-actin. Until recently it was unclear whether myosin V moves in a hand-over-hand manner, where the heads are alternating at leading positions, or whether it moves in a "worm" manner, where the same head remains at leading position all the time. Yildiz *et al.* [2003] showed that myosin V moves in a hand-over-hand manner. Myosin V takes 36 nm steps when attached to a bead moving over surface immobilised actin filaments. This step size of 36 nm is the helical repeat length of actin. The geometry of these experiments might force the myosin to bind to sites on the actin filament that are separated by 36 nm. This inspired Ali *et al.* [2002] to perform bead motility assays on suspended actin filaments. In this configuration myosin walks as a left-handed spiral motor over the right-handed actin helix, with step lengths of just below 36 nm.

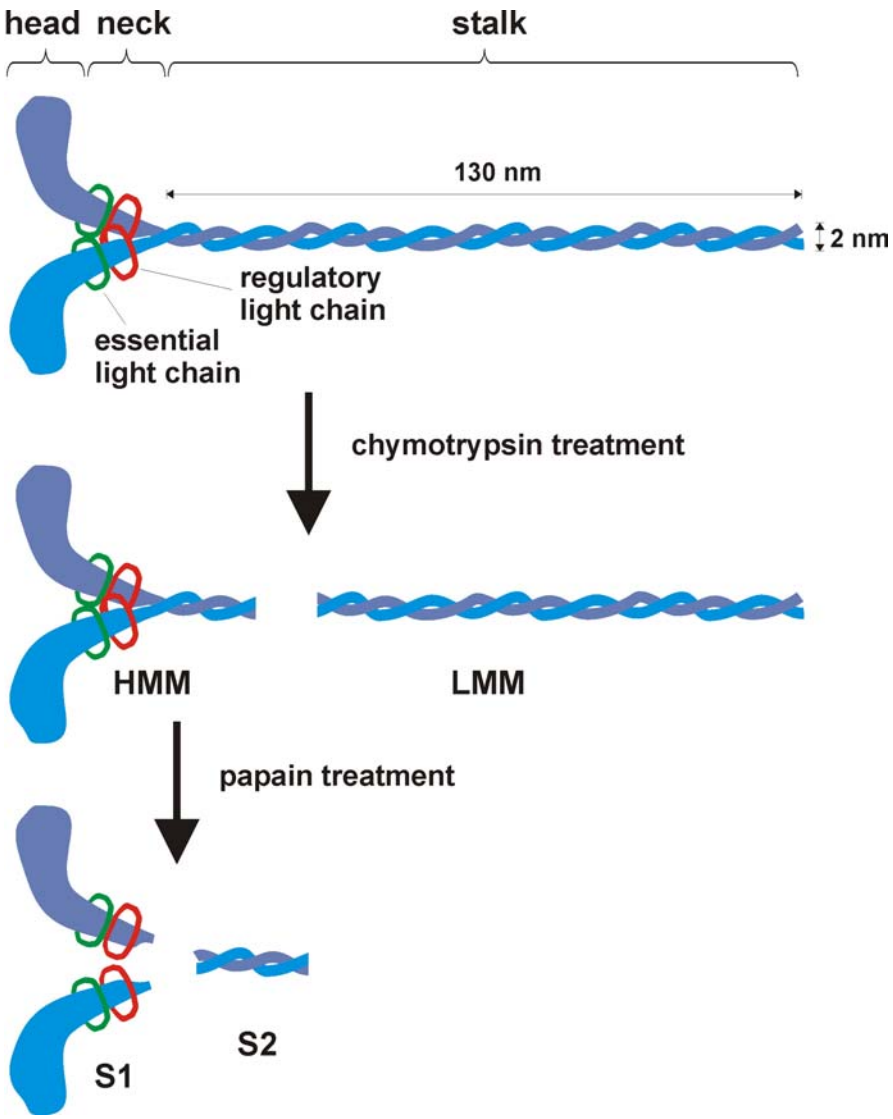

Fig. 1.2 Myosin II consists of two heavy chains and four light chains. The heavy chains are made up of three functionally and structurally different domains. These are the head domain, which incorporates the actin and ATP binding sites. Then comes a neck domain with light chains associated to it. These light chains regulate the activity of the head domain. Next to this lies the coiled-coil stalk domain. Proteases like chymotrypsin can cleave the myosin in heavy meromyosin (HMM) and light meromyosin (LMM). Subsequent digestion of HMM with papain results in a S2 and two S1 domains. The S1 domains are the single myosin heads. S1 can move actin filaments forward in gliding assays, because the head incorporates the nucleotide and the actin binding domains. After Lodish *et al*. [1999]

The microtubule associated motor protein kinesin family is made up from many subfamilies. Conventional kinesin is a processive motor, which moves organelles along microtubules towards its plus-end [Vale and Milligan, 2000]. Kinesin is a dimer with structural similarities to myosin II in having two heavy chains and two light chains [Alberts *et al*. 2002]. The step size of kinesin is 8 nm as determined by optical trapping interferometry [Svoboda *et al.*, 1993]. A different kinesin motor is Eg5. This mitotic motor is present in the mitotic spindle, a dynamic structure responsible for chromosome separation [Kapoor and

Mitchison, 2001]. Another subclass of microtubule motor proteins are dyneins, which move towards the microtubule minus-end.

1.2 Overview of cell experiments on special surfaces

Traditionally biologists and biophysicists study cells plated on coverslips. This is a convenient way to study the cells using light microscopy, because the glass is flat and transparent. In living organisms however, cells are embedded in a three dimensional matrix, called the extracellular matrix (ECM). This matrix consists of proteoglycans (polysaccharide chains linked to proteins) and fibrous proteins like collagen, fibronectin and laminin arranged in a network, which provides mechanical and biochemical support to cells [Alberts *et al.*, 2002]. Cells are connected to the ECM via integrin-based adhesion, which links the ECM to the cellular cytoskeleton. These integrins bind to fibronectin fibers in the ECM. The integrins are transmembrane proteins and a cluster of integrins is called focal contact, focal complex or focal adhesion. Cells do not adhere all over their surface to the environment, but only at the focal contacts and complexes. In vivo cells can move through the ECM and interact with it and with other cells. This migration is important for wound healing and embryonic development [Galbraith and Sheetz, 1998; Balaban *et al.*, 2001; see also references in both papers]. During motility, cells exert forces onto their environment and there is a close relation between adhesion assembly on the ECM and the forces fibroblasts can generate [Balaban *et al.*, 2001; and references therein].

Qualitatively these forces have been described, using flat flexible substrates. For instance Harris *et al.* [1980] plated individual chick heart fibroblasts on polydimethyl siloxane (PDMS). The PDMS was crosslinked by hanging a small layer (supported by a coverslip) of this viscous polymer over a Bunsen-burner flame for 2 seconds. During locomotion and contractility the cells exert force onto the surface and because the PDMS surface is flexible this results in wrinkling of the substrate. Observing the number and the extensions of the wrinkles gives some idea about the direction of the movement (fig. 1.3 A). Bell *et al.* [1979] plated human fibroblasts on hydrated collagen and observed how the ensemble of cells condensed the collagen lattice to a tissue-like structure within 24 h.

Quantitatively the contractile forces have been measured by using several types of surfaces. Lo *et al.* [2000] used flat, flexible polyacrylamide substrates, coated with type I collagen, to show that 3T3 fibroblast movement is guided by the rigidity of the substrate. Substrates that were more flexible on one side than on the other side were used. Cells approaching from the flexible side crossed the border to the stiff side. However, cells approaching from the stiff side did not want to cross the border and remained on the stiff side. Furthermore it is shown that the spreading and the traction forces of the cells were bigger on the stiffer part than on the more flexible part. Munevar *et al.* [2001] improved the technique of the polyacrylamide surfaces by mixing it with fluorescent beads. These beads were used as tracer particles and the result was in increase in spatial resolution of the traction pattern (fig. 1.3 B). Dembo *et al.* [1996] developed some of the mathematical and physical techniques needed to analyse the displacement field of the elastic substrate under stress and to relate this to the traction field of the locomoting cell.

Micropatterned flexible substrates (PDMS) were used by Balaban *et al.* [2001] to study the relation between local force applied by fibroblasts and cardiac cells to a surface and the assembly of focal adhesions. The force exerted by single focal adhesions could be followed in real time. In a different approach Galbraith and Sheetz [1997] used cantilever-

based devices made out of silicon to observe fibroblast traction forces. The cells moved over a surface patterned with cantilevers and on average one cantilever was below a cell to measure the traction forces at that point (fig. 1.3 C). Instead of observing cell motility Burton and Taylor [1997] measured traction forces of cytokinesis on flat, flexible phenylmethyl polysiloxane sheets. Besides force measurements some groups have micropatterned rigid substrates to study cellular behaviour under varying constraints.

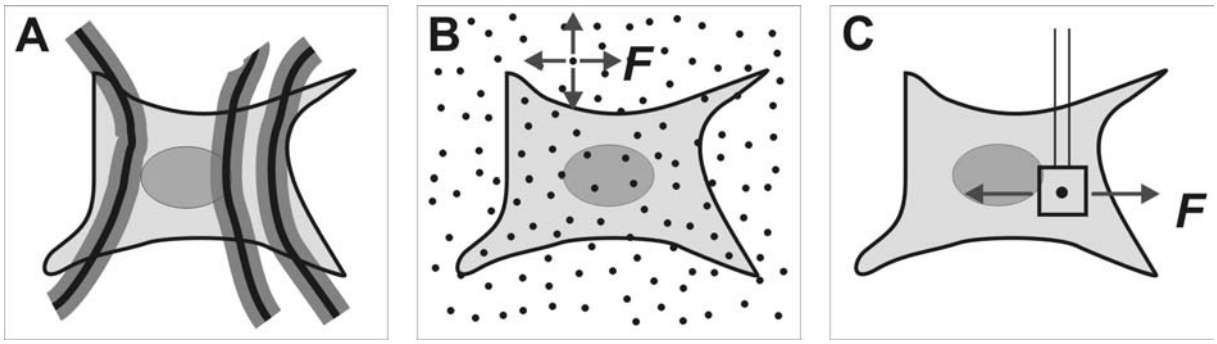

Fig. 1.3 Methods to study surface exerted forces during cellular locomotion and contractility reported in literature. (A) Wrinkles in flexible PDMS surfaces are observed during cellular locomotion. After Harris *et al*. [1980]. (B) Fluorescent tracer particles are embedded in a flexible polyacrylamide surface. By recording the displacement of the beads the force field the moving cell exerts can be computed. The substrate is flexible, but much more rigid than the substrate in (A). The result is that no significant wrinkles are observed, but the tracer particles do displace. After Munevar *et al.* [2001]. (C) A horizontal cantilever measures, in one dimension, the displacement of an adhering and locomoting cell. After Galbraith and Sheetz [1997]. All three schematic images are top views of the cell and the substrate.

Adhesive and non-adhesive areas can be created on gold coated glass cover slips by microcontact printing of self-assembled monolayers of alkanethiolates [Mrkisch *et al.*, 1997]. This was done by using a micropatterned PDMS stamp, which was coated with the alkanthiol. After stamping of the substrate it was immersed in a solution with an ethylene glycol terminated alkanethiol to inhibit adhesion to the parts that were not stamped. Next the substrate was immersed in a fibronectin solution and the protein only adhered to the stamped part. Consequently the cells only adhered to the stamped parts. Chen *et al*. [1997] used the microcontact printing technique to study apoptosis of endothelial cells. They used stamps with big patches, for adhesion of one cell onto one stamped area and stamps with many small, narrowly spaced patches. In the latter case the cells could lie over several adhesive islands. It was shown that not only the area of adhesion, but mainly the spatial distribution of the area of adhesion and thus of the focal complexes, was important for cellular viability. Arnold *et al*. [2004] changed this method by patterning surfaces with regularly spaced gold nano dots to study the adhesion of single integrins. These gold dots were chemically modified by a tripeptide sequence (arg-gly-asp, or RGD), which is part of the fibronectin molecule and which promotes cell adhesion. Instead of chemical patterning also topographical patterning of surfaces, like low aspect ratio silicon structures, has been applied to study cellular behaviour [Turner *et al*., 2000; Craighead *et al*., 2001]. Jungbauer *et al.* [2004] fabricated micrometer wide and nanometer high grooves in PDMS to observe dendrite orientation of melanocytes.

In the approach presented in this study the three methods described above are integrated into one sample. Flexible substrates are combined with biochemical and topographical patterning. Microfabricated pillar arrays of several materials are developed and used for cellular and protein filament studies. These micropillars are used as a template to study biomimetic protein assemblies and as a force sensor array. After plating cells on the microfabricated pillar arrays the forces these cells exert can be measured by analysing the bending of the pillars.

Three different types of pillar arrays are produced. These are gold capped silicon pillars, epoxy photo resist pillars and PDMS pillars. The dimensions of the pillars are in the micrometer range (diameter = 0.5 - 5 µm, height = 10 - 20 µm, inter pillar spacing > 2.5 µm). They are made by photolithographical techniques, either combined with ion and wet etching techniques (silicon pillars) or with replicate moulding techniques (PDMS pillars). The epoxy pillars are ready to use after the photolithography. Mouse fibroblasts and human pancreatic cancer cells are plated onto silicon and epoxy pillars. The morphology of adhesion is studied by light and electron microscopy. Chicken heart muscle cells are plated onto PDMS pillars. These cells contract regularly and the forces they exert to the surface are analysed by measuring the bending of the pillars. A schematic image of a cell lying on top of a pillar array is presented in figure 1.4.

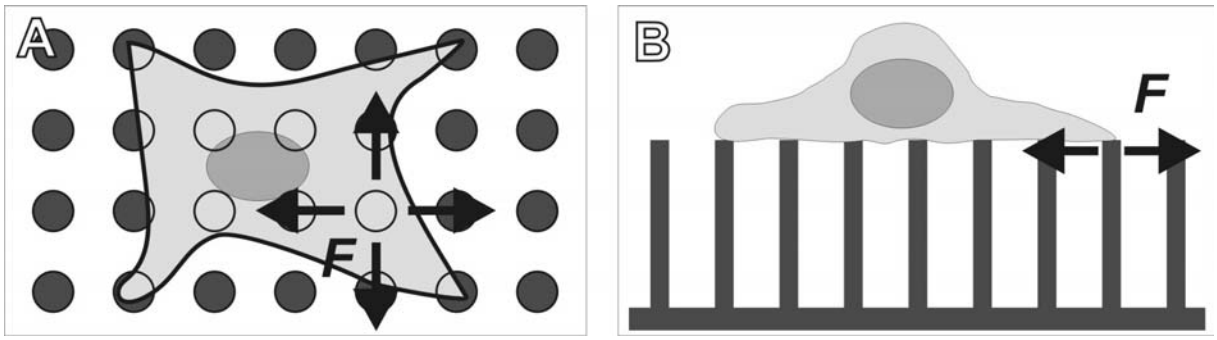

Fig. 1.4 Schematic images of pillar arrays used in this study to analyse cellular traction forces. (A) Top view of cell lying on a pillar substrate. Pillar bending is related to the forces a cell exerts to their environment. By measuring the displacement of the pillar heads in a top view approach, the exerted forces can be obtained. (B) Side view of a cell adhering onto a pillar array.

Galbraith and Sheetz [1997] used horizontal cantilevers to measure cellular traction forces, limiting the force measurements to one dimension (fig. 1.3 C). The pillar approach described here uses vertically standing pillars (fig. 1.4). This means that forces in two dimensions can be measured. During the course of this study methods using micropillars have been published [Tan *et al.*, 2003; Roure, du *et al.*, 2003]. They had however been preceded by Rovensky *et al.* [1991] in putting cells on microfabricated pillars.

Besides measuring forces the pillar arrays can be used to study focal adhesion assembly where the pillar heads function as islands of adhesion. In between these islands the cells will not have the possibility of interacting with a surface. Such a substrate is interesting to study filopodial extensions from motile cells and in general the spreading of cells. The formation of filopodial extensions and lamellipodia is based, for instance in neurons, on an interplay of microtubule polymerisation, actin cortex formation and the interaction with all the associated proteins (such as MAP1B, Myosin II, ARP 2/3) [Dickson, 2002]. Cells migrate by

extending filopodia, long thin actin supported membrane extensions, at their leading edge. Where the environment is favourable for adhesion the filopodia attach firmly and in between the filopodia a lamellipodium grows. Adhesion is released at the rear of the cell and the cell retracts, usually leaving some patches behind. Figure 1.5 shows images of two different cell types on two different, flat surfaces. On flat coverslips mainly qualitative studies can be performed. The pillar arrays make it possible to study quantitatively rigidity and extensions of filopodia and lamellipodia of growing, spreading and motile cells.

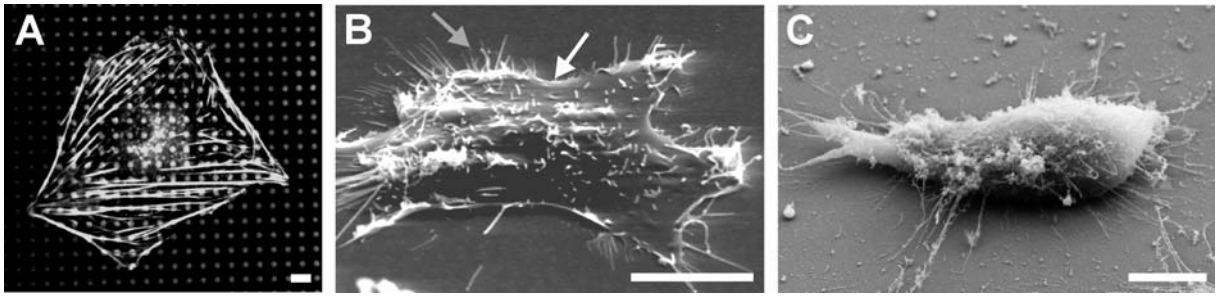

Fig. 1.5 Cells on flat surfaces. (A) Fluorescence microscopy image of GFP-actin fibroblast on fibronectin coated gold disks on glass. Actin stress fibers can be clearly seen. The actin cortex can not be imaged by light microscopy due to its limited resolution. (B) Electron micrograph of fibroblast on silicon. Filopodia (grey arrow) can be seen as thin long protrusions. A lamellipodium (white arrow) is a broad, flat extension, which is formed after several filopodia have made a tight surface adhesion. Angle of view 45º. (C) Electron micrograph of pancreas epithelial cell on silicon. The epithelial cell is less flat than the fibroblast. Angle of view 45º. Scale bar 10 µm.

Using microfabricated pillar arrays for cell plating is an approach to mimick in vitro the actual three dimensional environment that the ECM provides to a cell. Cells on micropillars can only build focal adhesions at the pillar heads. In between the pillar heads the cell is not adhering and is surrounded by the medium. The cell and thus the cytoskeleton is pending in between the adhesion sites. The cytoskeletal system, which is vital for controlling cell shape, cell motility and cell division, consists of the polymers microtubules, actin and intermediate filaments. These polymers and their properties can also be studied outside the cell, for instance grafted onto the micropillars. This allows topological and mechanical studies of cytoskeletal filaments and it allows studies of the actin cortex. Building an artificial actin cortex connected to only a few anchoring points has several advantages compared to having a surface everywhere. The main advantages are that surface interactions of the actin network are minimised and that two dimensional models can be probed.

1.3 Overview of actin and microtubuli experiments

The actin cortex of cells is a quasi two dimensional network of actin filaments and actin binding proteins, lying just below the cellular membrane. Whereas studying actin cortices in vivo gives an overall image of the mechanical properties of this network, it is difficult to separate the contributions of all the components it consists of. Observing actin

networks in vitro allows a better control of parameters. The influence of different actin binding proteins, like filamin, alpha-actinin, spectrin, myosin etc., can be analysed.

Mechanical properties of filamentous actin have been studied in one dimension (single filaments) [Gittes *et al*., 1993; Le Goff *et a*l., 2002] and in three dimensions (bulk in vitro actin gels) [Janmey *et al*., 1994]. Müller *et al*. [1991] and Hinner *et al.* [1998] used oscillating disk rheometry whereas Gardel *et al*. [2003] used microrheometry to study three dimensional actin gels. The former method addresses macroscopic parameters and the latter microscopic length scales. Experiments with entangled and with crosslinked gels are reported. By using magnetic bead microrheometry Bausch *et al*. [1998; 1999] performed viscoelastic measurements of the cytoplasm of fibroblasts and macrophages, from which information about the mechanical properties of the actin cortex in living cells can be deduced. Limozin and Sackmann [2002] studied polymorphism of crosslinked actin gels in giant vesicles. They polymerised actin inside the vesicles and used actin-binding proteins as crosslinker. Schmidt *et al.* [1989] employed quasi-elastic light scattering to characterise bulk actin solutions. Several methods to characterise bulk actin filament networks are described by Pollard and Cooper [1982]. These methods range from test tube inversion and low speed actin sedimentation to falling ball assays and various viscometric measurements.

The approach presented in this study is neither one nor three dimensional, but a two dimensional approach. Up to date this has always been difficult, because of either nearby surfaces that hinder the formation of a network or the absence of a surface to support the two dimensional network. The microscopic pillar arrays are a mixture of a surface that serves as anchoring points and the absence of a solid interface in between the attachment sites to promote free organisation of a two dimensional network. Crosslinking of the actin filaments is performed with the passive, protein crosslinker filamin and with divalant cations. The active crosslinker myosin II is also able to form two dimensional networks of actin. Besides actin networks also networks of microtubules and microtubule aster-like structures can be constructed on the pillar tops.

During cell division asters of microtubules are formed to pull the chromosomes apart. The positioning of these asters, with dynamic microtubules, has been studied in microfabricated chambers [Faivre-Moskalenko and Dogterom, 2002]. Dynamic asters are also studied with active motor proteins and stabilised microtubules [Surrey *et al.*, 2001]. In these experiments it is of great importance to understand the mechanical properties of microtubules and the dynamics of microtubule-motor interactions. Mechanical properties of microtubules are measured by Fourier analysis of undulating filaments [Gittes *et al.*, 1993]. The microtubule polymerisation force has been studied by shape analysis of buckling microtubules polymerising against a wall [Dogterom and Yurke, 1997]. Interactions of gliding microtubules with patterned, motor-coated surfaces are observed and analysed by Hess *et al.* [2002a, 2002b]. Going a step further it is explained in chapter 4 how pillar heads have been coated with kinesin motors to conduct microtubule gliding assays on the top of these pillars. The microtubules are prevented from gliding over the bottom surface by a passivation step, which does not allow for the binding of motors anywhere else as on the pillar tops. Gliding microtubules easily bridge gaps of over 10 μm without any support. The gliding velocity on PDMS pillars, on flat PDMS and on glass is then compared.

Chapter 2

Pillar formation

2.1 Introduction

Three types of pillar arrays, all consisting of different materials, have been successfully produced and implemented [Spatz *et al*., 2004]. These are silicon pillars, epoxy pillars and polydimethylsiloxane (PDMS) pillars. The silicon pillars have the highest aspect ratios (up to 20:1) and can be produced with diameters of 1 µm or more. Furthermore, the gold disks located at the top of the pillars permit easy and effective functionalisation of the pillar tips and passivation of the rest of the substrate. The major disadvantages of silicon include the fact that it is not optically transparent and its relatively high Young's modulus in comparison with that of cross linked polymers such as polydimethylsiloxane. The advantage of epoxy pillars is that they can be produced on glass, hence making the substrate transparent and suitable for transmission optical microscopy. The inherent fluorescent property of the epoxy pillars are advantageous when trying to localise fluorescent material and their distance to surrounding pillars. However, the fluorescent property of the epoxy pillars comes in as a disadvantage when imaging a fluorescent material on their tips. The fluorescent properties of the epoxy will be responsible for a significant background, which decreases the image resolution of the fluorescent material to be imaged. The PDMS pillars are transparent, non-fluorescent and their stiffness can be tuned by changing the crosslinker (curing agent) density. However, it is not possible to produce PDMS pillars directly on glass, because the pillars and the bottom surface are one and the same material, as for the silicon pillars. That is a result of the production process, which does not allow the separation of the pillars and their base. However the whole substrate can be put on a cover slip to enable transmission optical microscopy measurements.

Forces that are applied laterally to the pillar tops can be evaluated with conventional light microscopy coupled to a CCD camera, which records the displacement of the pillar tops. For small deflections, the bending stiffness, *b,* of a pillar can be calculated according to the formula below:

$$b = \frac{3}{4}\pi E \frac{r^4}{L^3} \qquad (2.1)$$

where E is Young's modulus, while r and L are the radius and the length of the pillar respectively [Landau and Lifshitz, 1991, problem 3, p101] (see figure 2.1). The dimensions of the pillars are obtained from electron micrographs. This can be done by making an image of the pillars under 45° and using the calibrated scale bar on the sem picture to measure the diameter and length of the pillar. Hereby the angle under which the image is taken needs to be taken into account.

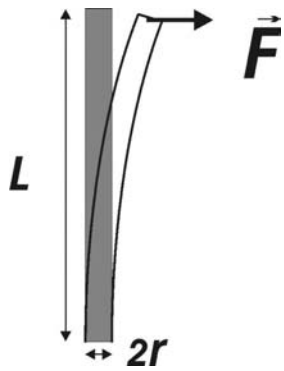

Fig. 2.1 Forces applied laterally to the pillar tops can bend the pillar. By recording the pillar top displacement the exerted force can be determined when the pillar stiffness is known. The pillar bending stiffness can be calculated from equation 2.1.

In the rest of this chapter the fabrication of the pillar arrays is described. The used parameters are printed in tables in the respective paragraphs. This chapter ends with a discussion about calibration of the pillars.

2.2 Gold capped silicon pillars

This section describes the fabrication of silicon pillars that have a gold disk attached to their tops. The production parameter section is followed by a section discussing problems that may arise during the fabrication of these pillars. A few examples are given of what the pillars look like when the production parameters are not correct.

2.2.1 Production process parameters

The first step in making silicon pillars is patterning the silicon wafer with gold disks. The successive steps are: 1) cleaning the silicon with distilled water, isopropanol and aceton, each five min in a sonicator. 2) Spin coating a 1 µm thick positive photo resist layer (AR-P 5350, Allresist, Strausberg, Germany) on top of the silicon pieces. 3) Illuminating the sample using a Karl Suss (München, Germany) MJB3 maskaligner with a master-mask consisting of circular holes (diameter 1 - 2 µm, spacing 2.5 µm, 5 µm or 7.5 µm). 4) Developing and

subsequently sputtering 5 nm chromium (Cr) and 80 nm gold (Au) on top. The Cr serves as an adhesion enhancer for the sputtered gold film. 5) Lift off results in silicon patterned with regularly spaced gold disks, which serve as masks for the Reactive Ion Etching (RIE) process.

The RIE is performed with a Surface Technology Systems plasma etcher (Multiplex Systems) in the Advanced Silicon Etching process. This process involves an alternate use of sulfur hexafluoride (SF_6), which plays a role of an etch gas and octafluorocyclobutane (C_4F_8), which acts as a passivating gas [Ayon *et al*. 1999]. During the passivation step, a "teflon-like" layer is formed on the pillar side walls to inhibit under etching. These pillars can have an aspect ratio (height : diameter) of up to 20 : 1 (see fig. 5.4). The height of the used pillars is about 10 - 15 µm. Table 2.1 summarises the employed parameters and the successive steps involved in the pillar formation. As an optional step, wet chemical etching is performed (see below of the following table).

Table 2.1 Parameters for fabrication of gold capped silicon pillars

process	*parameters*	*additional info*	*type / brand of product*
cutting silicon in pieces	10 x 10 mm		
cleaning	5 min in sonicator	subsequently in water, isopropanol and aceton	
spin coating	5 sec 200 rpm + 40 sec 4000 rpm	a few drops, medium acceleration	Allresist AR-P 5350
baking	100 °C, 15 min	in oven	
exposure	8 - 16 sec		Karl Suss MJB 3 Maskaligner
developing	20 - 40 sec	1 : 2 (developer : water) dilution	Allresist AR-300-47 or AR-300-35
sputtering	5 nm Cr or Ti + 80 nm Au		Bal-tec MED 020
removing	5 min, 50 °C		AR 300-70 or aceton
ion etching		reactive ion etcher	Surface Technology Systems
wet etching (optional)	5 - 10 sec under agitation	mixture of: [HF] = 4.3 M [HNO_3] = 5.0 M [CH_3COOH] = 4.3 M	

The stiffness of cylindrical objects can be decreased by increasing their aspect ratio, i.e. the ratio of length to diameter. This can be concluded from equation 2.1. The diameter of the silicon pillars is reduced by wet chemical etching, using a mixture of hydrofluoric (HF), nitric (HNO_3) and acetic (CH_3COOH) acid, this solution is also called HNA. The nitric acid oxidises the silicon and the hydrofluoric acid etches the silicondioxide [Williams and Muller, 1996], the acetic acid serves as a dilutant and helps to prevent the dissociation of HNO_3 in NO_3^- and NO_2^- [Kovacs *et al.*, 1998]. Figures 2.2 A and B show a pillar array before and after wet etching. Of interest is, that decreasing the overall concentration (see text by figure 2.2) by 7 percent, almost completely brings the etching process to a halt even when the etching time

is increased by a factor 80. Successful etching can result in an aspect ratio of approximately 25 : 1.

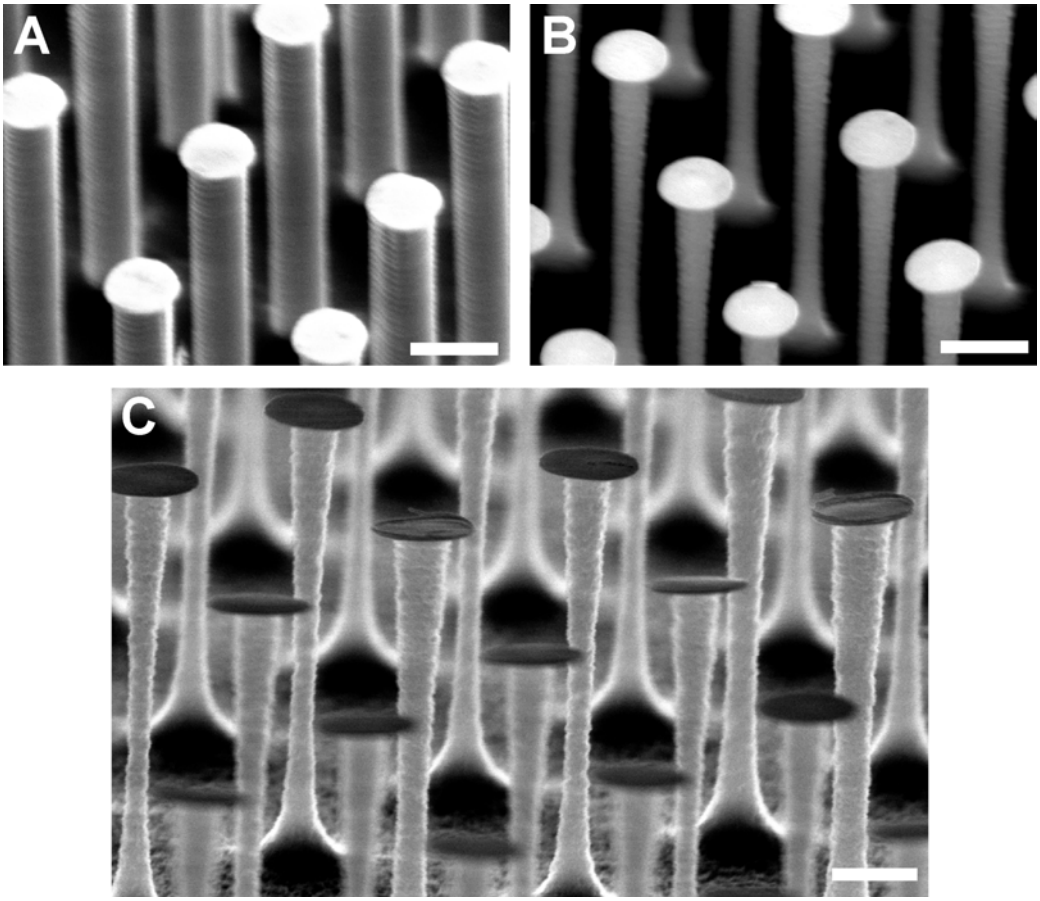

Fig. 2.2 Improving the compliance of Si pillars: (A) Silicon pillars after RIE and (B) the same pillar array after additional wet chemical etching ([HF]=4.3 M, [HNO_3]=5.0 M, [CH_3COOH]=4.3 M, 5 sec under agitation). The bright areas are the Au disks on top of the pillars. The bending stiffness of the pillars in (A) is 66 ± 6 N/m and in (B) it is 7 ± 2 N/m (viewing angle 45°). The aspect ratio before and after wet etching is 7 : 1 and 17 : 1 respectively. (C) High angle view of (a different) pillar array after wet chemical etching, viewing angle 71°. Scanning electron micrographs, scale bar 2 µm.

2.2.2 Etching artefacts

During the production process of the pillar arrays a series of problems may arise. One of which may be caused by the photolithography, whereby there is a possibility that the diameter of the gold disks may be larger or smaller than required. The gold layer sputtered on top might be too thin, hence ineffective as an etch mask. Another problem may lie in the reactive ion etching parameters, which may sometimes be inappropriate for proper pillar formation. Also, prolonged wet etching may result in pillars that are either too thin or completely etched away. Figure 2.3 shows scanning electron micrographs of pillar arrays that resulted from the previously stated problems. While the pillars shown in figure 2.3 A can be used for experiments without force measurements, the other two samples are clearly

inappropriate for experimental implementation. Due to the above stated problems it is necessary that the pillar arrays are checked before being used for experimentation. This can be done by aid of light microscopy or preferably by electron microscopy, because the latter has a higher spatial resolution.

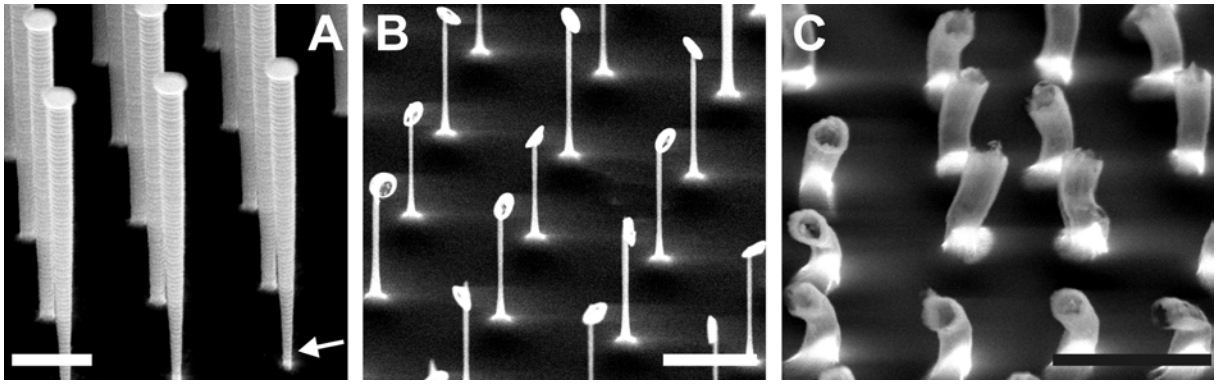

Fig. 2.3 Etching artefacts of gold capped silicon pillars. (A) Under-etching of the pillars becomes significant after extended reactive ion etching. The white arrow points to the base of a pillar, which is clearly smaller than the rest of the pillar. All the pillars would have collapsed, when the etching had been performed a bit longer. (B) Too long wet etching, combined with a too thin gold disk, which is a problem during the reactive ion etching. The pillar diameter is decreased too much to be able to support properly the gold disks. The aspect ratio of these pillars is 25 : 1. (C) These pillars are etched with improper reactive ion etching parameters and the gold etch mask is partially removed. The resulting pillars seem to be hollow and are clearly bent. Scanning electron microscopy images, angle of view in (A) 30º, in (B) and (C) 45º, scale bar 5 µm.

2.3 Epoxy pillars on glass

Epoxy pillars are made of an SU-8 negative photo resist (Microchem Corp, Newton MA, USA), which is widely used for micropatterning of surfaces and is known to produce high aspect ratio structures [Lorenz *et al.*, 1997; Shaw *et al.*, 1997; Hess *et al.*, 2002b]. SU-8 consists of a mixture of EPON SU-8, a photoinitiator and a solvent. EPON SU-8 is a molecule that has several epoxy groups (an oxygen bridge with two other atoms, in this case carbon). Upon illumination of the resist with UV light, an acid is formed, which opens the epoxy rings, making them reactive. Consequently a crosslinked matrix of the EPON SU-8 molecules is formed. This process is normally accelerated by a post-exposure bake at 95 °C. The final result is that the illuminated part of the resist will get insoluble and that the non-illuminated part can be dissolved. This is the typical feature of negative photo resists. For positive photo resists it is the other way around.

To fabricate the epoxy pillars a layer of 10 to 15 µm thick photo resist is spin-coated on aceton cleaned glass cover slips. The samples are then soft-baked on a hot plate. Using the same master-mask as employed in the silicon pillar preparation, the samples are illuminated with the maskaligner. During the illumination the exposed part of the photo resist starts to crosslink and this process continues during post-baking. Development of the resist removes only the non-illuminated part of the resist. After developing, free standing pillars with a

diameter of approximately 3 µm and height between 10 and 15 µm remain on the cover slips. Table 2.2 summarises the parameters and the successive steps employed in the formation of the epoxy pillars.

Table 2.2 Parameters for fabrication of epoxy pillars on glass

process	*parameters*	*additional info*	*type / brand of product*
use glass cover slip	24 x 24 mm		
cleaning	5 min in sonicator	in aceton	
spin coating	10 sec 500 rpm + 30 sec 3000 rpm	0.5 ml, medium acceleration	Microchem SU-8 10
soft-baking	65 °C, 2 min 95 °C, 5 min	on a hotplate	
exposure	8 sec		Karl Suss MJB 3 Maskaligner
post-bake	65 °C, 1 min 95 °C, 2 min	on a hotplate	
developing	2 min		Microchem SU-8 developer
rinsing		with isopropanol	

The main problems encountered with epoxy pillars are that either most of the pillars collapsed after developing and drying or, they are standing on a kind of baked epoxy layer, which is all over the sample. This baked epoxy layer depreciates the image quality, because it partially disrupts light transmission. The implementation of an epoxy silane as an adhesive in between the glass and the photo resist does not significantly improve the adhesion quality of the epoxy pillars on the glass substrate. Normally a nitrogen blow drying technique is employed to dry the sample after rinsing with isopropanol. A spin coating step to dry the sample does not give improved results. It seems that there is quite a small range within which the parameters are optimal to produce the free standing epoxy pillars on glass. Due to the fact that humidity, temperature and other unknown influential parameters change from experiment to experiment, it is difficult to obtain a high degree of reproducibility.

2.4 PDMS pillars

The third method to make pillar substrates is based on replicate moulding techniques. A transparent polymer, mixed with a crosslinker, is poured onto a substrate with regularly spaced holes. After curing and removing the pillar substrate is obtained.

2.4.1 Production process parameters

The first step in this process is again photolithographic. This step is the inverse method that is used to make the epoxy pillars. Instead of making pillars out of photo resist, cylindrical holes are made in photo resist. Before making the cylindrical holes in the SU-8 resist however, a master-mask needs to be fabricated.

The master-mask is made with a mask writer (DWL 66, Heidelberg Instruments, Germany). For this the desired pattern has to be designed and drawn. Then it is written with a laser into a photo resist layer (AZ-1505, Microchemicals, Germany), which is previously spin coated on a glass plate. After developing a non-transparent (i.e thicker than 100 nm) layer of chromium is sputtered on top and a lift off is performed. This is now the master-mask. The master-mask can be used many times to make cylindrical holes in a thick SU-8 photo resist layer, using a master-mask patterned with disks. The cylindrical holes in the SU-8 photo resist are employed in the following steps.

Polydimethyl-siloxane (PDMS) is mixed with a thermo-crosslinker (curing agent) at a weight-ratio 10:1. Directly after mixing, so before it is crosslinked, this mixture is poured on the substrates with the cylindrical cavities. By evacuating the air around the substrate and out of the holes, the mixture runs into the holes. Curing in an oven results in a flexible PDMS layer, which can be peeled off the substrate. The formed negative of the hole-substrate is a PDMS pillar array. In table 2.3 the parameters for the production of PDMS pillars are printed. The steps until developing is performed in the clean room. The PDMS mixing and curing can easily be performed in a normal chemical laboratory. The chemical reactions involved in this step are described in the following.

Crosslinking mechanism of PDMS

This section discusses the crosslinking reaction of PDMS [Campbell *et al.*, 1999]. PDMS (Sylgard 184, Dow Corning) is sold as a kit consisting of a base and a curing agent. The base consists of the PDMS and a platinum-based catalyst that cures the elastomer by an organometallic crosslinking reaction. The PDMS is a polymer consisting of siloxane (molecule with alternating Si and O atoms) oligomers, terminated with vinyl groups (i.e. $H_2C{=}CHR$, with R the siloxane). Base and curing agent include crosslinking siloxane groups. In each molecule of the curing agent at least three silicon-hydride bonds are present. Mixing everything together lets the Si-H bonds of the curing agent react with the double bonds of the vinyl groups in the PDMS and a $Si\text{-}Ch_2\text{-}Ch_2\text{-}Si$ link is formed. Now a flexible, crosslinked, three dimensional matrix is formed. The curing process can be performed in an oven, it takes a minimum of four hours at 65 °C.

Table 2.3 Parameters for fabrication of PDMS pillars

process	*parameters*	*additional info*	*type / brand of product*
use a silicon wafer	Ø 100 mm		
cleaning	no cleaning		
dehydration	200 °C, 5 min	on a hotplate	
spin coating	10 sec 500 rpm + 30 sec 1750 rpm	4 ml, medium acceleration	Microchem SU-8 10
soft-baking	65 °C, 2 min 95 °C, 5 min	on a hotplate	
cutting	10 x 10 mm	cut with diamond and subsequent breaking	
exposure	4 - 5 sec		Karl Suss MJB 3 Maskaligner
post-bake	65 °C, 1 min 95 °C, 0.5 - 3 min	on a hotplate	
developing	0.5 - 6 min		Microchem SU-8 developer
rinsing		with isopropanol	
PDMS mixing and applying	10 : 1 (PDMS : cross linker)	poured on substrate with holes	Dow Corning
evacuating	2 h		
curing	65 °C, > 4 h	in a oven	
peel off			

For all three types of pillars the following remark needs to be made. In general, even when using the same production parameters, there is not an exact reproducibility possible of the pillar production. This holds even for experiments performed on the same day. Possible reasons for this could be changes in humidity and temperature of the working environment. However it is not quite clear how these effects influence the pillar formation. In other words the parameters printed here are just an indication. Even with parameters differing from these, good results are sometimes obtained. The three methods to produce pillar arrays are summarised in the tables in the respective paragraphs. A visualised scheme of the production process of all three methods is shown in figure 2.4.

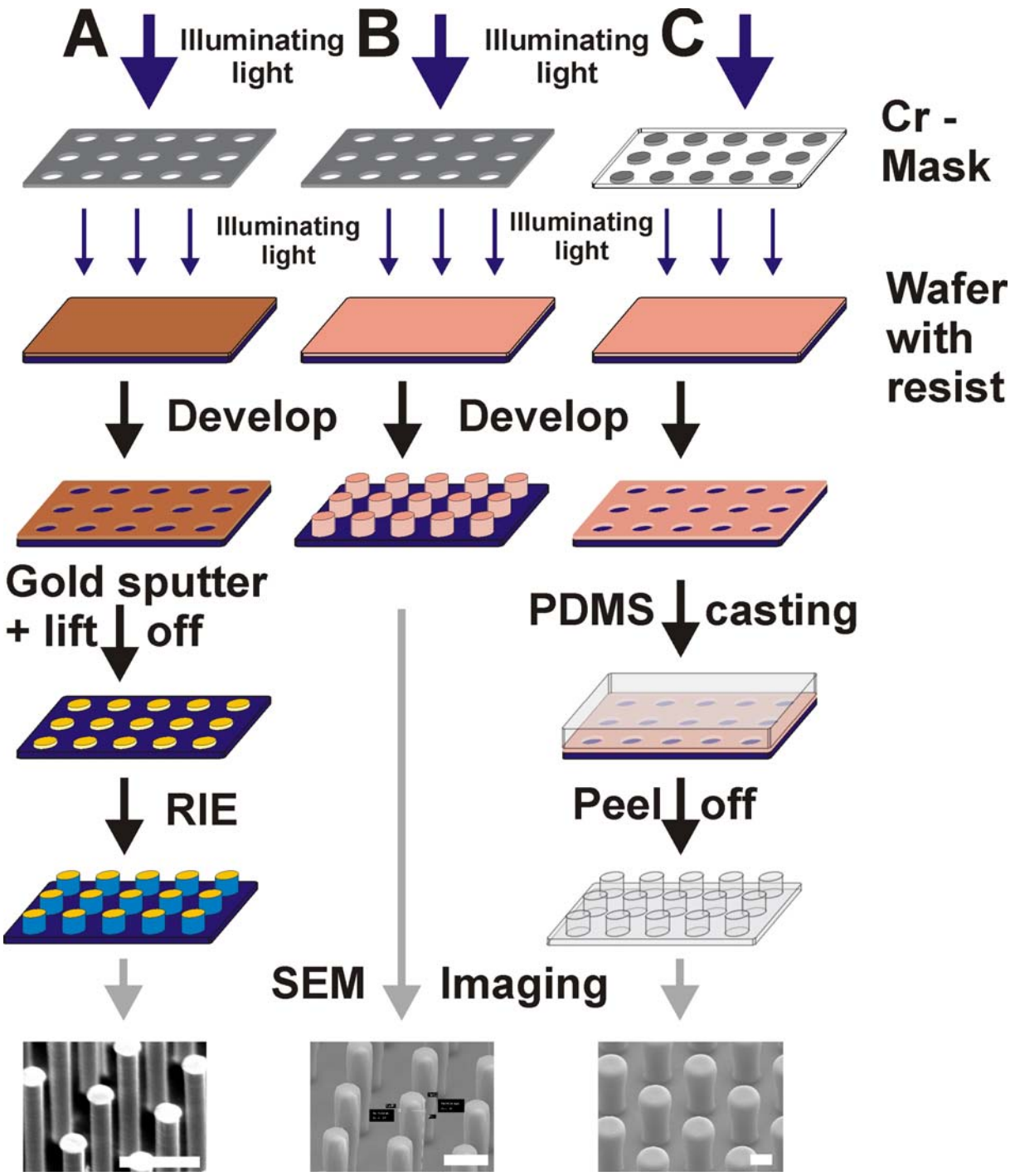

Fig. 2.4 Schematic view of three methods to produce microscopic pillar arrays. (A) A silicon wafer with a positive photo resist layer on top is illuminated through a chromium master-mask with holes in it. After a developing step, gold is sputtered on top and a lift-off is performed. Finally Reactive Ion Etching (RIE) results in silicon pillars with gold disks on top. (B) A silicon or glass slide is coated with a layer of negative photo resist and it is illuminated through a chromium master-mask with holes in it. After developing pillars of photo resist (epoxy) remain. (C) A silicon or glass slide with a layer of negative photo resist is illuminated through a chromium master-mask with disks on it. After developing holes remain in the resist and the PDMS mixture is poured onto this mask. Curing is performed at 65 °C and subsequently the PDMS pillars can be peeled off. The three images at the bottom show electron micrographs of the pillars at a 45° angle. Scale bar is 5 µm.

2.4.2 Gold caps on PDMS pillars

The precious metal gold is used in an approach to coat the PDMS pillars with a material that is easy to functionalise. The idea is to attach gold particles covalently to the pillar heads and to subsequently merge these particles by electroless plating. Two methods to attach the gold to the pillars are presented, of which the first one is successfully probed. A layer of 30 - 50 nm gold is sputtered onto a silicon wafer. Next, the previously described photolithography is performed with the wafer as template. Photo resist coated silicon wafer pieces with holes in the resist are obtained. The holes traverse the whole resist layer down to the gold layer. The substrates are incubated over night in a propene-thiol atmosphere under low pressure. The propene-thiol binds covalently to the gold and remains on the gold after evacuating the environment for two hours to remove the molecules that are not covalently bound. The PDMS is mixed with crosslinker and poured onto the substrate. The previously described reaction between the crosslinker and the vinyl groups of the PDMS results in an elastic material. Because the propene-thiol also has a vinyl-end, this molecule is incorporated in the crosslinked matrix as well. This means that there is a covalent bond between the PDMS and the gold on the silicon substrate. When the PDMS is now carefully removed from the mould, a gold coated pillar array is obtained.

The disadvantage of this method is that the moulds can only be used once. After peeling off the PDMS, the photo resist and the whole gold layer come of together with the PDMS. As a next step the photo resist layer needs to be peeled off mechanically and during this process the gold layer will break apart. The part of the gold that is covalently bound to the PDMS remains on the pillars, the rest stays on the photo resist. This photo resist layer can not be used again, because it normally breaks into pieces. This means that for every experiment new moulds need to be produced. The proposed second method will enable reusage of the moulds. Gold colloids, whose diameter can be tuned from 2.5 - 125 nm, will be prepared from $HAuCl_4$ solutions [Grabar *et al*., 1996]. These solutions are poured over the hole substrate and left to evaporate. The gold colloids will be pushed into the cavities due to the capillary forces during drying. After the sample has completely dried there are gold colloidal particles on the bottom of the holes. Now the previously described steps to bind propene-thiol to the gold can be performed. After pouring the PDMS onto the substrate and curing at 65 ºC, a crosslinked matrix, linked with the gold colloids, is formed. Subsequent removal of the PDMS should result in pillar arrays with gold colloids on the heads. In this case the photo resist will stay on the silicon, as it is usual. The resist-silicon adhesion is strong enough to ensure that the resist, with the holes, stays onto the silicon after peeling off of the PDMS. The mould can now be reused to deposit gold colloids and to make new PDMS pillars.

For both methods the gold particles on the pillar tops have to be merged to form a closed layer on every single pillar head. This can be done by electroless plating of gold, of which first results look promising. Meltzer *et al*. [2001] describes a method of hydroxylamine seeding of colloidal gold. By this method gold particle growth is induced by immersing the substrate for a few minutes in an aqueous solution containing 0.01% $HAuCl_4$ and 0.4 mM NH_2OH. The deposition is stopped by removing the sample and rinsing with water.

The advantage of having substrates with gold capped pillars is that thiol based biochemistry can be used to selectively functionalise the pillar heads. This is already successfully done with the gold capped silicon pillars. The rest of the substrate can then be passivated selectively and thus a well controlled system is obtained.

2.5 Calibrating the pillars

The pillars need to be calibrated to determine their stiffness. The easiest way is to measure the dimensions by electron microscopy and to use equation 2.1 to calculate the stiffness. Next to the dimensions of the pillars the E-modulus (Young's modulus) of the used material needs to be known for this calculation. For silicon and epoxy this can be looked up in literature [Schweitz, 1992; Lorenz *et al.*, 1997], for PDMS it depends on the ratio of cross linker to polymer and on the curing conditions. This means that the E-modulus needs to be measured experimentally. An easy experiment described by Pelham and Wang [1997] uses gravity. A rectangular beam of PDMS hangs down from a freely suspended anchor and the rest length l_0 is measured. Now a force F is applied by hanging a weight at the lower end of the PDMS and the elongation Δl is measured (fig. 2.5). The E-modulus E can now be calculated by [Landau and Lifshitz, 1991]

$$E = \frac{F / A}{\Delta l / l_0} \tag{2.2}$$

with the area A of the cross section of the PDMS beam. This formula is valid when the elastic material is subject to a small strain, which does not irreversibly change the material.

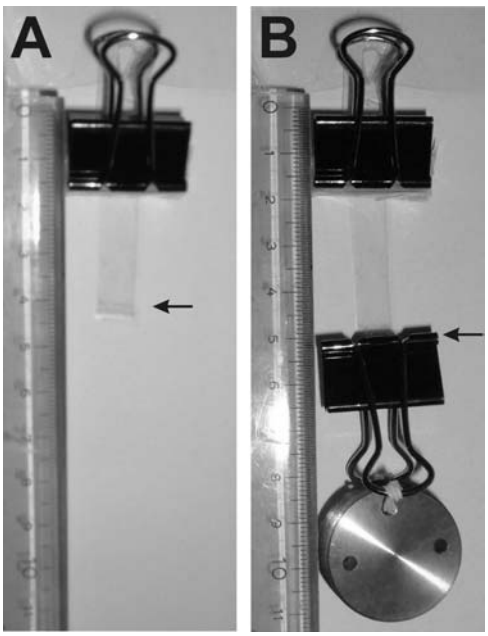

Fig. 2.5 E-modulus determination of PDMS. (A) Relaxed PDMS (B) Stretched PDMS under a force = 0.65 N. Arrows point to the part where the clamp is attached. Ruler from 0 - 11 cm on the left of each image.

Performing the experiments on beams of PDMS mixed with the crosslinker at a ratio of 10 : 1, cured overnight at 65 °C and left at room temperature for three weeks, leads to a

result of E = 1.2 ± 0.1 MPa (mean ± error, N=6). Here the mean $\bar{x}$ is calculated as an average of weighted measurements [Barlow, 1989]

$$\bar{x} = \frac{\sum x_i / \sigma_i^2}{\sum 1/\sigma_i^2} \tag{2.3}$$

with the individual measurements x_i having an error σ_i. The error is estimated during the measurements as the maximum likely difference from the measured value. The error σ in the mean is given by

$$\sigma = \sqrt{\frac{1}{\sum 1/\sigma_i^2}} \tag{2.4}$$

As an alternative approach to measure Young's modulus an apparatus consisting of two clamps, a spring scale and a micrometer positioning screw as described by Watari [2003] can be used. With this machine calibration experiments are performed with the same pieces of PDMS as used before. Comparing the results of both methods gives similar values, within the range of error of the measurements.

Further experiments are performed with PDMS cured at 65 °C for 4 hours and 24 hours respectively. Experiments are conducted directly after removal from the oven and after 7 days, where the samples are stored at room temperature in between. No significant difference is observed and the mean result is 8 ± 5 MPa (mean ± error, N=127). In this case the error is estimated by the standard deviation, which is plausible due to the large amount of data points. In the previous case N = 6 and the standard deviation could easily be biased, therefore the error is estimated by the estimated failure in the measurements.

The discrepancy between the two values (1.2 MPa and 8 MPa), might be explained by a differences in the PDMS to crosslinker ratio. A ratio of 10 : 1 is not exact and can therefore give rise to significant fluctuations. Further measurements are planned with commercial machines to obtain a better understanding of all the involved parameters. For all experiments it is advisable to make samples of flat PDMS for calibration purposes in parallel to the pillar substrates.

A method to measure the pillar stiffness directly uses a microplate with known stiffness to bend a single pillar [Watari, 2003]. The glass microplate is obtained by using a laser micropipet puller and it can be calibrated by using an AFM cantilever of known stiffness. Then a pillar can be bent and by analysing the displacement of the pillar head the stiffness can be found. The biggest source of error for this method is estimating the exact position of the microplate along the height of the pillar. Equation (2.1) shows that the stiffness of the pillars depends on the power 3 of the height of the pillar. As the pillars are used as a force sensor for forces applying to the pillar tops, it is important to calibrate to pillars at the pillar tops. Due to the limited z-resolution of the microscopy system used, this leads to a significant error in the calibration. Nevertheless, Watari's microplate measurements are comparable to the measurements obtained by measuring the E-modulus and the dimensions of the pillars and subsequently calculating the stiffness.

Comparison of the different pillar types

In table 2.4 the pillar stiffness for several types of pillars is given. On the left of the table the pillar material is written. In the successive columns the minimum radius r_{min}, the corresponding maximum length L_{max}, Young's modulus E and the resulting pillar stiffness k is given. The dimensions of the pillars are obtained from electron microscopy. Literature values are taken for Young's modulus of silicon [Schweitz, 1992], who published a table with references for thin silicon films oriented along the 100 and 110 direction and for polycrystalline silicon. There is a rather large spread in the values published by different groups. The only value for the 100 direction in this paper is taken here. For epoxy also literature values are taken [Lorenz *et al.*, 1997]. Young's modulus of PDMS is experimentally obtained as described before. In the last row pillars made from a new and promising material, crosslinked polyethylene glycol (PEG), are mentioned. These pillars have been made recently, but have not yet been used in experiments. The handling of these pillar arrays is not trivial, because the PEG can take up a significant amount of water. This means that drying of these pillars changes substantially their structure. The dimensions are estimates, because it is difficult to perform electron microscopy measurements with these substrates. Young's modulus is also estimated. Despite difficulties in handling the PEG, this material seems to be promising for force measurements.

Table 2.4 Pillar stiffness k for several pillar substrates

	r_{min} (μm)	L_{max} (μm)	E	k (N/m)
epoxy	1.3	15	4 GPa	9
silicon	0.3	15	131 GPa	0.7
PDMS	1.2	15	1 MPa	0.001
PEG*	3	15	1 kPa	0.00006

* *approximate values*

The different types of pillar arrays show big differences in flexibility. Below follows a summary with applications of the different arrays. The silicon, epoxy and PDMS pillars are used in a wide range of applications. Next to serving as a template for cell and filament adhesion, they are also used as force sensors. The pillar arrays are employed to measure contractile forces that play a role during fixation and drying of cells. These forces are not actively exerted by the cells, but they are a result of the shrinking of the cell during these treatments. Living cells consist for a significant part of water and when this water is removed during drying, the cell naturally contracts. The pillar arrays are not only used to study cell fixation and drying, they are also used to measure traction forces of living cells.

Table 2.5 gives a rough estimate of the range of forces in which the different types of pillar arrays can be used. Examples of what they are used for are shown in the following chapters. The PEG pillars are fabricated to study contracting filament networks where molecular motors provide the contractile forces. However, this application has not yet been probed on these pillars.

Table 2.5 Applications and relevant force regimes of different pillar types

	application	*range of forces*
silicon, epoxy	fixation and drying forces of cells	10 - 10000 nN
PDMS	traction forces of living cells	0.01 - 100 nN
PEG	dynamic filament-motor protein networks*	0.1 - 100 pN*

* *proposed application and estimated force range*

Acknowledgments:

Thanks to J. Konle (Daimler-Chrysler Ulm), S. Gräter, J. Ulmer and J. Raskatov (Universität Heidelberg), E. Arzt and F. Thiele (MPI Stuttgart) for help with the pillar preparation. A. Plettl (Universität Ulm) is thanked for support in the clean room.

Chapter 3

Biomimetics of the actin cytoskeleton

3.1 Introduction

Numerous chemo-mechanical processes of cells, such as pseudopod formation during cell locomotion [Stossel, 1993; Cunningham *et al*., 2001; Janmey, 2001a], the propulsion of Listeria bacteria in infected cells [Gerbal *et al.*, 2000] and the capping process preceding the engulfment of pathogens by macrophages during immunological responses [Bear *et al*., 2002; Maly *et al*., 2001], are mediated by the actin-based cytoskeleton. In quiescent cells, the actin cytoskeleton consists of a partially crosslinked network of actin filaments lying just below the cell membrane. It forms a several 100 nm thick shell, which is called the actin cortex. On the other hand, the activation of cells (e.g. of endothelial cells, lining the inner wall of blood vessels, by inflammation mimicking agents such as thrombin) often leads to the formation of actin bundles coexisting with the random actin network [Fenteany *et al*., 2000; Bausch *et al*., 2001]. Several families of actin manipulating proteins control the structure and viscoelastic properties of the actin cytoskeleton. These proteins include (i) sequestering molecules which control the fraction of polymerised actin, (ii) severing proteins which control the filament length and (iii) linker proteins mediating crosslinking between actin filaments and coupling of actin filaments to membranes.

Several studies of the structural reorganisation of the actin-based cytoskeleton during pseudopod formation [Svitkina and Borisy, 1999], centripetal contraction of endothelial cells by inflammational signals such as thrombins [Garcia and Schaphorst, 1995], or formation of focal contacts to stabilize cell adhesion [Geiger and Bershadsky, 2002; Balaban *et al.*, 2001] yielded insight into the regulation of the actin cytoskeleton by biochemical signaling. Micromechanical studies of cell membranes provided some information of the correlation between the viscoelastic behaviour of cells and the structure of the actin cortex [Bausch *et al.*, 1999]. These studies also provided insight in the role of the cytoskeleton for the generation of forces [Evans, 1993].

The quantitative interpretation of such studies, however, is hampered by the complex structure of the actin cortex and its coupling to the cell's plasma membrane. One strategy to overcome this problem is to design realistic in vitro models of the actin cortex, which allow

for controlling the network complexity and the consideration of theoretical investigations [Bowick *et al*., 2001; Lakes, 2001].

Since actin filaments in vitro exhibit contour lengths of 10 to 30 µm, the structure and molecular motions of single filaments within networks may be visualized through labelling with fluorescent chromophores or gold nanoparticles [Dichtl and Sackmann, 1999]. This allows for relating macroscopic viscoelastic moduli of actin gels to distinct motions and relaxation processes of single filaments [Howard, 2001]. Scaling laws can then be established which relate the cortex's macroscopic physical properties to characteristic length scales of the structure and dynamics of the network [Tempel *et al*., 1996].

Up to present most biophysical studies are performed with bulk in vitro models of the actin cytoskeleton [Humphrey *et al*., 2002; Janmey *et al.*, 1994; Helfer *et al*., 2001]. However, the physical properties and structural phase transitions (e.g. bundling) of such extended three dimensional networks are expected to differ from those of networks confined to a thin sheet (thickness small compared to the actin persistence length) of finite lateral extension [Bowick *et al.*, 2001].

Two-dimensional arrays of micro pillars open new possibilities to develop realistic models of the actin cortex [Roos *et al*., 2003]. Such locally surface grafted actin networks exhibit structural similarities with the actin cortex in cells. They can therefore be applied with other added proteins to study the adaptation of the cytoskeleton to external mechanical and biochemical stimulations. Self-assembly of freely suspended quasi two-dimensional actin networks that mimic biophysical, biochemical and structural properties of the intracellular actin cortex of cells can be achieved by using these microscopic pillar arrays.

3.2 Materials and methods

Proteins

Actin and all the actin binding proteins used, are provided by E. Sackmann (TU München). Actin is prepared from rabbit skeletal muscle as described by MacLean-Fletcher and Pollard [1980] and Pardee and Spudich [1982] with an additional purification step using gel column chromatography (Sephacryl S-300).

G-Actin is polymerised in a polymerisation buffer (table 3.1) for 20 minutes at room temperature or alternatively for 30 minutes on ice. The monomer concentration at the start of polymerisation is 5 µM (210 µg/ml). After polymerisation the actin is labelled with phalloidin-TRITC (Sigma) in an equimolar ratio of phalloidin-TRITC to G-actin. Phalloidin is a fungal toxin isolated from the poisonous mushroom *Amanita phalloides*. It only binds to actin in the filamentous form, while it does not bind to actin monomers. By binding, it stabilises actin filaments. The resulting F-actin can no longer depolymerise. A further advantage of this labelling is that fluorescent visualisation of the F-actin is possible due to the fluorescent dye TRITC, which is conjugated to the phalloidin.

The composition of the buffer solution used for diluting F-actin is also described in table 3.1. As an oxygen scavenger, 1 mM DTT, 2.3 mg/ml glucose, 0.1 mg/ml glucose-oxidase and 0.02 mg/ml catalase are added just before use. The water is degassed in an ultrasonic bath for 5 minutes. The undiluted polymerised actin can be used in experiments for one up to two weeks.

Table 3.1 Actin buffers

Actin polymerisation buffer		*Actin dilution buffer*	
TRIS	2 mM	Imidazol	25 mM
$MgCl_2$	2 mM	EGTA	1 mM
KCl	100 mM	$MgCl_2$	4 mM
$CaCl_2$	0.2 mM	KCl	25 mM
DTT	0.2 mM		
ATP	0.5 mM		
pH = 7.4		pH = 7.4	

Myosin II and HMM is prepared following the procedure of Margossian and Lowey [1982] with additional modifications as described by Hynes *et al*. [1987]. N-ethylmaleimide modified heavy meromyosin (NEMHMM) is prepared as described by Cande [1986]. Filamin is purified from chicken gizzard as described by Shizuta *et al*. [1976]. Myosin V is abundant in neural tissue and is therefore purified from chick brain following the procedure of Cheney [1998] with additional modifications as described by Zhang [2004]. Monoclonal antibodies against myosin V are obtained from cell lines following the procedure described by Zhang [2004].

Myosin II is fluorescently labelled with 5-iodoacetamidofluorescein (5-IAF) a dye from Molecular probes (Invitrogen, Breda, Netherlands). This is a thiol-reactive reagent which binds to myosin II. DeBiasio *et al.* [1988] showed that this labelled myosin is still active. The protocol to label the myosin is similar to the one provided by Molecular probes. The buffer solution is the same as for F-actin dilution, but additionally containing 600 mM KCl. Myosin is diluted to 2 nM and 300 µl of this solution is mixed with 25 µl of 250 nM 5-IAF. In this mixture the dye is ten times as concentrated as the myosin. The mixture is incubated overnight at 4 °C. A molar excess volume, compared to the dye, of DTT is added to consume excess dye. This solution is spun a few times in a Micron YM-100 100 kDa centrifugal filter (Millipore) to remove excess dye. The part of the solution which does not pass the filter contains the labelled myosin II. The labelled myosin is diluted to a volume of 80 µl.

The buffer solution for diluting the NEMHMM and filamin is the same as for F-actin dilution. Myosin II is diluted in the same buffer, except for the concentration of KCl. The KCl concentration in the myosin buffer needs to be below 0.3 M to obtain filaments and above 0.3 M to obtain single myosin II dimers [Margossian and Lowey, 1982]. The myosin V motility assay is performed in the actin dilution buffer with additional 1 mM ATP.

Flow cell protocol

The gold disks on top of the silicon pillars are chemically modified by self-assembling alkanethiol monolayers (CH_3-$(CH_2)_{17}$-SH) [Mrkisch *et al*., 1997] to render them hydrophobic. The pillars are incubated in a 2 mM solution of octadecanethiol (Sigma-Aldrich) in ethanol for 12 hours. After rinsing with ethanol they are dried under a nitrogen stream. The flow cell is built on a cover slip with double sticky tape (50 µm thick) as a spacer. The prepared hydrophobic surfaces serve the adsorption of NEMHMM.

This is done by immersing the substrates into a buffer solution containing 5 µM NEMHMM. After adsorbing NEMHMM, the substrate is treated with a 250 µM BSA buffer solution to prevent unspecific binding of actin to hydrophobic Au-disks. Actin oligomers (obtained by mechanically shredding F-actin by pulling the solution up and down several times in a pipette) are then grafted to the pillar tops through the inactive myosin fragments. These oligomers act as seeds for actin polymerisation. To initiate prolongation of the filament's fast growing end, 1.25 µM G-actin in polymerisation buffer is added to the measuring chamber. After a polymerisation time of 10 minutes, the actin is fluorescently labelled and stabilised by the addition of TRITC-Phalloidin.

Finally crosslinking is initiated by addition of filamin ([filamin] = 500 nM), myosin II ([myosin II] = 400 nM and [KCl] = 200 mM) or divalent cations (for instance [Mg^{2+}] = 80 mM). The protocol for the epoxy and PDMS pillars is similar. The difference is that the NEMHMM is directly physisorbed on top of the pillars. That is done either via stamping of NEMHMM by putting a droplet on top of the pillars or by immersing the whole substrate in the NEMHMM solution.

Microscopy

A Zeiss Axiovert 200 microscope with a 100x Plan-Neofluar oil immersion and a 40x C-Apochromat water immersion objective is used. Either the normal fluorescence mode or the confocal microscopy mode (Zeiss, LSM 5 Pascal) is used. The images are recorded with a Hamamatsu Orca-ER camera, which has a maximum acquisition rate of 50 Hz. Experiments are performed at ambient conditions.

3.3 Freely suspended actin cortex models on pillars

Pillar arrays are microfabricated from silicon substrates, epoxy-based polymers or PDMS as described in chapter 2. The micropillars exhibit a minimum diameter of 1 µm and a height of 15 µm with a lattice spacing of 5 or 7.5 µm. Actin filaments are grafted to the tops of the pillars and consequently crosslinked by actin binding proteins, or divalent cations. Due to the height of the fabricated pillars (comparable to the actin filament contour length) physisorption of the filaments to a solid surface between the pillars is impeded. Additionally, the discrete nature of the pillar substrate allows for mimicking the point-like membrane anchoring of actin characteristic for the situation in cells (e.g. in focal complexes). It is demonstrated that the local anchoring of the actin filaments results in self-assembly of networks the structure of which is determined by the arrangement of the pillars.

Actin binding and crosslinking proteins are responsible for the formation of actin bundles and networks in cells. Looking at an electron micrograph of a fixed cell of which the membrane is removed, one can see the actin bundles and the seemingly random actin network, which is present in cells [Lodish *et al*., 1999; Svitkina *et al*., 1995]. Both bundles and networks serve as a supporting framework for the plasma membrane. The actin filaments in bundles are closely packed and aligned parallel to each other. In the network they form angles of various degrees to each other and they are loosely packed. Two types of actin networks are present in cells [Lodish *et al.*, 1999]. A three dimensional one, which gives the cytosol gel-like properties and a locally quasi two dimensional network associated with the

plasma membrane. The term locally refers to the fact that the plasma membrane is all around the cell, hence it must be three dimensional. However, locally it can be regarded as two dimensional. To be more precise, quasi two dimensional, because the network has a finite thickness. For a physicist a two dimensional network means that it has zero thickness. The actin network that is associated with the cell membrane, can be spread over several tens of micrometers, but its thickness is about 200 nm. This thickness is almost negligible compared to the lateral extensions of the network and therefore one can speak from a quasi two dimensional network.

The quasi two dimensional actin networks are made by crosslinking the actin filaments with actin binding proteins or with divalent cations. Actin binding proteins can be divided into passive and active proteins. The active binding proteins are the myosin molecular motors. Myosin II can bind to F-actin and is released after performing a force stroke. Subsequently the myosin can bind again. When no ATP is present the myosin binds, but does not release anymore, because there is no energy to perform the force stroke. So without ATP myosin is essentially a passive actin binding protein.

To form actin crosslinks the binding proteins need to bind to two actin filaments. Not all actin binding proteins possess two binding pockets for actin. For instance CapZ and tropomodulin are actin capping proteins that bind to actin extremities to inhibit polymerisation and depolymerisation. These proteins can not make crosslinks of actin filaments. In the study presented here no such proteins are discussed. Only proteins that have two actin binding domains and hence can make crosslinks between actin filaments, are of relevance here. Myosin II can act as an actin crosslinker when it is present in the filamentous state, i.e. at low salt concentrations. At [KCl] > 0.3 M the myosin II is present as a dimer and is difficult to use as crosslinker.

Examples of passive actin binding proteins are for instance filamin, α-actinin and spectrin. These actin crosslinking proteins belong to the calponin-homology-domain superfamily [Lodish *et al*., 1999]. Such proteins have a pair of actin binding sites, whose sequence is homologous to calponin, a muscle protein. The actin binding domains in these proteins are linked by repeated helical coiled-coil or β-sheet motifs. One of the shortest of the calponin-homology-domain binding proteins is α-actinin, a protein which is found in actin bundles that are present in filopodial extensions. Filamin and spectrin are among the longest actin crosslinking proteins. They are found in the actin networks that are associated with the plasma membrane. In the next section quasi two dimensional actin networks that are crosslinked by filamin will be discussed.

3.3.1 Crosslinking by filamin

Figure 3.1 A shows a fluorescence image of actin filaments in buffer solution, which are grown from the top of single silicon pillars. The filaments are firmly bound to the tops of the pillars by one of their ends. The other end is extending into the bulk of the sample, out of the focal plane of the objective. These filaments show strong spatial fluctuations due to thermally induced motion. This motion is much faster than the shortest exposure time of the camera, such that the dangling end of filaments bound with one end to pillar tops can only be seen as a blurred background in figure 3.1 A. However, several filaments are attached to two or more pillars (arrows and inset in figure 3.1 A). The contour of these filaments can be focused well.

To generate these hair-like assemblies of dangling actin filaments with defined polarity on the pillars, the hydrophobic gold disks are used to physisorbe inactivated myosin fragments (NEMHMM). Actin oligomers are then grafted to the pillar tops and further polymerisation of the seeds is induced by addition of G-actin. Due to the lag phase of F-actin seed polymerisation, the relatively low G-actin concentration used in these experiments delayed spontaneous actin polymerisation in the bulk. The prolongation of the surface grafted oligomers has no lag phase [Ruddies *et al*., 1993; Engel *et al*., 1977]. Since the bulk solution is depleted of G-actin during the growth of the surface grafted filaments, actin polymerisation in the bulk or between the pillars is completely inhibited. The actin is fluorescently labelled and stabilised after polymerisation.

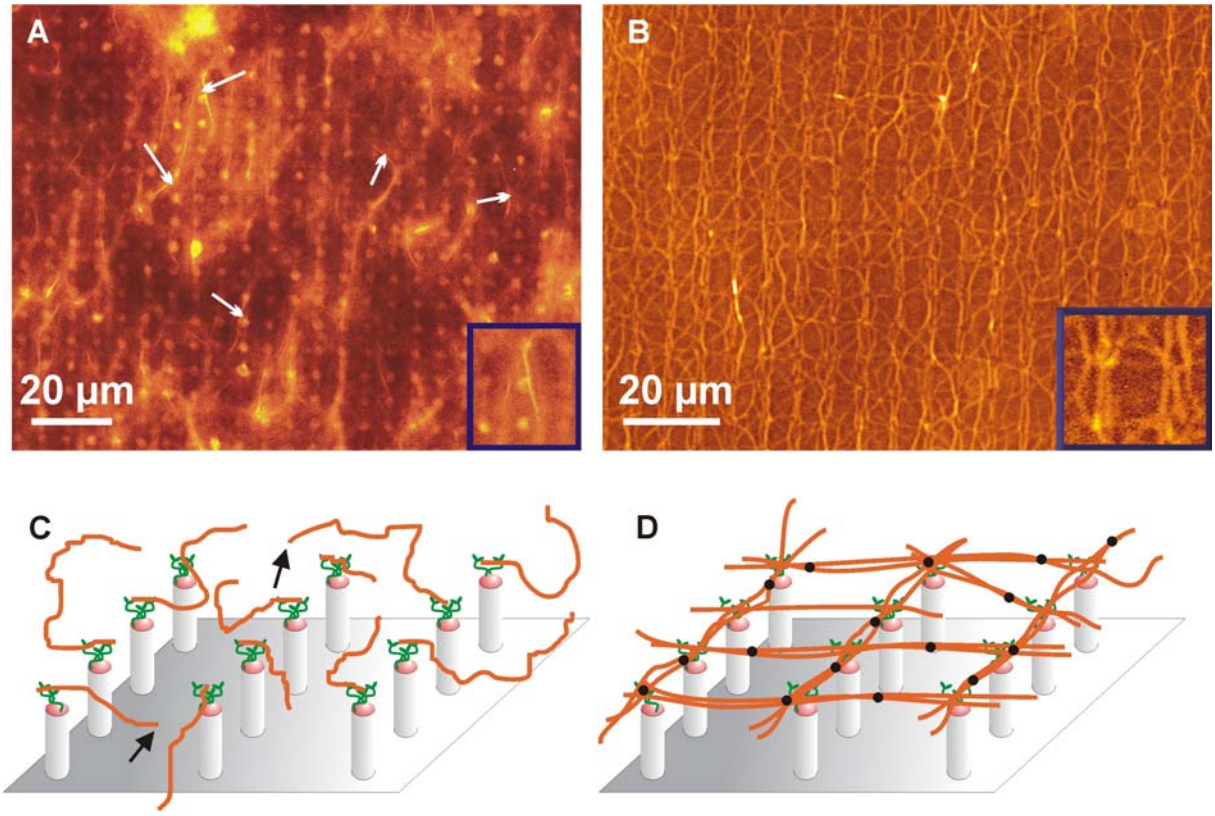

Fig. 3.1 Assembly of a freely suspended actin cortex. (A) Fluorescent microscopy image of actin filaments on top of silicon pillars. Note that only filaments fixed to more than one pillar can be seen as well focused strings (some are indicated by arrows and shown in the inset). The fast growing end of filaments which are only fixed to one top of a pillar are freely dangling in the bulk of the sample. These filament ends are sometimes out of the focal plane and move too fast to be captured by the camera. The image shown is taken 15 minutes after the beginning of polymerisation. The filaments exhibit a preferred orientation in the vertical direction due to the hydrodynamic flow used to incubate the bulk solution with various agents. (B) Fluorescent micrograph of a two-dimensional network of actin bundles. This pillar-grafted, quasi two-dimensional actin network, is formed by injecting filamin (500 nM) into the chamber that contained the substrate with the dangling filaments. The image is taken 5 minutes after the addition of filamin. Here, filaments are bundled and attached to the pillar tops, which reduces their thermal fluctuations to an extent that sharp images of their contour are obtained. (C) Schematic view of dangling actin filaments (fig. 3.1 A). The loose ends of the actin filaments can move freely in solution. Arrows are pointing at two of these free ends. (D) Schematic view of freely suspended 2-dimensional actin network (fig. 3. 1 B), generated by crosslinking F-actin by filamin.

When filamin (a dimeric actin binding protein with a fork-like structure known to favor F-actin coupling [Nakamura *et al.*, 2002; Janmey *et al.*, 2001b, Stossel *et al.*, 2001]) is injected into the liquid chamber, the formation of a 2-dimensional network of actin bundles is observed (Figure 3.1 B). Apparently, the formation of an orthogonal network on the pillar substrate is initiated by crosslinking the highly mobile dangling ends of actin filaments in the bulk. Further crosslinking resulted in the complete confinement of the actin network to the plane defined by the pillars tops. Remarkably, the network of fiber bundles assumes a predominantly orthogonal structure correlated with the pillar array. However, also diagonal bridging of the tops of the pillars is observed. The micro-network of actin bundles is extended over several millimeters of the pillar substrate with the structural quality shown in figure 3.1 B. The structure of the spontaneously formed quasi two-dimensional network exhibits a similarity with the network formed in cells by arrays of focal contacts [Geiger and Bershadsky, 2002; Balaban *et al.*, 2001]. Figure 3.1 C and figure 3.1 D summarise schematically the observations of actin organisation on pillar substrates.

A similar experiment is performed on "flat" surfaces covered with two-dimensional arrays of 25 nm thick circular gold disks of 2 µm diameter. The gold disks are functionalised with alkane thiols and NEMHMM. Experiments are performed with substrates which are passivated between the gold disks by polyethylene glycol molecules (CH_3-(CH_2-CH_2-O)$_{17}$-O-C=O-NH-CH_2-CH_2-CH_2-Si(OEt)$_3$) [Arnold *et al.*, 2004] to minimise non-specific actin adsorption. Only an ill-defined network is formed on this sample, even when filamin is added. This is attributed to the presence of a stiff boundary causing non-specific surface interaction of the actin filaments, demonstrating the different behavior of freely suspended and surface interacting actin filaments.

Experiments are also performed to produce actin networks on pillar arrays with different gap sizes. The formation of these networks is only possible when the interpillar distance is not too large. In figure 3.2 a Z-stack of confocal microscopy images is shown of a two dimensional network of actin filaments on top of PDMS pillars that have a spacing of 5 µm. Some pillars, however, are spaced by 15 µm and it can be seen that no actin network is formed on top of these widely spaced pillars. At such wide gaps the actin filaments are not located on top of the pillars anymore, but they lie in between the pillars, near the bottom surface. The average length of polymerised actin filaments is 20 to 30 µm whereas the persistence length is only 15 µm. Therefore the persistence length might be a limiting factor that prevents the formation of stable networks for large interpillar spacings.

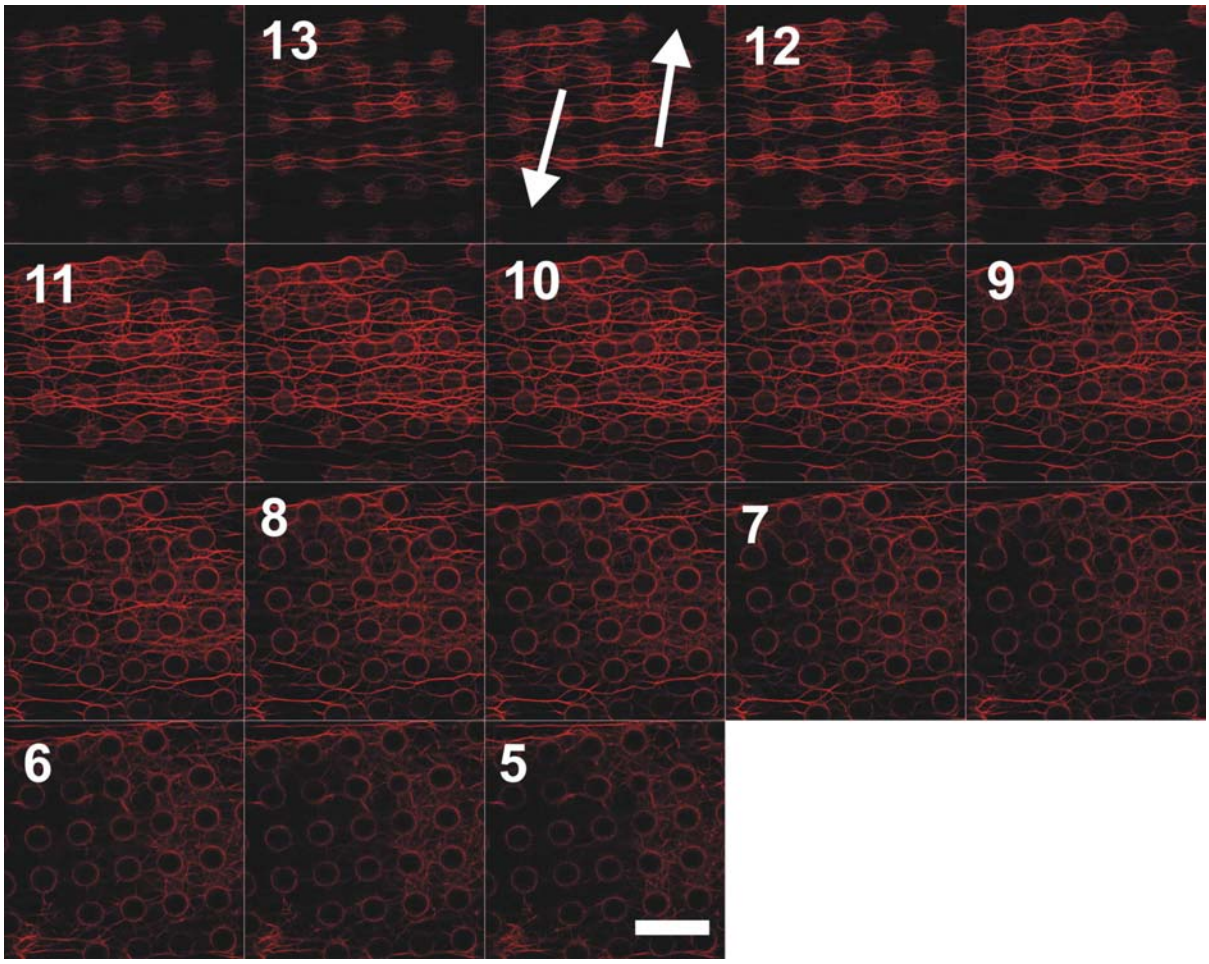

Fig. 3.2 Confocal microscopy images of TRITC- labelled actin network on PDMS pillars. The actin filaments are crosslinked by the actin binding protein filamin (500 nM). Z-stacks are taken with 0.5 µm intervals. The distance from the bottom of the pillar substrate is written in every second image in units of µm. In the middle of the substrate the interpillar spacing is 5 µm. It can be seen that the network forms mainly on top of these pillars instead of between them. The white arrows point to two parts of the substrate where the interpillar gap is 15 µm. These pillars are too far apart from each other to act as a template for forming a two-dimensional actin network on top. In this case, the network forms predominantly close to the bottom of the pillar substrate that offers mechanical support for the actin filaments. Scale bar 20 µm.

3.3.2 Crosslinking by fluorescent myosin II

Not only passive binding proteins like filamin are used for crosslinking. Also active actin binding proteins can crosslink actin filaments on top of pillar substrates. The active binding proteins used, are myosin II molecular motors. These molecular motors form small filaments at KCl concentrations of about 200 mM. Every myosin filament has multiple myosin heads that can bind to several actin filaments and serve as crosslinkers. To observe the specific binding of the myosin II to the F-actin, myosin labelled with fluorescein, a fluorescent dye, is used. Figure 3.3 shows a pillar substrate with actin filaments that are crosslinked by myosin II. It is observed that the actin filaments and the myosin are

colocalised. During control experiments with fluorescent actin, but with non-fluorescent myosin, a fluorescent signal in the fluorescein range is absent. Therefore, it can be concluded that the fluorescence, which can be observed in figure 3.3 B, is coming from the fluorescein labelled myosin.

Myosin in buffer solution without ATP can bind to actin filaments, but they can not detach. In this case myosin acts as a passive crosslinker. The result is that the myosin-actin networks without ATP are similar to the networks formed by filamin. However, the myosin crosslinked networks can also be decrosslinked, which is not possible for filamin crosslinked networks. At the end of this chapter an example of decrosslinking of myosin-actin by ATP is presented.

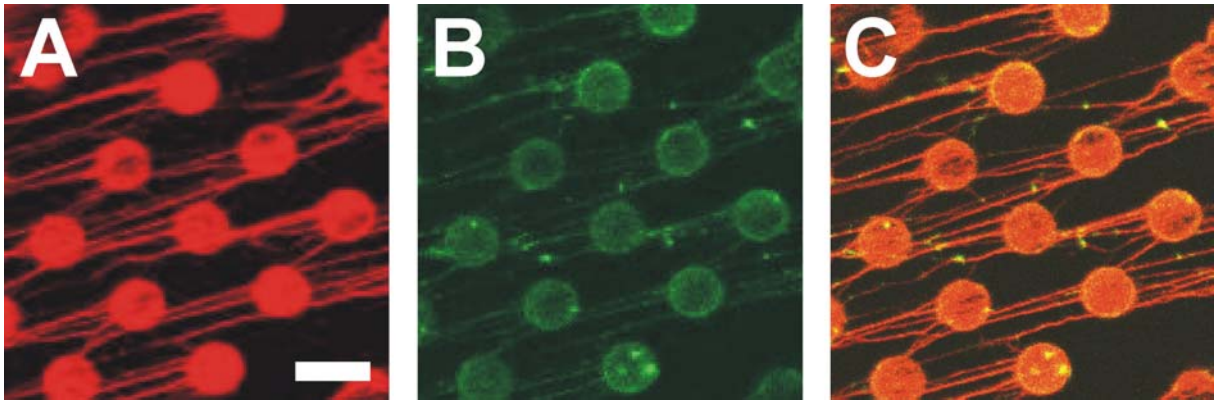

Fig. 3.3 Actin crosslinked by fluorescent myosin on PDMS pillars. The actin flows into the flow chamber in the filamentous form. (A) The TRITC channel shows the fluorescently labelled actin filaments. (B) The fluorescein channel shows the fluorescently labelled myosin II. (C) In this image the pictures of both channels are put on top of each other. A correlation between the position of the actin filaments and that of the myosin is observed. [Actin] = 50 nM, [Myosin] = 400 nM, [KCl] = 200 mM. Confocal microscopy image, scale bar 10 µm.

3.4 Myosin V motility assay on actin networks

Another intriguing application of the pillar device is to study the transport of particles by processive motor proteins on freely suspended self-assembled two-dimensional actin networks. This allows to mimic the transport of cellular compartments on the interface between the actin cortex and the cytoplasm. A typical movement of a myosin V coated bead is presented in figure 3.4, where in a section of the actin network around four pillars one bead is moving along the network from one pillar to the next.

Overall many tens of myosin V coated beads move simultaneously for several micrometers on the 2-dimensional actin-filament network before they unbind from the actin track. The analysis of 47 moving beads with single particle tracking techniques shows an average velocity of 330 nm/s ± 50 nm/s. This velocity is comparable to the results of Mehta *et al*. [1999] who performed actin gliding assays over myosin V coated surfaces. Since the network can be treated with controlling agents, myosin mediated transport in complex actin cortex like networks can be studied under controlled biochemical and structural boundary conditions.

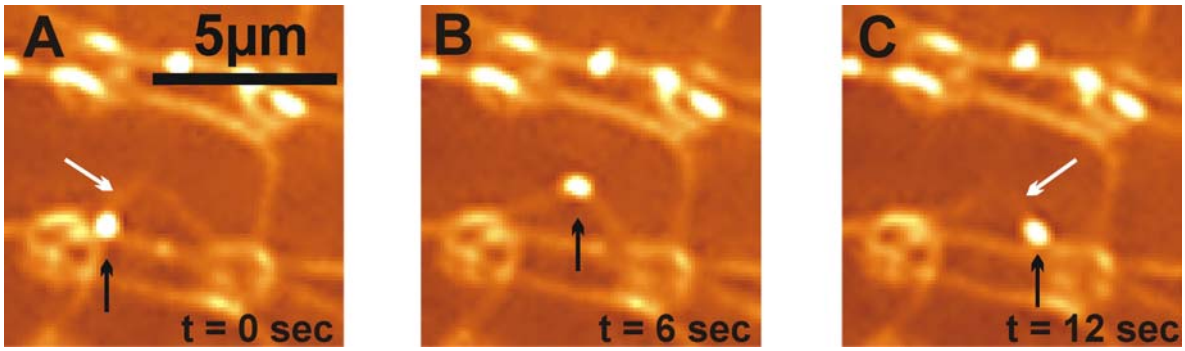

Fig. 3.4 (A-C) 40 nm fluorescent polystyrene, carboxyl-terminated beads are coated with Protein A and subsequently with monoclonal antibodies. The antibodies bind to the actin associated processive motor myosin-V, which is the last reagent to be added to adhere onto the beads. In the presence of 2 mM ATP, a large number of beads are observed to simultaneously move along an actin network structure as shown in figure 3.1 B. The black arrow indicates the location of a bead moving on an actin filament (white arrow), extending diagonally between two pillar tops. At the intersection with another filament, the bead apparently changes its track and continues along on this filament (white arrow). The average velocity of this bead is determined with single particle tracking to be 273 nm/s (± 2nm/s).

3.5 Single filament fluctuations

3.5.1 General considerations

While the physical theory of highly flexible chain molecules is comparably well understood, the statistical mechanics of semiflexible chain molecules has received some attention lately, as several problems remain unresolved [Wilhelm and Frey, 1996]. The rigidity of a polymer can be described by its persistence length l_p. The persistence length is a measure for the correlation of the movement of two segments on a chain a distance s apart, where s is the arc length along the chain. For $s \leq l_p$ the movements of the two segments are said to be correlated. The movements become uncorrelated for $s \geq l_p$. For synthetic polymers, l_p is normally on the order of a few nanometer. Such polymers can be classified as freely jointed chains [Frey, 2002]. Semiflexible polymers normally have a persistence length comparable to their contour length. Values for l_p of actin reported in literature range from 0.1 µm to 21 µm. As the length of in vitro polymerised actin can be around 50 µm, this polymer can be classified as a semiflexible chain. A corresponding model for semiflexible polymers, which takes into account the bending stiffness of the polymer and which supposes inextensibility is the Kratky-Porod model, also called the wormlike chain model [Doi and Edwards, 1986; Harris and Hearst, 1966; Wilhelm and Frey, 1996].

The persistence length is proportional to the bending stiffness, also called flexural rigidity. The bending stiffness κ is sometimes denoted as EI, where E is Young's modulus, or the elastic modulus and I is the geometrical moment of inertia of the cross-section. When I is known, Young's modulus of actin can be calculated as it is a common parameter for bulk materials. The problem is that I can not be determined precisely because F-actin is not a

homogeneous cylindrical rod. The filaments are better described as two-stranded helical polymers of the protein actin, with a helix periodicity of 36 nm [Lodish *et al.*, 1999]. The cross-section of F-actin can be modelled as an ellipse with major and minor radii of 3 and 2 nm respectively, yielding a cross-sectional area of 19 nm^2 (effective radius r of 2.4 nm) [Gittes *et al.*, 1993]. With these assumptions and $I = \pi r^4/4$ [Landau and Lifshitz, 1991, p83], Young's modulus can be determined from the bending stiffness.

3.5.2 Literature overview

The persistence length of actin is measured by a variety of techniques. Fujime [1970] performed quasi-elastic light scattering experiments on solutions of actin and found l_p = 4-12 µm. Götter *et al.* [1996] characterised semidilute actin solutions, also by quasi-elastic light scattering. They measured the bending stiffness of actin with and without tropomyosin-troponin complexes bound to it. For actin without the complex, a value for l_p of 2 µm is found. A note is written in the publication that the technique is not optimised for determining absolute values, but more for revealing relative changes in the stiffness. The applied technique is described in more detail by Schmidt *et al.* [1989]. Müller *et al.* [1991] employed oscillating disk rheometry to probe actin solutions and found l_p = 0.1-0.3 µm.

The techniques described above are applied to bulk solutions of actin filaments. So the persistence length is determined by a procedure that leads to a result which is an averaged value over the whole actin solution. Below techniques that target single filaments are presented.

Takebayashi *et al.* [1977] looked at dried actin filaments under the electron microscope and supposed that the filaments on the mesh sheet keep the shape they have in solution. From these images they measured the end-to-end distance and calculated l_p = 6.3 ± 0.8 µm. Yanagida *et al.* [1984] measured the end-to-end distance of single actin filaments in solution with and without myosin and with and without tropomyosin-troponin complexes in the presence and absence of Ca^{2+} and ATP. The persistence length of bare actin filaments is determined to be 16 µm. Käs *et al.* [1994] analysed the end-to-end distance of single fluorescent filaments in a bulk of non-fluorescent filaments and found l_p = 4 ± 1 µm. Le Goff *et al.* [2002] measured the end-to-end distance of filaments labelled with short fluorescent tags at the extremities in a 1 µm thick chamber. They found l_p = 16.1 ± 0.1 µm.

Ott *et al.* [1993] recorded the Brownian movement of single flickering filaments confined to a cell of height ~1 µm. By calculating the "cosine correlation function" (eq. 3.2) they found l_p = 16.7 ± 0.2 µm. Gittes *et al.* [1993] observed single filament flickering in a cell of height < 3 µm, performed a mode analysis and found l_p = 17.7 ± 1.1 µm.

A microneedle approach was used by Kojima *et al.* [1994] to measure the stiffness of single actin filaments with and without tropomyosin. The filaments are attached via myosin to a stiff needle on one side and to a flexible glass needle on the other side. A sinosoidal force is applied to stretch the filament. Combined with micromanipulators and a microscope they are able to determine l_p = 21 µm for the bare filament with this set-up. Dupuis *et al.* [1997] optically trapped monomeric myosin coated polystyrene 1 µm diameter beads with an actin filament in between them. Knowing the trap stiffness they displaced one of the beads and observed the force it underlies due to the stretched filament. Considering a possible exerted torque on the beads they found l_p = 4 µm. In a different approach Riveline *et al.* [1997] covalently attached 1 µm diameter polystyrene beads to F-actin via carbodiimide and anti-

actin antibodies. The filaments are oscillated in a direction perpendicular to their long axis by an optical tweezer. In this way the bending stiffness is probed under influence of external forces and viscous drag and they determined $l_p = 7.4 \pm 0.2$ µm.

In the following a technique is described, based on the known mode analysis, to determine the bending stiffness of actin with novel boundary conditions for the filaments.

3.5.3 Determining the persistence length by mode analysis

Because of the well-defined boundary conditions of the pillar substrate, this technique offers excellent possibilities of precisely measuring the elastic properties of individual actin filaments fixed at both ends. This is done by Fourier analysis of thermal bending fluctuations. Since the silicon devices reflect the excitation light strongly, the fluorescence images are too blurred to analyse shape fluctuations. This problem is overcome by the use of an epoxy resin instead of silicon as pillar material (fig. 3.5 A). Since the epoxy pillar heads are not covered by gold, single actin filaments are coupled to the pillar heads through NEMHMM physisorbed to the substrate. After passivating the rest of the substrate with BSA a 100 nM solution of fluorescently labelled actin filaments is flowed into the flow cell. After 5 min the unbound filaments are washed out. The projection of the momentary contour of a fluctuating filament can be reconstructed by recording the fluorescence intensity distribution along sections perpendicular to the straight line between the attachment points on the pillars (denoted as x-axis in figure 3.5 B). The distribution of each section is fitted by a Gaussian function, the maximum of which defines the local deflection $y(x_i)$ of the filament at position x_i.

The filament undulations of a wormlike chain are determined by the bending elastic energy E_b, which is a path integral over the squared curvature weighted by the bending stiffness κ [Landau and Lifshitz, 1991, p87]

$$E_b = \frac{\kappa}{2} \cdot \int_0^l \left(\frac{\partial^2 y}{\partial x^2} \right)^2 \cdot dx \qquad (3.1)$$

where l is the length of the filament[1]. The persistence length l_p of a semiflexible filament is defined over the correlation of the tangent vectors $\vec{t}(s)$ along the filament contour s [Doi and Edwards, 1986, p317; Wilhelm and Frey, 1996]

$$< \vec{t}(s) \bullet \vec{t}(s') >= \exp(-|s - s'| / l_p) \qquad (3.2)$$

[1] A more rigorous analysis would require to account for the internal tension τ of the filament due to the extension. The free elastic energy then becomes [Landau and Lifschitz, 1991, p100]

$$E_b = \frac{1}{2} \cdot \int_0^l \left[\kappa \left(\frac{\partial^2 y}{\partial x^2} \right)^2 + \tau \left(\frac{\partial y}{\partial x} \right)^2 \right] \cdot dx$$

Due to the small amplitudes of the oscillations in our experiments, the tension term leads only to a correction of less than 2% and will be neglected.

with (s - s') the arc distance between the two observed points. This function decays exponentially, where the characteristic length is the persistence length

$$l_p = \kappa / k_b T \tag{3.3}$$

with the Boltzmann constant k_b and the absolute temperature T. This equation can be found by writing down the partition function for finding a particular tangent at time t given the tangent at time 0 and explicitly calculating the correlation function (eq. 3.2) with equation 3.1.

Neglecting filament stretching and following previously reported procedures [Gittes *et al.*, 1993] the bending modulus can be determined by Fourier analysis of the bending undulations in terms of eigenmodes of excitation and application of the equipartition theorem. The deflection of the filament is expressed as

$$y(x,t) = \sum_j u(q_j, t) \cdot e^{iq_j x} \tag{3.4}$$

where $u(q_j,t)$ is the amplitude of the eigenmode with wavevector q_j. The equipartition theorem in statistical physics states that all independent degrees of freedom contribute a value of ½ $k_b T$ to the total energy [Landau and Lifshitz, 1987, §44]. As the modes of fluctuation are independent, any mode can be used, together with the equipartition theorem, to calculate κ from equation 3.1.

The equation of motion for transverse waves in thin rods is given by [Landau and Lifshitz, 1991, p124]

$$\frac{\partial^4 y}{\partial x^4} = -C\ddot{y} \tag{3.5}$$

with a constant C and where the dots denote the second derivative with respect to time. Inserting

$$y = y_j(x)cos(\omega t+\alpha) \tag{3.6}$$

into equation (3.5) yields

$$\frac{\partial^4 y_j}{\partial x^4} = q_j^4 y_j \tag{3.7}$$

with $q_j^4 = \omega^2 C$. For a general solution to equation 3.7, where successive derivatives vanish at the boundaries, a solution can not just be constructed from the familiar sum of sin's and cos's from Fourier space [Wiggins *et al.*, 1998]. The solution is found when hyperbolic trigonometric functions are included. A general solution to equation 3.7 is [Landau and Lifshitz, 1991, problem 4, p125]

$$y_j = A_1\cos(q_j \cdot x) + A_2\sin(q_j \cdot x) + A_3\cosh(q_j \cdot x) + A_4\sinh(q_j \cdot x) \tag{3.8}$$

Furthermore $y(x,t)$ must fulfil the boundary conditions

$$y\,(0,t) = y\,(l,t) = y'\,(0,t) = y'\,(l,t) = 0 \tag{3.9}$$

where the prime denotes the derivative with respect to x. The boundary conditions are determined by the fact that the filaments are fixed at several points at their ends to the pillar tops and thus do not exhibit an angular degree of freedom. By considering the filaments as homogeneous, freely undulating, clamped rods, above written boundary conditions need to be fulfilled and the wave vectors q_j of the eigenmodes are determined by

$$\cos(q_j \cdot l) \cdot \cosh(q_j \cdot l) = 1 \tag{3.10}$$

For large q_j the solutions of equation 3.10 resemble the familiar solutions of $\cos(q_j \cdot l) = 0$. Only for small q_j there is a significant deviation to these solutions. The eigenmodes themselves may be expressed as

$$y_j(x,t) = A_j(t)\ \{(\sin(q_j \cdot l)-\sinh(q_j \cdot l))\cdot(\cos(q_j \cdot x)-$$

$$\cosh(q_j \cdot x))-(\cos(q_j \cdot l)-\cosh(q_j \cdot l))\cdot(\sin(q_j \cdot x)-\sinh(q_j \cdot x))\} \tag{3.11}$$

with the amplitude A_j of the eigenmodes and

$$y(x,t) = \sum_j y_j(x,t) \tag{3.12}$$

In order to determine the bending stiffness κ by the application of the equipartition theorem and equation 3.1, a set of 500 images is analysed by fitting the first four eigenmodes

$$y(x,t) = \sum_{j=1}^{4} y_j(x,t) \tag{3.13}$$

to the measured momentary deflections $y(x_i)$ in each image. The corresponding bending stiffness is calculated from the averaged amplitudes for each eigenmode. The value obtained for the first mode is $\kappa = 6.3*10^{-26} \pm 0.6*10^{-26}$ Nm^2 (persistence length $l_p = 15.0 \pm 1.5$ µm). This value agrees well with data obtained by fluctuation analysis of filaments in bulk solutions [Ott *et al.*, 1993; Gittes *et al.*, 1993; Le Goff *et al.*, 2002]. It does not agree with the values obtained by rheology and quasi-elastic light scatter experiments (values discussed before). A possible explanation is that for the latter two techniques a bulk solution of actin is probed and that this might give some uncertainties when translating the results to the properties of a single filament. This in contrast to the analysis of the fluctuation of single filaments as described in this chapter.

The κ-value obtained for the second mode is by a factor of 2.5 smaller, $\kappa = 2.4*10^{-26}$ Nm^2. This apparent decrease of the bending stiffness with decreasing undulation wavelength is attributed to artefacts associated with high resolution analysis of fluorescence images. The high noise level may artificially generate intensity fluctuations of the images, which can feign undulations of the filament. These artefacts become more important with decreasing undulation wavelengths [Gittes *et al.*, 1993]. This is shown by the apparent values for the bending modulus, when it is calculated from the amplitudes of the third ($\kappa = 1.7*10^{-26}$ Nm^2) and of the fourth mode ($\kappa = 1.3*10^{-26}$ Nm^2). Figure 3.5 B shows the fit of a snapshot of the undulating filament.

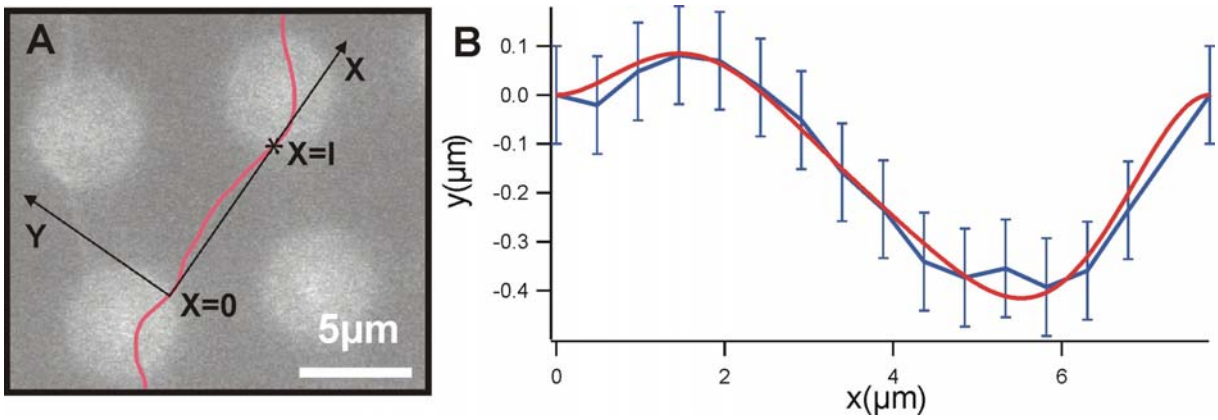

Fig. 3.5 (A) Fluorescent microscopy image (snap-shot) of thermally fluctuating actin filament extending between the tops of two epoxy based pillars. In this image the filament is accentuated by a line for clarity. (B) Fit of the set of filament positions $y(x_i)$ with $y(x)$ containing the sum of the first four modes of equation 3.11. The line with the error bars is obtained by Gaussian fits of segments of the filament in the recorded image. The smooth line is the fit of equations 3.11 and 3.12 to the measured positions of the segments.

The accuracy of the evaluation of the mean square displacements of the higher-order modes is mainly determined by the relatively low time-resolution of the image processing system (≈0.02 s) and the spatial resolution of the undulations of the fluorescent filaments. The lifetime of the longest wavelength mode is considerably larger than the time resolution of the image processing system and the spatial resolution is sufficient to analyse the longest wavelength excitation, which is the distance between two pillar heads. Therefore, the accuracy of the measurement of the amplitude is determined by the ratio of the mean square amplitude of the undulation to the mean square amplitude of the camera noise. A signal-to-noise ratio of ≈ 1 : 2 for the longest mode is found. Since the mean square amplitude is obtained by evaluating 500 images, the error is of the order 10%.

It should be noted that it is also possible to determine the persistence length by measuring the probability distribution function of the fluctuation of the filament at a point along the contour of the filament, which can be achieved by observing the Brownian motion of a colloidal bead coupled to the filaments [Dichtl and Sackmann, 1999]. A similar approach is adopted by Le Goff *et al.* [2002] who evaluated the distribution of the end-to-end distance of filaments.

3.6 Actin bundles formed by proteins and divalent cations

3.6.1 Static bundles

The pillar substrates offer the possibility of determining the elastic properties of individual actin bundles (mimicking F-actin stress fibres) crosslinked by different actin bundling proteins (such as filamin, alpha-actinin, or myosin), or by divalent cations. As an

example, figures 3.6 A and B show how actin-filamin bundles can be immobilised on the pillar substrate. Due to the higher stiffness of the bundles, the thermal shape fluctuations could not be resolved by fluorescence microscopy. However, measurements of the mechanical properties with improved microscopy techniques are in progress. Next to the passive binding protein filamin, also the motor protein myosin II, at KCl concentrations below 300 mM, is able to form actin bundles.

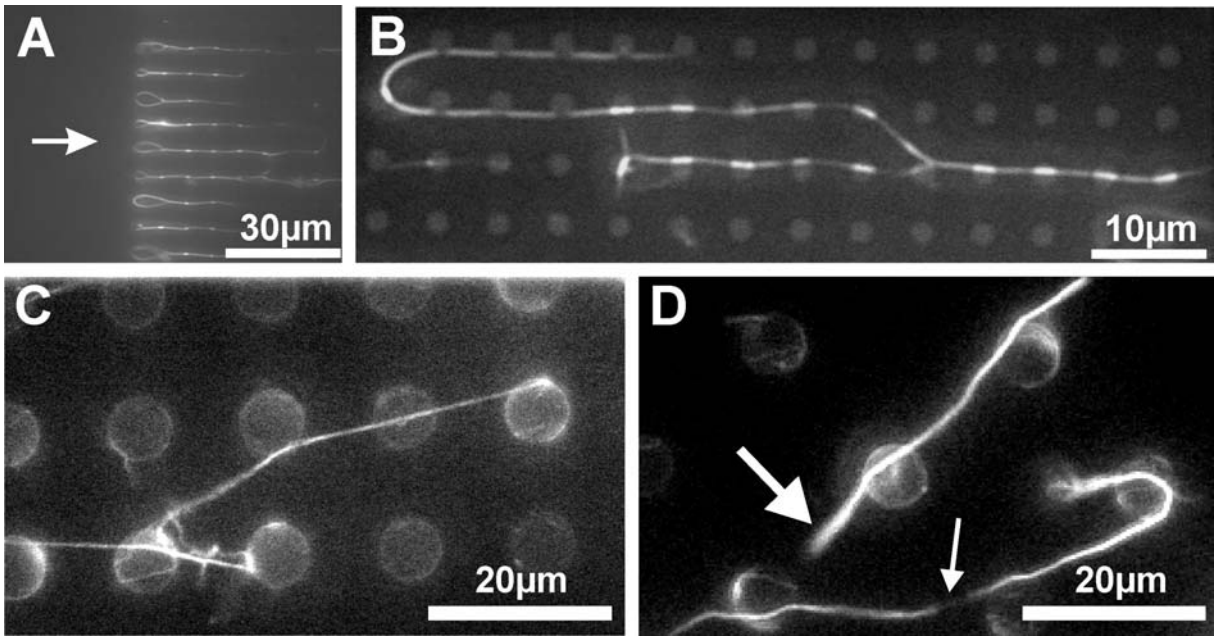

Fig. 3.6 Fluorescent optical microscopy image of actin bundles on silicon (A and B) and PDMS (C and D) pillars. (A) Actin bundles, formed by crosslinking of actin filaments with filamin in bulk solutions, is flowed into the liquid chamber from the left side (arrow) where no pillars are located. The arrow indicates the flow direction. Folding of the bundles is observed. (B) Example of branched actin bundle immobilised on top of pillars. (C) Bundles crosslinked by 80 mM Mg^{2+}. (D) Bundles crosslinked by 25 mM Ba^{2+}. It can be observed that the bundles are made up of filaments that do not go along the whole bundle. The small arrow shows a section where the bundle only consists of one filament. The big arrow shows the free end of a bundle, which is blurred due to Brownian motion. The sensitivity of the camera does not allow a higher capture rate, the result is a smeared image.

Literature review of bundle formation by divalent cations

Figures 3.6 C and D show images of immobilised actin bundles crosslinked by divalent cations. Actin is a highly negatively charged polyelectrolyte and therefore attracts cations from the buffer solution, resulting in so-called counterion condensation. Fluctuations in the counterion charge density along the polyelectrolyte lead to long range attractions and can sometimes overcome the electrostatic repulsion between polyelectrolytes [Wong *et al.*, 2003]. This is described by the Manning counterion condensation theory and it explains not only actin bundle formation by divalent cations, but also DNA condensation. At physiological conditions F-actin has a charge density of 4 e/nm [Tang and Janmey, 1996]. This is sufficiently small compared to the Bjerrum length λ_b for the counterion condensation to be relevant. The Bjerrum length is the distance between elementary charges at which the

electrostatic interaction energy equals the thermal energy k_bT, i.e. $\lambda_b = e^2/4\pi\varepsilon_0\varepsilon k_bT$. For example for water at 20 ºC, $\varepsilon = 80$, a value for $\lambda_b = 0.71$ nm is found.

Several theoretical papers considering counterion condensation have been published. Borukhov *et al.* [2001] described the attraction between two semiflexible polyelectrolytes from the point of view of the flexibility of the chain, instead of studying how the counterions modify the effective interactions between the monomers on the chain. Golestanian *et al.* [1999] described the collapse of stiff polyelectrolytes due to counterion fluctuations. Rouzina and Bloomfield [1998] addressed DNA bending by small, multivalent cations. In literature many reports can be found of experiments that support the counterion condensation theory.

Kawamura and Maruyama [1970] studied polymorphism of actin at acid pH by electron microscopy. They distinguished between three types of paracrystals of which the type III paracrystal is a bundle-like aggregate. Tang and Janmey [1996] performed light scattering experiments on actin solutions with several cations. They showed that a threshold concentration of polycations is required for bundling and that this threshold value is strongly dependent on the valence of the cation. The threshold concentration also increases with the ionic strength of the solution, in this case [KCl]. Wong *et al.* [2003] studied actin bundle formation by confocal microscopy and synchrotron small-angle x-ray scattering. They observed the bundle formation, induced by several alkali earth metals as a function of the ion concentration. It was also discovered that a lamellar phase of crosslinked actin rafts exists for concentrations just below that at which bundles are formed. At neutral pH, it seems that monovalent cations can not form actin bundles, even at [KCL] > 600 mM.

Experiments with several cations

In what follows bundle formation that is initiated by the addition of divalent cations to a diluted actin solution, is discussed. Both magnesium ions and barium ions appear to bundle actin at cation concentrations above 15 mM (Fig. 3.6 C and D) at an actin concentration of 4 µg/ml. At such concentrations, some bundles can be found, but single filaments are still present. For higher concentrations, the single filaments are increasingly incorporated into bundles. These experiments are carried out in the presence of 25 mM KCl and in the case of Ba^{2+} in the absence of Mg^{2+}. Additionally zinc, copper, manganese, nickel and calcium ions are able to bundle actin filaments as will be discussed in the following.

Calcium ions start bundling actin filaments at almost the same concentration as magnesium ions do, with only a small difference in the exact concentration of the cross-over regime. To investigate the difference in bundle formation with these two cations in more detail, the additive comportment of calcium and magnesium is studied. The experiments are performed in flow cells of two cover slips with double sticky tape as a spacer. It is observed whether bundle formation takes place for different cation concentrations. The threshold concentration for calcium ions is slightly lower than that for magnesium ions as shown in figure 3.7. Below the line only single filaments are present and there is no difference observed for varying concentrations. At the line the first bundles are observed in solution. Above the line an increased amount of bundles is observed. Far above the cross-over regime no single filaments are present anymore. The experiments show that there is a straightforward additive behaviour of the crosslinking of actin filaments as a function of the relative amount of ions. This is to be expected, since both ions will compete for binding sites along the negatively charged actin filaments.

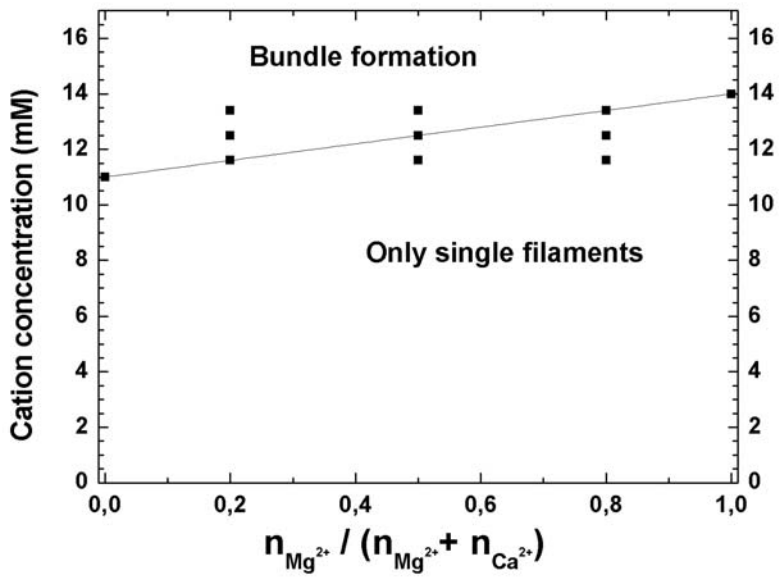

Fig. 3.7 Actin bundle formation with mixtures of calcium and magnesium ions. On the x-axis the relative molar amount of magnesium ions is plotted, with the molarity of the magnesium ions n_{Mg}^{2+} and the molarity of the calcium ions n_{Ca}^{2+}. This means that for 0 there are only calcium ions present and for 1 there are only magnesium ions present. The dots show the concentrations at which experiments are performed. For solutions with only calcium ions present, bundling starts around $[Ca^{2+}]$ = 11 mM. When only magnesium ions are present, bundling starts at $[Mg^{2+}]$ = 14 mM. The drawn line separates the regimes where only single filaments are present and where bundle formation starts to take place. For the measurement data points below this line, no bundles are observed. Above this line bundles are present. Actin concentration is 1 µg/ml.

Experiments with other divalent cations are performed, similar to the experiments with only calcium ions and only magnesium ions present. Figure 3.8 shows a graphical representation of actin bundle formation as a function of the concentration of various cations. Crosslinking experiments are performed with copper, zinc, nickel, manganese and barium ions. The observed qualitatively differences in the actin bundle formation as a function of the ion concentration are divided into four groups. These are: no crosslinking observed, a few bundles present, many bundles present and only bundles present. Combining with the results from figure 3.7, it can be seen that for the alkali earth divalent ions there is an increase in crosslinking efficiency with increasing atomic number. Magnesium ions need to be present at a concentration of about 14 mM for bundle formation to start. For calcium ions a concentration of 11 mM is sufficient and for barium ions the concentration at which bundle formation takes place is about 10 mM. The atomic numbers of these ions are 12, 20 and 56 respectively. The effect of the dependence of actin bundle formation on the atomic number is also observed by Tang and Janmey [1996] for calcium and magnesium ions. In the study presented here, barium is additionally studied and it is observed to be in agreement with this description.

The description of the dependence of actin bundle formation on atomic number of the ion can also be applied to elements from the transition metal group. Manganese, nickel and zinc, with atomic numbers 25, 28 and 30 respectively, are increasingly efficient in initiating bundle formation in this respective order. However copper, with the atomic number 29, does not fit into this description. The concentration with which copper ions bundle actin filaments

is the lowest for all the elements observed. Tang and Janmey [1996] also observed this peculiarity of copper and their explanation is that this might be due to specific binding of copper ions with a high affinity to the C terminus of actin. It should be noted that for the experiments presented here, where copper ions are involved, a very low fluorescence intensity is observed. This might be related to the special behaviour of copper.

Whereas the theory of increasing crosslinking efficiency with increasing atomic number can be applied to the alkali earth elements and the transition metals alone, this can not be applied to the studied ions of the combined groups. It seems that in general the transition metal group elements are more efficient in bundling actin filaments than the earth alkali elements. There is also a qualitative difference observed in the bundling by the ions from these different groups. Whereas the ions in the earth alkali group make mainly linear aggregates of actin filaments, the transition metal ions form predominantly crosslinked irregular close packed aggregates of actin filaments. The varying observations of the bundle formation inducement of actin filaments by several divalent cations should be the topic of further research. This will help to be able to refine the counter ion condensation theory. Tang and Janmey [1996] noted that some cation specific effects can not be explained by the Manning counterion condensation theory. They suggested that ionic radius and extent of hydration of the ions will play a significant role in the cation induced bundle formation of actin filaments.

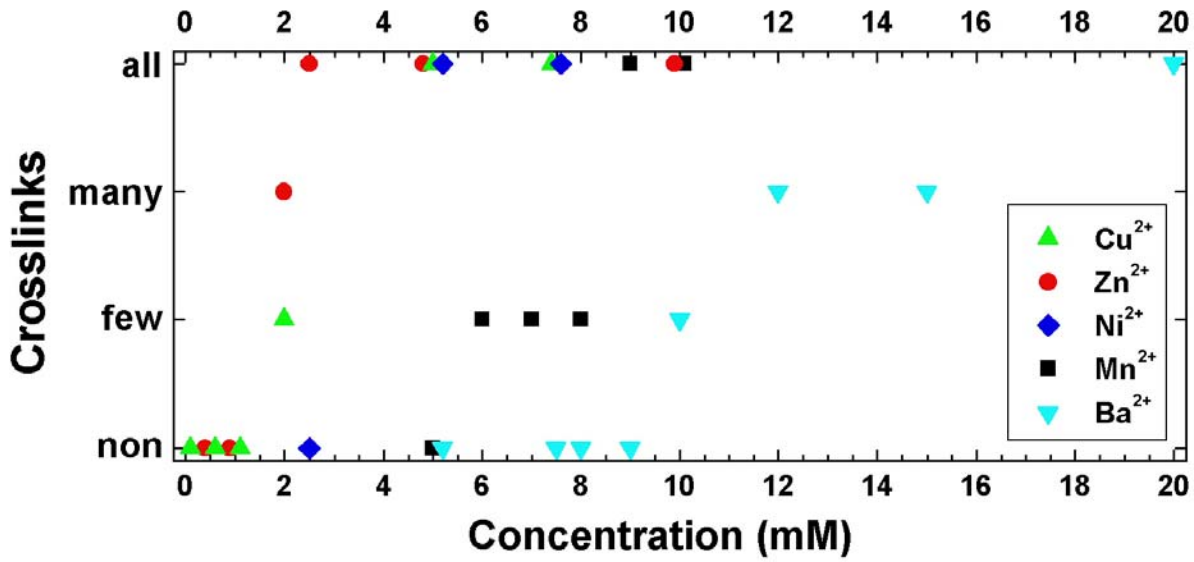

Fig. 3.8 Actin bundle formation with several divalent cations. The x-axis denotes the concentration of the specific ions. A qualitative measure for the amount of crosslinked filaments is depicted on the y-axis. The studied ions are copper, zinc, nickel, manganese and barium. Actin concentration is 1 µg/ml. Results for magnesium and calcium are shown in figure 3.7.

3.6.2 Dynamic bundle formation

In the previous experiments, the bundles are formed prior to flowing them into the measuring chamber. In what follows, filaments that are imaged during bundle formation are

discussed. Bundle formation is a stochastic process where the crosslinker first needs to get into contact with one filament and then with another filament. The first contact is difficult to observe. However when the second contact is made, necessarily two filaments come into contact. If there is a high enough amount of crosslinkers on one or both of the filaments, an increased association rate is observed. A so called zipper-like connection [Uhde *et al.*, 2003] is made and bundle formation takes place.

Bundle formation by magnesium ions

Figure 3.9 shows an example of this process. F-actin is loosely bound near to a glass surface. When Mg^{2+} ions at a concentration of 80 mM are flowed into the chamber, gradually the free filaments get crosslinked. A zipping behaviour is observed on the subsecond level. The velocity with which the crosslinking takes place can be above 20 µm/sec as seen in the images in figure 3.9. This velocity is considerably higher than the velocity with which myosin V motors move along actin flaments (see section 3.4).

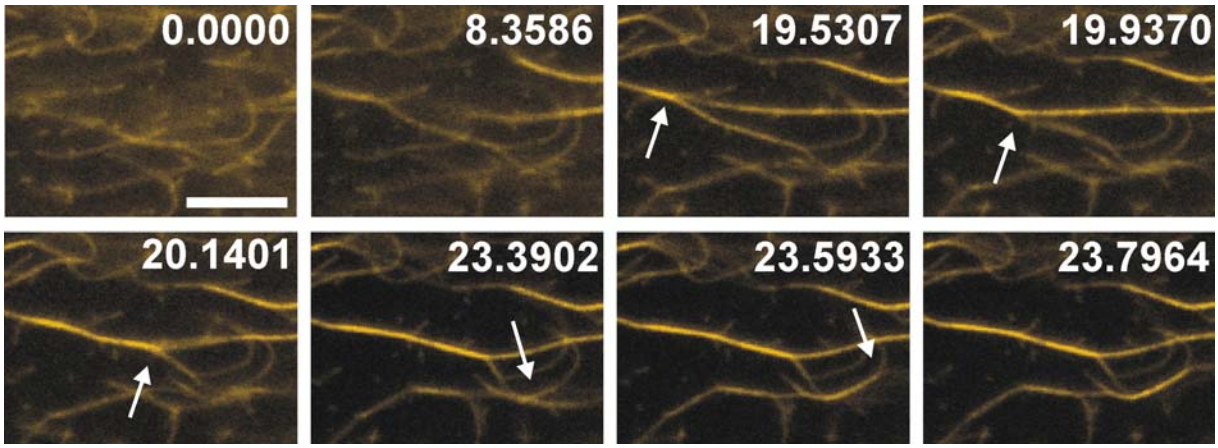

Fig. 3.9 Crosslinking of actin filaments on glass, by influx of Mg^{2+} ions. The magnesium ions are added at t = 4 seconds (actin concentration 50 nM, Mg^{2+} concentration 80 mM). The velocity with which the crosslinking takes place between the third and the fourth image is approximately 9 µm/sec. Between the fourth and the fifth image this is approximately 25 µm/sec. Arrows are added to accentuate areas where crosslinking takes place. Fluorescence microscopy image, time in seconds, scale bar 10 µm.

Crosslinking and decrosslinking by myosin II motors

Not only crosslinking but also decrosslinking is observed. Whereas passive actin binding proteins like filamin can only bundle actin filaments, myosin and divalent cations can also be dissociated from the bundle. This dissociation leads to the split up of the bundle into the filaments it is composed of. Divalent cations can be dissociated by diluting the actin bundle solution with enough divalent cation-free buffer solution. When the divalent cation concentration falls below a critical value there are not enough cations left to keep the filaments together, the resulting effect is decomposition of the bundle.

The dissociation of myosin II can be induced by the addition of ATP. Without ATP, myosin binds to actin, but can not dissociate. With ATP present, there is a dynamic situation between association and dissociation, of which the latter process proceeds with a force stroke. However, the set-up presented here does not have a sufficient spatial and temporal resolution to image this force stroke. After dissociation of myosin II from the actin filament, the myosin can easily diffuse away. Due to the three dimensional flow chamber used in the experiments presented here, there is a small chance the myosin II will associate again to the actin filament.

In buffer solutions with a KCl concentration of more than 0.3 M myosin II is present as a dimer. There is a different situation at KCl concentrations of 25 mM. In this case myosin II forms long filaments, because the stalk of myosin II (see figure 1.2) is insoluble at low salt concentrations. In the experiments presented here, an intermediate state of myosin II organisation is used. At KCl concentrations of 200 mM myosin II forms mini-filaments. These mini-filaments consist of a few myosin dimers that are associated to each other. Figure 3.10 shows images of actin filaments on PDMS pillars. The first image shows single actin filaments adhered to the pillar tops. The actin filaments are subsequently crosslinked by flowing in a solution of myosin II mini-filaments. Actin bundles can be observed. Next the filaments are decrosslinked by the addition of ATP and single filaments are present again. Finally these filaments are crosslinked again by the addition of magnesium ions at a 80 mM concentration.

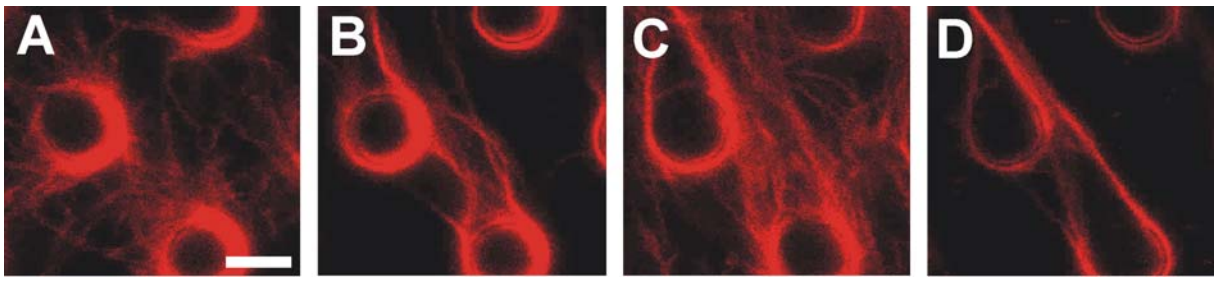

Fig. 3.10 Dynamic crosslinking of actin filaments on PDMS pillar substrates. (A) F-Actin (50 nM) is flowed into the flow chamber and adheres to the pillar tops as single filaments. (B) Myosin II (500 nM), diluted in a buffer solution with a KCl concentration of 200 mM, is added and bundle formation can be observed. (C) ATP (1 mM) is flowed into the chamber and a decrosslinking of the actin bundles is observed. The single filaments are visible again. (D) Mg^{2+} ions (80 mM) are added and a renewed crosslinking is observed. There are actin bundles again. Confocal microscopy image, scale bar 5 µm.

In muscle there are always some myosin heads that are attached, some that are producing a force stroke and some that are rebinding again. Due to this fact and mainly due to geometrical considerations, myosin and actin filaments are tightly packed in muscle tissue, no myosin filaments will diffuse away during or after muscle contraction. The experiments in figure 3.10 show a different situation. After addition of ATP the myosin-actin bundles dissociate from each other and the actin is again present as single filaments. Apparently the myosin II filaments in the set-up described here are so short that there is not enough time for reassociation after all the heads made their force stroke. Furthermore the three dimensional set-up on which the bundles are located, does not provide sufficient boundary conditions to hinder the filaments from diffusing away. The result is that after the addition of ATP most or

all of the myosin II mini-filaments diffuse away with a small probability of rebinding. Even when they rebind, force strokes are produced again and subsequently the myosin mini-filament can diffuse away. These experiments show that variations in the ATP concentration can be used as a switch to turn crosslinking of actin filaments by myosin II on and off.

Acknowledgments:

J. Zhang, M. Bärmann, M. Rusp and H. Kirpal (TU München) are thanked for the careful preparation of actin, filamin, NEMHMM and myosin V motors. Thanks to E. Sackmann (TU München) for providing the actin and the actin binding proteins and enabling the author a one month stay as a visiting scientist in his group. A. Roth (TU München) is thanked for introduction to actin and for the longstanding collaboration. Thanks to J. Blümmel (Universität Heidelberg) for the PEG preparation and to S. Schulz, S. Quint (Universität Heidelberg) and A. Sugiharto (Universität Karlsruhe) for actin bundling experiments with myosin II and different divalent cations.

Chapter 4

Microtubule gliding assays

4.1 Introduction

Microtubules play an important role in intracellular vesicle transport and cellular division. Microtubules are vital in, for instance, neuronal axons, where they stabilise the axonal structure. The presence of microtubules prevents the axons from retracting. They serve however multiple purposes in axons. Next to stabilising the neuron they also serve as tracks for intracellular vesicle transport [Lodish *et al*., 1999]. Neurons release neurotransmitters at synapses with other cells in order to transmit electric impulses. Due to the continuing exocytosis at the neuron terminal, proteins and membranes need to be replaced continuously. Ribosomes are not present in axons and in synaptic terminals, which means that proteins can not be synthesised in either of them. Therefore, membranes and proteins are synthesised in the cell body and they are transported through the axon, which can extend over meters, to the synaptic terminals. This transport takes place along microtubules, which are directed with their plus end to the synaptic terminal. Transport in both directions takes place in neurons. Anterograde transport proceeds from the cell body to the synapses and serves axonal growth and synaptic releases. Transport in the opposite direction, called retrograde transport, is associated with the transport of membranes, which needs to be degraded in lysosomes in the cell body [Lodish *et al.*, 1999]. The fastest transport is that of membrane-bound vesicles, which move at speeds of about 3 μm/s.

During cell division a large microtubule structure is formed, called the mitotic apparatus. This apparatus is responsible for partitioning newly replicated chromosomes. Three groups of microtubules can be distinguished in the mitotic apparatus. All of them are organised with their minus end in spindle poles or microtubule organisation centers (MTOC), from which there are two present in the dividing cell. At their plus ends, a part of the microtubules is connected to chromosomes by kinetochores. Another part is connected to the plus end of microtubules originating from the opposite spindle pole. The last group of microtubules radiates outward to the cellular cortex to position the mitotic apparatus [Lodish *et al*., 1999]. The chromosomes are finally separated by a combination of microtubule polymerisation and depolymerisation and by active transport processes.

During the two processes described above, motor proteins like kinesins and dyneins move along the microtubules. One of the differences of these motors is that they are respectively plus-end and minus-end directed. This means that kinesins are responsible for

anterograde transport in neuronal axons and dyneins are responsible for retrograde transport. In vitro, microtubules are shown to glide over kinesin-coated surfaces and one kinesin motor is able to push an entire microtubule forward. Kinesin is a processive motor protein with a high duty ratio [Young *et al*., 1998]. Processivity means that a motor remains attached to the filament during many catalytic cycles. A high duty ratio indicates that the velocity with which one motor can push a microtubule forward is similar to that with which many motors can push.

In the experiments described here, microtubules are shown to glide over the top of microfabricated pillars, whereas the sidewalls and bottom of the substrate are passivated and inaccessible to the microtubules. This in contrast to experiments performed on microstructured surfaces where the microtubules moved over the bottom instead of on the structure tops [Hess *et al*., 2002a]. Via stamping techniques kinesin motors are attached to the pillar heads and prepolymerised microtubules glide from one pillar to the next. This is a combination of the chemical patterning and the topographical patterning, which is reported as separate systems by Hess *et al*. [2002b]. The advantage of the microfabricated pillar surfaces compared to flat substrates is that the positioning of the motor proteins can be controlled. The motors can only adhere to the pillar heads. At the height of the pillar heads, but in between them, there is no surface present, only buffer solution. The result is a minimisation of surface interactions of the gliding microtubules. This in turn, results in a decreased possibility of frictional encounters of the microtubule with the environment. On the pillar substrates the distances that moving microtubules can gap without having a support is studied. Such experiments can be related to processes like axonal outgrowth in the extra cellular matrix, which leans heavily on the high rigidity of microtubules. The gliding microtubules on the pillar surfaces gap distances of more than 10 µm without difficulties.

Figures 4.1 A and B show a schematic image of the experimental set-up and a picture of microtubules on the pillar tops. In this study, it is shown that the velocity of the gliding microtubules is geometry independent. This means that there is no significant difference observed in the mean velocity of moving microtubules on PDMS pillar structures and on flat PDMS surfaces. The average velocity is also similar on glass and on flat PDMS substrates. Buckling of microtubules is observed in many cases and those experiments show that the microtubules are attached to several motors per pillar top.

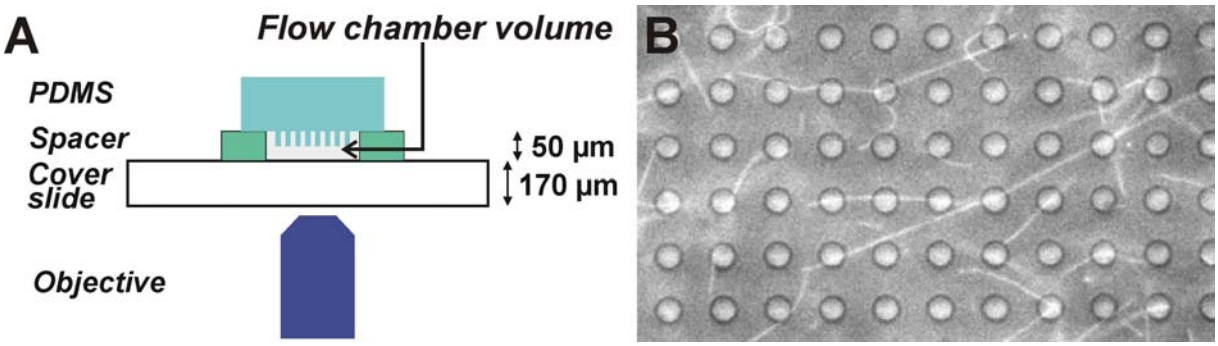

Fig. 4.1 (A) Schematic view of flow chamber and microscope. The flow is in the in plane direction. (B) Microtubules gliding over pillar tops (snap-shot). Full image width 95 µm.

4.2 Materials and methods

Protein preparation

Tubulin is purified from pig brain [Mitchison and Kirschner, 1984] and stored in liquid nitrogen. Unlabelled and carboxy-tetramethylrhodamine-labelled (TAMRA) tubulin is mixed at a 5 : 1 ratio. The tubulin, with a final concentration of 2 mg/ml, is polymerised with 1 mM GTP at 37 °C in BRB80 buffer (see table 4.1) for 20 minutes. Next, the microtubuli are stabilised with 2 µM taxol in BRB80 (denoted by BRB80/taxol). This solution is spun in an ultracentrifuge (Beckman Coulter TLX, 200,000 * g, 15 min, 37 °C) to get rid of the non-polymerised tubulin. Biotinylated tubulin is prepared by coupling a *N*-hydroxysuccinimide (NHS)-biotin to tubulin. In a similar way, TAMRA labelled tubulin is prepared with TAMRA-NHS. Both methods follow the procedure of Hyman *et al*. [1991]. Biotinylated HA-kinesin is produced as described by Surrey *et al*. [1998]. Full length Eg5 is expressed in SF9 cells by the method of Kapoor and Mitchison [2001]. Microtubuli are diluted in the BRB80/taxol buffer. All other protein solutions are diluted in BRB80 unless otherwise stated.

Table 4.1 Microtubule BRB80 buffer

BRB80	
PIPES / KOH	80 mM
$MgCl_2$	1 mM
EGTA	1 mM
pH = 6.8	

Flow cell protocol

The PDMS pillar substrates are produced as described in chapter 2. PDMS is a hydrophobic material and PDMS pillar substrates are even more hydrophobic, which can be explained by the lotus effect [Patankar, 2004]. This means that a drop of liquid on the pillar substrate will only wet the pillar heads, but it will not wet the region between the pillars when it is left for a limited time. To functionalise only the tops of the pillars, a drop of 100 µg/ml biotin-BSA (Sigma) is left for 30 sec on top of the pillar substrate. This results in functionalised pillar heads and no functionalisation of pillar side walls and bottom. A simple flow cell, comprised of two stripes of 50 µm thick double sticky tape (Tesa 4972, Winterhalder, Heitersheim, Germany), a glass cover slip and the pillar substrate, is constructed. To passivate the glass and the non-functionalised parts of the sample, 10 mg/ml Bovine Serum Albumin (BSA; in 5 mM TRIS buffer) is flowed into the chamber for incubation. Additionally, the BSA binds to free regions on the pillar tops, therefore suppressing non-specific binding of microtubules to the pillar tops. Following a washing step with buffer solution, 100 µg/ml streptavidin (Molecular Probes) is flowed into the chamber. After washing again, the biotin-kinesin solution is flowed into the sample. Finally, the prepolymerised microtubules, diluted in buffer solution containing 1 mM ATP, are flowed into the chamber and the sample is observed.

Microscopy

Experiments are performed with a Zeiss Axiovert 135TV Microscope at ambient conditions. A 63x Plan-Neofluar oil immersion objective and a 40x Plan-Neofluar oil immersion objective are used. Images are recorded with a Visitron Coolsnap HQ camera. Due to little reflection at the condenser, the pillar tops of the non-fluorescent PDMS could be imaged together with the fluorescent microtubules.

4.3 Gliding assays

Gliding assays are performed on flat and pillar structures. It is shown that it is possible for microtubules (having lengths of approximately 15 to 30 µm) to glide from one pillar to the next, bridging distances of over 10 µm. Microtubules have a persistence length of several millimeters [Gittes *et al.*, 1993] and this can explain why the microtubules can easily bridge the gap in between the pillars during motility. Similar experiments with actin filaments (having lengths of approximately 20 to 30 µm) did not show positive results, probably due to the fact that filamentous actin has a much smaller persistence length (around 15 µm) than microtubules [Roos *et al.*, 2004]. The microtubules do not always move continuously over the pillar heads. Sometimes they get stuck at their front and buckling of the microtubule takes place. This buckling is discussed in section 4.3.1. The velocity distribution of gliding microtubules on several substrates is presented in section 4.3.2. To show the effectiveness of the stamping technique to selectively bind kinesin on pillar heads, some control experiments are performed. These experiments are presented in section 4.3.3

4.3.1 Microtubule buckling

A straight and rigid rod, which is subject to a compressive force parallel to its long axis will buckle after a critical force is reached. The difference between buckling and bending of a rod is that the former is the result from a force parallel to its axis and the latter from a force in a different direction. For buckling to occur, a critical force is required. When this force is exceeded the rod jumps into a buckled state. Bending of rods however, starts already after an infinitesimal small force is applied.

Buckling of microtubules has been the subject of various studies. Dogterom and Yurke [1997] analysed buckling of polymerising microtubules against a wall. The microtubules are attached at their minus end to a surface and polymerisation continues at the plus end, even when it encounters a wall. Subsequent buckling is the result. Gittes *et al*. [1996] studied buckling of microtubules that are attached to a flat surface at their minus end and these microtubules are pushed forward at the other end by surface immobilised kinesin motors. Both these buckling experiments are performed to improve the understanding of fundamental microtubule and molecular motor properties, like microtubule polymerisation and directed motor movement.

In figure 4.2 some images of a microtubule gliding assay on pillars are shown. At 61 seconds, it can be seen that the microtubule has buckled. The microtubule front end got stuck

for a short time. This is probably the result of inactive motors or non-specific surface interactions with the microtubule. At the rear of the microtubule there are still motors pushing, which leads to buckling. It can be seen that the microtubule is still lying straight on the upper left pillar. This means that it is bound to at least two kinesin motors [Gittes *et al.*, 1996]. For the buckling microtubule on top of the pillars a reference frame with the connecting line in between the two pillars denoted as the x-axis and an axis perpendicular to this line as the y-axis, is taken. In this frame of reference the following boundary conditions are relevant: $y(0) = y(L) = 0$ and due to the rigidity of the microtubules also $y'(0) = y'(L) = 0$ is supposed (fig. 4.3). The variable L denotes the pillar gap and the prime denotes the derivative with respect to x. The critical buckling force F_c of a microtubule fixed at two sides is given by [Landau and Lifshitz, 1991, problem 2, p104]

$$F_c = \frac{4\pi^2\kappa}{L^2} \tag{4.1}$$

where κ is the microtubule bending elasticity and L is the microtubule length between the attachment points at the onset of buckling.

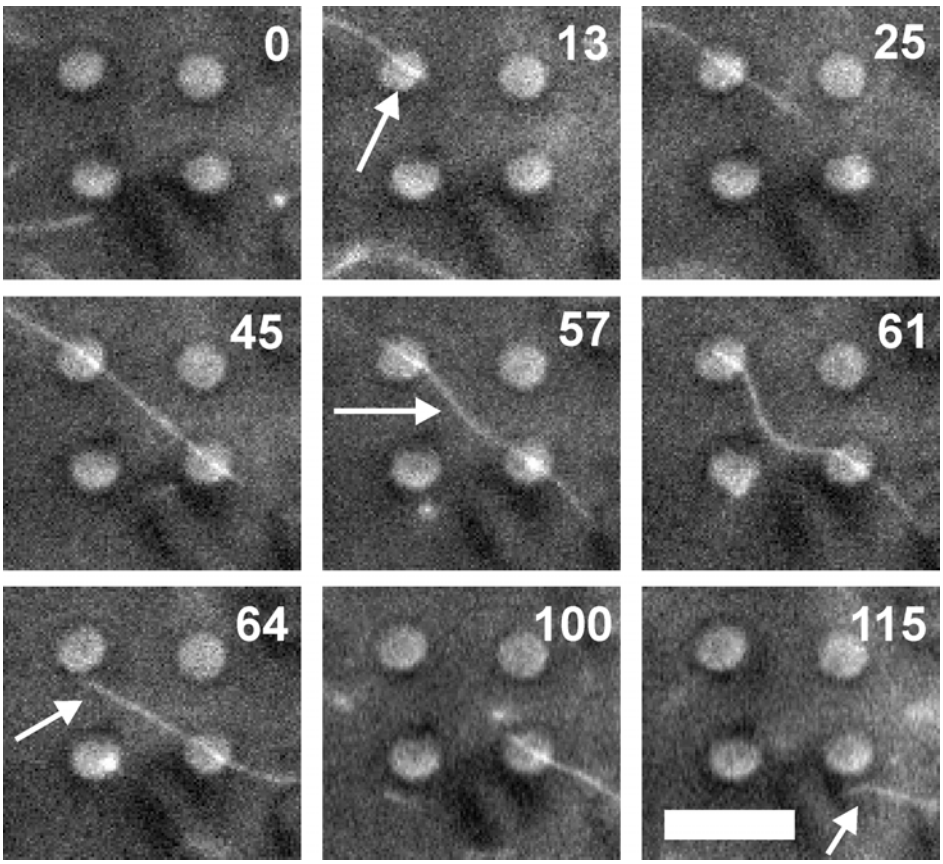

Fig. 4.2 Microtubule motility assay on top of pillars. At 0 seconds and at 115 seconds no microtubule is bound. In the intermediate time the microtubule attaches to one pillar (at 13 seconds), glides over it to the next pillar and finally detaches from the second pillar. The microtubule buckles around 57 seconds and continues after 61 seconds. The average velocity of the gliding microtubule is 500 nm/s. Arrows pointing at the microtubule are added in some images, for emphasis only. Time is indicated in seconds, scale bar 10 µm.

Various values for κ can be found in literature. Gittes *et al*. [1993] measured $\kappa = 2.2 * 10^{-23}$ Nm^2 for taxol-stabilised microtubules by analysis of thermal fluctuations in shape of microtubules in between two coverslips separated by 3 µm (effectively limiting the fluctuations to two dimensions). Elbaum *et al.* [1996] analysed buckling of unlabeled microtubules in artificial phospholipid vesicles and found $\kappa = 2.6 * 10^{-23}$ Nm^2. Dogterom and Yurke [1997] and Janson [2002] analysed the thermal fluctuations of growing microtubules with one side attached to a glass cover slip and found $\kappa = 3.4 * 10^{-23}$ Nm^2 and $\kappa = 2.0 * 10^{-23}$ Nm^2, respectively.

Using the value $\kappa = 2.2 * 10^{-23}$ Nm^2 [Gittes *et al*., 1993] and $L = 9.6$ µm, a critical buckling force of 9.4 pN is calculated for the buckling presented in figure 4.2. Two kinesin motors would have been able to generate this force as the typical force per motor is around 5 pN [Svoboda and Block, 1994] as obtained by optical tweezer experiments of in vitro motility assays of kinesin coated beads. As discussed before after analysis of the images, it is plausible that more than one motor pushes the microtubule forward. Figure 4.3 shows a schematic configuration of the buckled microtubule on top of two pillars with the active and the rigid motors drawn as small circles.

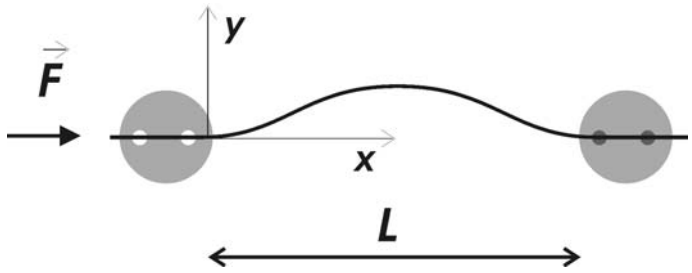

Fig. 4.3 Schema of buckling of microtubule on pillars. On the right pillar the microtubule is stalled by to at least two rigid motors (small, dark circles). On the left pillar at least two motors (small, white circles) push the microtubule forward.

For all the buckling experiments on pillar tops, it can be observed that the buckled microtubule remains in focus. The flat surface of the pillar tops probably prevents the microtubule of buckling downwards. On flat surfaces, it is also observed that buckling normally takes place in lateral directions. This implies that both a flat surface and the pillar tops prevent the microtubule from buckling upwards. This is probably due to the fact that a surface hinders the upward buckling as the microtubule will exert a force in the opposite direction of buckling during this process.

Microtubule experiments are performed on PDMS pillars, flat PDMS and on glass surfaces. In general it can be said that on all substrates sooner or later a microtubule buckles. This is a result of unspecific surface interactions of gliding microtubules and with rigid motor heads. These are kinesin motors that can adhere to microtubules, but that are not able to perform a force stroke. Even in the presence of ATP they remain attached to the microtubule and therefore they present a frictional effect to the gliding microtubule. Some rigid heads are always present in a kinesin preparation, excluding them completely is a difficult task. It is also possible that active motors turn into rigid heads during the experiment.

4.3.2 Velocity distribution of gliding microtubules

The average speed of the gliding microtubules is calculated for in total 235 microtubules with lengths in between 5 µm and 35 µm. The values are obtained for experiments on PDMS pillar substrates, on flat PDMS and on glass. A difference between the flat and the pillar structures is that the amount of motors that attach simultaneously to the microtubule will probably be lower for the pillar surface than for the flat surfaces. However, as discussed before the duty ratio of kinesin motors is high, which means that the gliding velocity is independent of the kinesin density on the surface.
There is no significant difference observed in the mean speed of the moving microtubules on the different samples (immobile microtubules are not counted for). This means, that there is no averaged significant friction contribution from the substrates or from motors, which attach but do not move. However, the distribution of the velocities is different on the different substrates, as will be discussed later. Figure 4.4 shows a scatter plot of the velocity distribution on the different substrates. The average speed is in the range of 200 nm/s to 800 nm/s for time intervals of 15 sec to 135 sec. However, on the flat and the pillar PDMS substrates about half of the microtubules got stuck. On glass more than 95% of the microtubules moved. The measured speeds are comparable to measurements reported by Surrey *et al.* [1998] with the same motor construct and by Young *et al.* [1998] with a different kinesin construct.

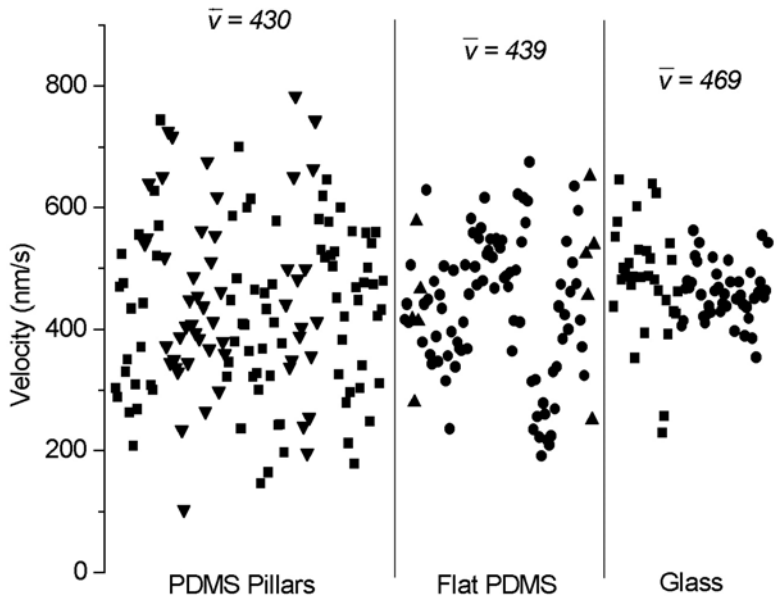

Fig. 4.4 Scatter plot of velocity distribution of microtubules on several kinesin coated substrates. Experiments on PDMS pillars, on flat PDMS and on glass are performed. The average velocity $\bar{v}$ in nm/s is printed above the respective columns. On the pillars 94 microtubules are analysed, the mean velocity is 430 ± 140 nm/s where the error is the standard deviation. On flat PDMS 82 microtubules are analysed and the mean velocity is 439 ± 115 nm/s. On glass 59 microtubules are analysed, the mean velocity is 469 ± 70 nm/s.

The data points that are plotted in figure 4.4 are also drawn in a histogram with a velocity binning of 25 nm/s. Figure 4.5 shows these histograms for the different substrates. The velocity distribution on glass is clearly the smallest of the three distributions. The distributions on either of the PDMS substrates is relatively large.

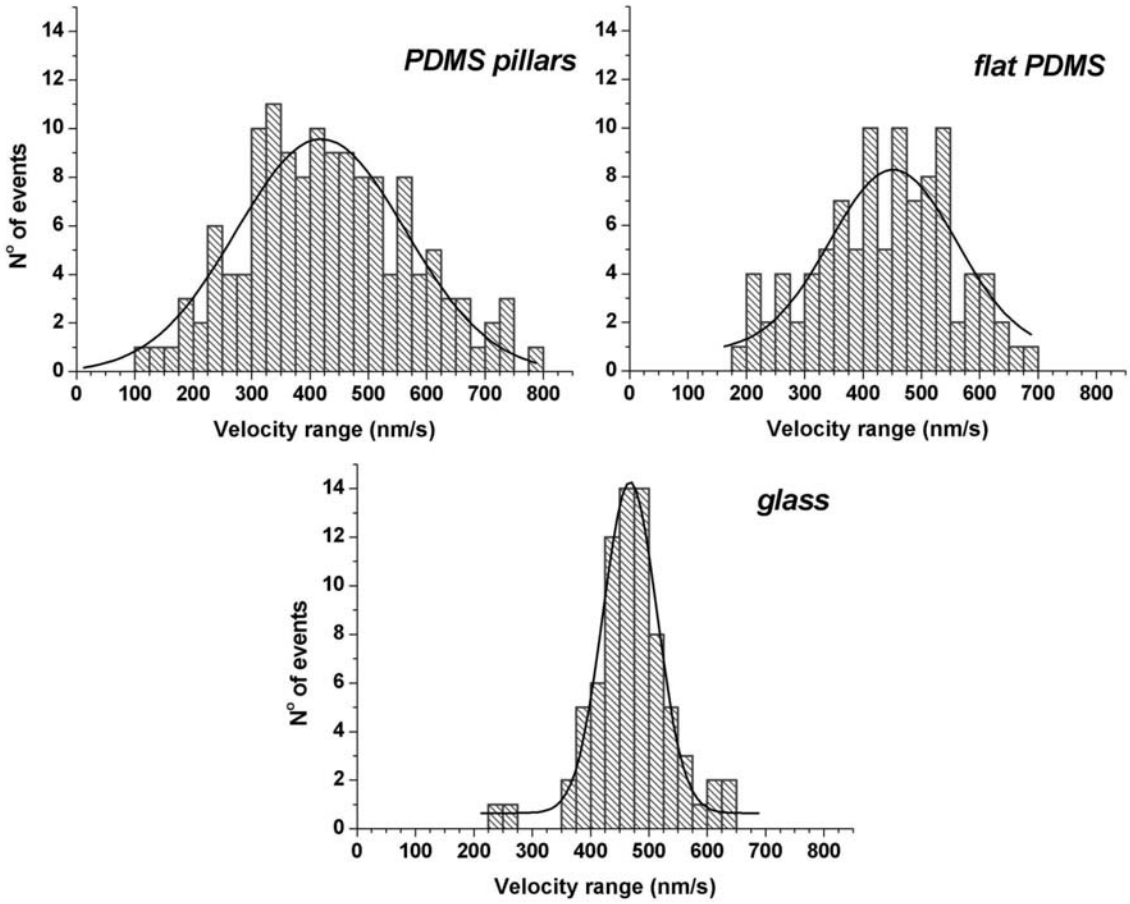

Fig. 4.5 Histogram of gliding velocities on PDMS pillars, flat PDMS and on glass. The velocities of which the values are plotted in figure 4.4, are used. Bin width is 25 nm/s. A gaussian fit to the histogram data is plotted, as a black line, in all plots.

It seems that on the pillar substrate there is a slight tail on the high velocity side. On the flat PDMS there is a tail on the low velocity side. A possible explanation is given for these results. On the flat PDMS the events in the low velocity regime might be due to the high hydrophobicity of PDMS. This can result in increased hydrophobic interaction between the proteins and the surface, which in turn can slow down the moving microtubule. The pillar substrates have a two-fold effect on the gliding velocity of the microtubules. From one side it can be argued that there is less substrate present, which means less friction of the gliding microtubule with the environment. With less friction that brakes the microtubule, a higher velocity can be achieved. The result is a significant number of events in the 600 - 700 nm/s regime. On the other hand, it can be argued that for the pillar arrays there can also be a decrease in velocity due to the three dimensional geometry. That can happen when the gliding microtubule does not directly attach to the kinesin on the next pillar. Microtubules are semi-

flexible polymers and they fluctuate due to Brownian motion. This can result in a fluctuation towards the pillar base at the moment the microtubule reaches the next pillar. It bumps into the upper part of the pillar and it brakes. The result is a significant amount of events in the 200 - 300 nm/s velocity range. To verify these assumptions further experiments are needed to improve the statistics of the experiments presented.

4.3.3 Specific adhesion experiments

The effectiveness of the biotin-BSA stamping and the BSA passivation of the rest of the substrate is tested on flat PDMS substrates. For this experiment, the streptavidin is mixed with Alexa 488 fluorescent streptavidin (at 100:1 ratio). Figure 4.6 A shows that the border between the stamped and the non-stamped region can be distinguished clearly. After binding of the biotinylated kinesin motors, microtubules without ATP are flowed into the sample. The microtubules only adhere to the stamped part of the PDMS (fig. 4.6 B). The same experiment is performed with microtubules mixed with ATP and it could be seen that the microtubules only adhere and move on the stamped parts. However, due to stochastic release of the motors in the presence of ATP, the concentration of adhering and moving microtubules is lower than under conditions without ATP.

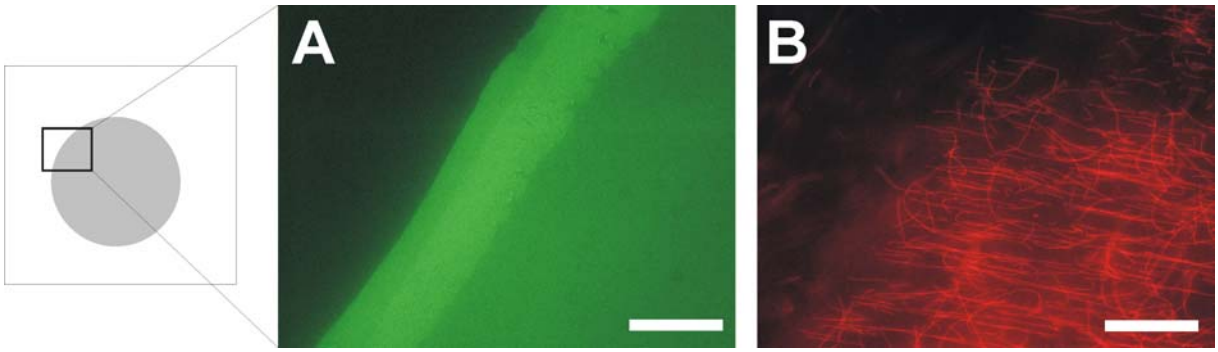

Fig. 4.6 Effectiveness of biotin-BSA stamping for selective microtubule adhesion on flat PDMS surfaces. On the left side a schematic image of the stamped area (grey) on the flat PDMS is shown. Figures (A) and (B) are an enlargement, which is denoted by the thick lined box in the schematic picture. (A) Fluorescent image of streptavidin Alexa 488, which adheres to the biotin-BSA. The black part of the image is passivated with BSA. (B) Microtubules adhere to the biotin-kinesin, which only adheres to the stamped parts of the PDMS. Scale bar 50 µm.

The experiments shown in figure 4.6 are performed on flat PDMS substrates. These experiments are repeated on PDMS pillar substrates. Figure 4.7 shows the results for the stamping control experiments on pillar surfaces. From figure 4.6 it can be concluded that the kinesin binding only takes place at the stamped part and that the other part is successfully passivated. Figure 4.7 is an example for the reproducibility of these results on pillars. First, only microtubules adhere onto the stamped part of the pillar arrays. Second, by focusing up and down it can be seen that the microtubules only adhere to the pillar tops. They do not

adhere to the pillar side walls or to the bottom of the pillar substrate, because these surfaces are passivated by BSA.

In figure 4.7 A it can be seen that most of the stamped part is at the bottom right of the image. However, a few small spots are present at the left part of the image. These spots are directly correlated with microtubule adhesion, which can be seen by comparison with figure 4.7 B. The small spots can not be prevented during stamping and they are normally present near the border area. Further away from the stamped part such spots are not present anymore.

The experiments presented in this section show that specific adhesion of microtubules can be obtained by a combination of stamping and passivation techniques. This works on flat as well as on pillar structures.

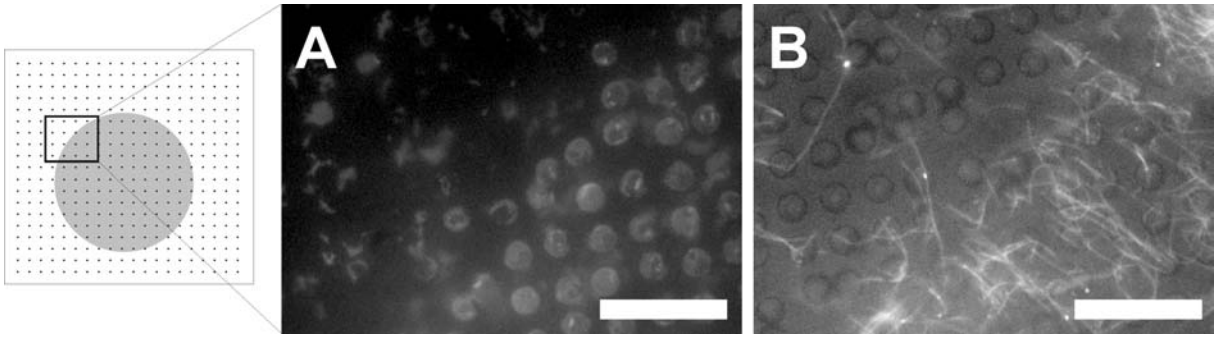

Fig. 4.7 Effectiveness of biotin-BSA stamping for selective microtubule adhesion on PDMS pillars. On the left side a schematic image of the stamped area (grey) on the pillars is shown. Figures (A) and (B) are an enlargement, which is denoted by the thick lined box in the schematic picture. (A) Fluorescent image of streptavidin Alexa 488, which adheres to the biotin-BSA. Over the whole sample the pillar side walls and the bottom of the pillar substrate are passivated with BSA. Outside the stamped area also the pillar heads are effectively passivated by BSA. (B) Microtubules adhere to the biotin-kinesin, which only adheres to the stamped parts of the PDMS. Scale bar 20 μm

4.4 Microtubule networks and asters

In addition to the gliding assays, the pillar arrays are used to study network formation of microtubules. Biotinylated microtubules are employed to promote the adhesion of microtubules directly to the streptavidin coated pillar tops. Biotin-tubulin is incorporated into the microtubules during polymerisation. Via the biotin-BSA/streptavidin linkage these microtubules are attached to the pillar heads. The microtubules are crosslinked by the mitotic kinesin Eg5, without ATP present. For pillar gaps of about five μm it can be observed that two-dimensional networks are formed (fig. 4.8 A). By increasing the pillar gaps one gets to a regime where the pillars are too far apart to get effective global crosslinking of the microtubules. The crosslinking becomes local and on each pillar aster-like structures of microtubules are formed (fig. 4.8 B).

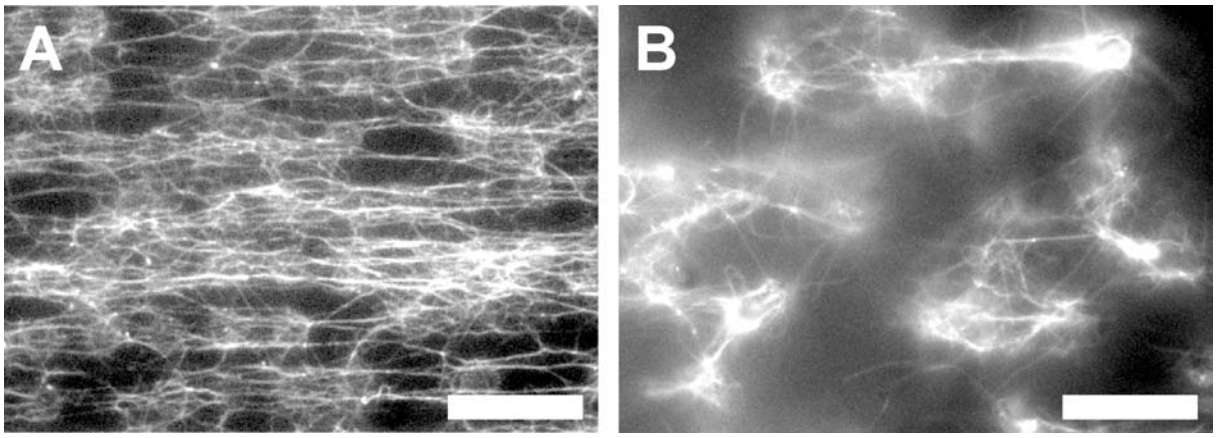

Fig. 4.8 Biotin-labelled microtubules crosslinked by Eg5. (A) Pillars with a minimum distance of 5 µm. On this part of the substrate the microtubules form a network. (B) Pillars with a minimum distance of 11 µm. On this part of the substrate the pillars are too far apart to serve as a scaffold for network formation, instead aster-like structures are formed. Scale bar 20 µm.

Networks and aster structures formed by microtubules are interesting to study spindle pole formation which precedes the pulling apart of chromosomes during cell division [Surrey *et al.*, 2001; Heald *et al.*, 1997]. During this process the microtubules are ordered in a controlled way, which resembles asters. It also resembles parts of the network which can be seen in figure 4.8 A. The pillar structures are ideal to study these asters as surface interactions are minimised, but at the same time anchoring points are present to immobilise the structures. In this way formation of the asters can be observed and force measurements can be performed when active molecular motors are added that will pull the microtubules along each other.

Acknowledgments

Thanks to T. Surrey (EMBL) for providing the proteins and for sharing his laboratory to perform the experiments.

Chapter 5

Cellular mechanics

5.1 Introduction

Adhesion to surfaces or to other cells is necessary for many cell types to perform specific functions. For instance migration of cells during wound healing and embryonic development can not take place without any type of adhesion. Cell migration takes place by exerting forces to the extracellular matrix and to exert these forces a contact with the environment is needed [Galbraith and Sheetz, 1998; Horwitz and Parsons, 1999; Balaban *et al.*, 2001]. To describe cell adhesion and migration a thorough understanding of the cellular mechanics is needed. Cellular mechanics is directly related to the mechanics of the cellular cytoskeleton, as discussed in previous chapters. This chapter focuses on the mechanical properties of cells as an entity.

In vitro adhesion of cells to substrates can be promoted by coating the substrate with extracellular matrix molecules, such as fibronectin. Fibronectin is a protein with specific binding sites for other matrix macromolecules and for receptors on the cell surface. It is a dimer consisting of two similar, but not identical, polypeptide chains linked by disulfide bonds. Some of the binding sites are for: self-association, collagen binding and cell binding. One of the cell binding domains is the tripeptide sequence Arg-Gly-Asp, also called RGD. The RGD sequence is recognised by cellular transmembrane adhesion proteins, the integrin receptors [Alberts et al., 2002]. These integrins are again connected to the intracellular cytoskeleton, which gives shape and rigidity to cells. RGD alone can bind cells comparable to the way fibronectin does this. The binding to extracellular matrix proteins enables a cell to get a firm contact with the surroundings and it represents a way to exert forces to the environment during contractile and migratory movement. Microscopic pillar arrays are used to study the effects of cell adhesion, migration and contraction. These pillar arrays serve as both a template for cellular adhesion and as force sensor.

Experiments are performed with human epithelial pancreas cancer cells, mouse fibroblasts and chicken heart muscle cells. In vertebrates the major tissue types are blood, nerve, lymphoid, muscle, epithelial and connective tissues [Alberts *et al.*, 2002]. Connective tissue and epithelial tissue are two extremes from the organisational point of view. In connective tissue the sparsely distributed cells (often fibroblasts) are embedded in a large extracellular matrix complex, with collagen, fibronectin and other fibers running in between the cells. It is the matrix which is responsible for a large part of the mechanical properties of

this tissue. Stress and strain of the connective tissue is taken up by the matrix rather than by the cells. The extracellular matrix is secreted by the fibroblasts it embeds.

Under normal conditions the cells in the connective tissue are not directly attached to each other. In epithelial tissue a completely different organisation is observed. Epithelial cells are lined up in a tight manner and are attached to each other by cell-cell adhesions. Most of the mechanical stress to which this tissue is subject, is taken up by the cells and their attachment points. Therefore a high amount of intracellular proteins are present in these cells and they cross the whole cytoplasm to make connections to neighbouring cells via transmembrane proteins. The extracellular matrix of epithelial tissue only takes up a small volume and consists of the basal lamina, a small mat lying below the epithelium. Epithelial cells line the inner wall of, for instance intestines. The first three tissue layers coming from the inside of intestine are epithelial tissue, connective tissue and smooth muscle tissue. In general epithelial cells cover, in a closed packed single cell layer or in multiple cell layers, surfaces and cavities.

This chapter is organised in the following way. After a section discussing the materials and methods, there are two sections discussing experiments with epithelial cells and with fibroblasts. Mechanical properties of muscle cells are discussed in the last section of this chapter.

5.2 Materials and methods

The gold disks on top of the silicon pillars become hydrophobic due to chemical modification of the gold by self-assembling alkanethiol monolayers (CH_3-$(CH_2)_{17}$-SH) [Mrkisch *et al.*, 1997]. The pillars are incubated in a 2 mM solution of octadecanethiol (Sigma-Aldrich) in ethanol for 12 hours. After rinsing with ethanol they are dried under a stream of nitrogen. These hydrophobic surfaces serve for specific adsorption of fibronectin (Sigma-Aldrich). Proteins normally consist of hydrophilic and hydrophobic domains. Due to hydrophobic interactions of parts of the fibronectin, this molecule adheres onto the alkanthiol coated gold disks. The pillars are incubated with fibronectin for 3 hours at a concentration of 25 µg/ml in Phosphate Buffered Saline (PBS). After washing with PBS, which removes the fibronectin that is not physisorbed, the fibroblasts are plated. The pancreas cells shown in figure 5.3 are plated directly on the pillars, without previous fibronectin functionalisation. The other pancreas cells are plated on fibronectin treated surfaces. The fibronectin functionalisation of the gold caps of the silicon pillars promotes preferential binding of the cells to the pillar heads. The rest of the substrate is less favourable for adhesion. The adhesion to the silicon can be totally inhibited by coating the silicon with a poly-ethylene-glycol (PEG) layer [Arnold *et al.*, 2004].

Panc-1 human pancreatic cancer cells are a kind gift of T. Seufferlein from Universitätsklinikum Ulm, Germany. GFP-actin transfected 3T3 swiss mouse fibroblasts are a kind gift from B. Wehrle-Haller, Université de Genève, Switzerland. Both the cell lines are maintained in DMEM supplemented with 10% fetal bovine serum (FBS) at 37 °C in a humidified atmosphere of 5% carbon dioxide. Pancreas cells are plated in serum free medium [Beil *et al.*, 2003]. Fibroblasts are plated in medium containing serum.

After a certain incubation time the cells are fixed, dehydrated and dried as described in table 5.1 As a last step before scanning electron microscope visualisation the cells need to be

covered by a layer of conducting material. Otherwise the SEM imaging is not possible because of charging effects.

Table 5.1 Fixing, dehydrating and drying of cells for SEM visualisation.

removal of medium			
wash with PBS (37 ºC)	this is an optional step to remove free proteins from environment		
glutaraldehyde fixing	2.5 % in PBS (37 ºC)	2 h	
wash 3x with PBS		10 min each	
dehydration with ethanol	70%, 80%, 90%, 96%, 100% ethanol successively, diluted in distilled water (except for the last step)	30 min each step	
critical point drying	in absolute ethanol	8 CO_2 cycles	Bal-tec CPD 030
carbon or gold sputtering	5 - 10 nm		Bal-tec MED 020

A slightly different method of fixation is used for the cells depicted in figures 5.3 and 5.4 A. At the indicated incubation time, cells are fixed with a solution consisting of 2.5 % glutaraldehyde, 0.1 M phosphat buffer, 1 % saccharose and a pH of 7.3. After dehydration with ethanol the cells are critically point dried and a layer of carbon is sputtered on top. Scanning electron microscopy is performed with a Zeiss DSM 962 microscope and a Zeiss Leo 1530 Gemini microscope.

Chicken heart muscle cells are prepared as described by Rutz [2003] and the preparation is only briefly described here. Heart muscle cells are isolated from chicken embryo of 9 day old eggs. The cells are plated in DMEM containing 5% FBS, 1% amphotericin, 1% L-glutamin and 1% penicillin/streptomycin at 37 ºC and 10% CO_2. After 24 hours the medium was exchanged for L-glutamin free medium and two hours later the cells started contracting spontaneously.

5.3 Pancreatic cancer cells

5.3.1 Effect of critical point drying on cells

Cells are normally imaged by phase contrast light microscopy, fluorescence light microscopy or by electron microscopy. In the case of light microscopy the cells can be imaged while being in a fluid medium. Electron microscopy is normally performed in vacuum and therefore the cells need to be dried. For water or a buffer solution under ambient conditions there is a clear interface between the fluid phase and the gas phase. This interface gets smaller and smaller during drying until it vanishes and only water in the gaseous phase is left. So during drying the liquid-gas interface has to pass all the structures in the liquid. The

hereby present capillary forces destroy all the fine details present on cell surfaces. A method to overcome this is critical point drying. At a temperature and pressure above the critical point there is no clear distinction between the gaseous and the liquid phase. This means that a fluid can be dried without passing any clear transition from liquid to gas and without the consequent destructing capillary forces of such a transition. Figure 5.1 shows a phase diagram of a simple substance with the trajectory to perform critical point drying.

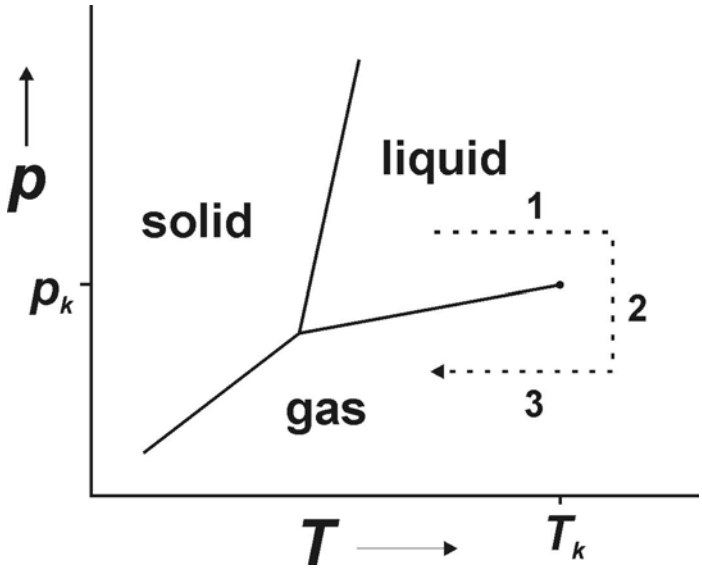

Fig. 5.1 Phase diagram of an element or a simple compound with the temperature T and the pressure p. The critical point is denoted by the critical temperature T_k and the critical pressure p_k. The dotted line shows the trajectory the solvent has to pass during critical point drying. 1) the solvent is heated, 2) the pressure is decreased, 3) the temperature is decreased. Now the solvent has turned into gas without passing a clear transition from liquid to gas.

Water has a critical point of p_k = 229 bar and T_k = 374 °C. These conditions are difficult to achieve with standard laboratory equipment. So water is not a suitable medium for critical point drying and another solvent needs to be found that can be used. Carbon dioxide is more favourable as a transition medium than water. CO_2 has a critical point of p_k = 74 bar and T_k = 31 °C. These conditions are not so difficult to achieve.

First the cell is dehydrated by exchanging the buffer solution for ethanol. This can be done at room temperature and a pressure of 1 bar. Next, the absolute ethanol, in which the cells are immersed, needs to be exchanged with liquid carbon dioxide. The samples can now be placed in a chamber, which resists to high pressures and is partially filled with absolute ethanol. The next step is to decrease the temperature to 10 ºC. Now liquid CO_2 is flowed into the chamber and when it is completely filled half of the ethanol-CO_2 mixture is released. This process is repeated several times until there is almost only liquid carbon dioxide present in the chamber. Now the temperature is increased to 40 ºC and the CO_2 passes from the liquid phase to the undefined liquid-gas phase. Next the pressure can be decreased slowly and the mixture turns into gaseous CO_2 at atmospheric pressure. The temperature can be decreased and the dried sample can be taken out of the chamber. Now the cells are dried, but they still have the fine structures that were present when they were still alive. For visualisation under the

electron microscope the cells need to be covered with a small layer of conducting material, like carbon or gold.

Figure 5.2 shows examples of cells that are air dried and that are critical point dried. A clear difference can be seen in the fine structure on the membrane. Moreover the air dried cell (fig. 5.2 A) is completely flat, but the other cells kept their original three dimensional structure they had when they were still alive. These examples clearly show that critical point drying is indispensable when studying cellular structures under the electron microscope.

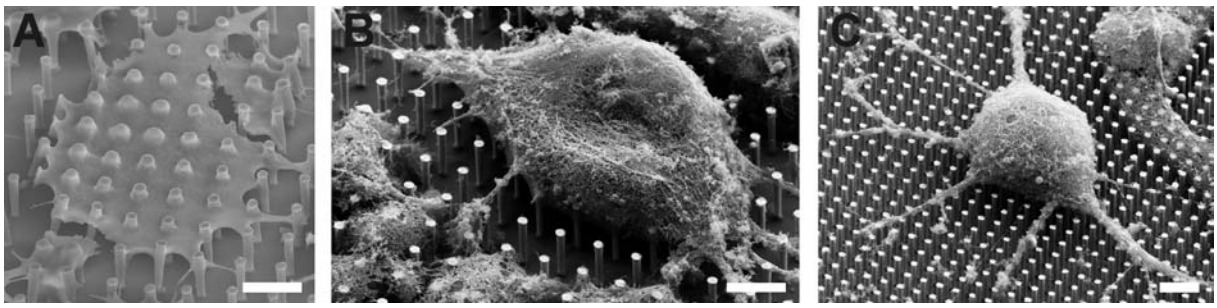

Fig. 5.2 Difference between air drying and critical point drying of cells. (A) Air dried epithelial cell. The cell is totally flat, no fine structure can be seen on the cell surface. On the left side in the middle of the image, it can be seen that a pillar is broken due to the high forces that are exerted during fixing and drying of the cells. (B) and (C) Critical point dried epithelial cells. When performing a critical point drying procedure on fixed cells many of the fine surface details are made visible. Next to the fine structure on the cell membrane also thin extending filopodia can be seen. Pillar gap in (A) and (B) 5 µm, pillar gap in (C) 2.5 µm. The pillar diameters are 1.5 µm, 1.4 µm and 1.9 µm respectively for (A), (B) and (C). Sample A is fixed one day after plating, samples B and C five days after plating. Silicon pillars with gold disks that are fibronectin coated are used. Electron micrographs with an angle of view of 45º, scale bar 10 µm.

5.3.2 Pillars embedded by pancreas cells

The stiffness of the silicon pillars is too high to resolve the bending induced by the traction forces of living cells. However after fixing and critical point drying of the cells the pillars did substantially bend. This is probably due to the removal of the water in the cell during the drying procedure. As cells consist mainly of water, they normally shrink during drying. Instead of rupturing, the dried cell cytoskeleton exerts high forces on the pillars, upon which these bend. These forces can be calculated using equation 2.1. Figure 5.3 shows a critical point dried cell with the exerted forces printed next to the pillars. This is an example of how drying can increase the stiffness of cells. The living cell was not able to bend the pillars substantially. Interestingly, it has been shown by Atomic Force Microscope (AFM) measurements that even the fixation itself (without drying) increases the stiffness of cells [Hoh and Schoenenberger, 1994; Braet *et al*., 1998].

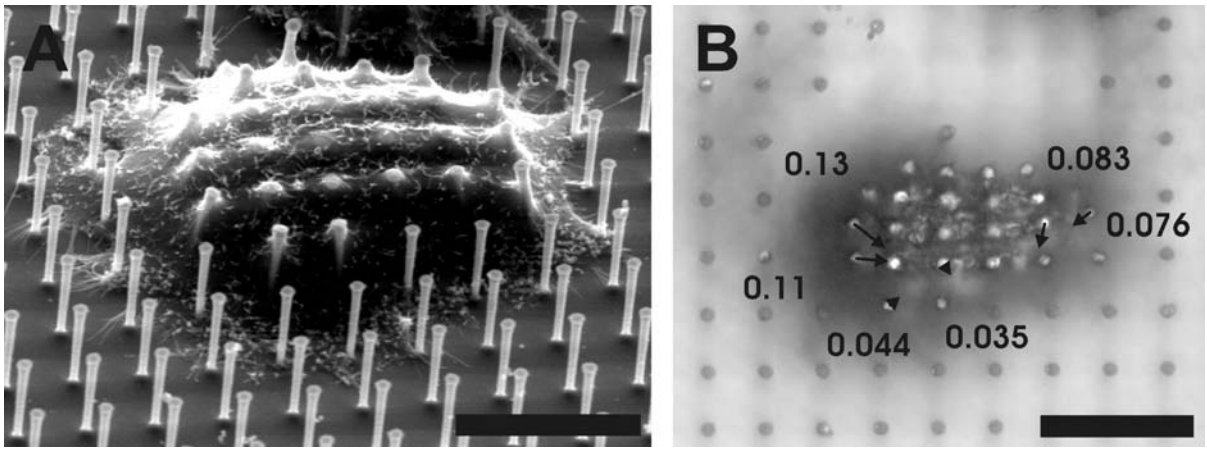

Fig. 5.3 Penetrating cell and forces that play a role during drying of cells. Critical point dried pancreatic cancer cell in between an array of silicon pillars. (A) Electron micrograph at 45° angle. (B) Dark field microscopy image of the dried cell, top view. Next to several pillars the force that bends them is printed in mN (error 25 %). Pillar stiffness is calculated as 25 ± 6 N/m. The pillars are not coated with fibronectin, they are only sterilised before plating the cells. Fixation is performed after 15 hours. Pillar gap is 5 µm and pillar diameter is 1.2 µm, scale bar 20 µm.

Comparing figure 5.2 B with figure 5.3 A it can be seen that the same cell type, on pillar arrays with the same inter pillar distance of 5 µm, can grow on top of the pillars or can embed the pillar arrays. The difference between these experiments is that for the former the pillar heads were fibronectin coated (fig. 5.2 B) and that for the latter there was no fibronectin functionalisation (fig. 5.3 A). Apparently the cells are so much attracted to fibronectin that they will guide their growth towards the places where fibronectin is present, even when the have to bridge distances of 5 µm without any possible adhesion. This means that the filopodia that the cells extend must be rigid over at least 5 µm. Probably will the actin filaments inside the filopodia be supported by other proteins or they will be crosslinked with each other to obtain the desired stiffness. As indicated in figure 5.3 A, there is no stimulus for a cell to remain on the pillar tops when there is no fibronectin present on the pillar heads. In this case they just easily spread by using the whole substrate surface, seemingly undisturbed by the presence of the pillars. Tan *et al*. [2003] observed a similar behaviour of smooth muscle cells on PDMS pillars. Without specific fibronectin coating the cells are in between the pillars, with specific fibronectin coating of the pillar heads the cells lie on top of the pillars.

5.4 Fibroblasts

After plating fibroblasts on specifically functionalised silicon pillars with a small inter pillar gap it can be observed that cells have a preference to remain on top of the pillars (fig. 5.4 A). However, fibroblasts plated on epoxy pillars placed at double spacing, do sink in between the pillars (fig. 5.4 B). This will be partially due to the increased spacing, but also due to the fact that the epoxy pillar heads can not be specifically functionalised with fibronectin. This because the epoxy pillars are homogeneous and do not have a gold cap, like the silicon pillars. The whole substrate is evenly functionalised and the cell spans the volume

in between a few pillars. The cell seems however to be hindered by the pillar substrate and does not spread completely. In contrast, the pancreas tumor cells fill a big volume in between the pillars and they completely enclose many of them (fig. 5.3 A), seemingly unhindered by the presence of the pillars. This demonstrates different mechanical behavior of fibroblasts and pancreas tumor cells. Such a difference should be correlated with a difference in cytoskeletal architecture. In pancreas cells the intermediate filament keratin makes up for 5% of the total protein amount. This keratin extends from the perinuclear region towards the periphery of the cell and it is (partially) responsible for cell shape and rigidity. Actin is also present, but it seems to have less influence on the mechanical properties of the cell [Beil *et al.*, 2003]. In fibroblasts actin plays a more important role in the cellular rigidity. A difference between intermediate filaments and actin is that the latter is stiffer. However, the stiffness of cells is also dependent on the amount and types of crosslinking of the cytoskeletal filaments. This means that crosslinking, filament rigidity and the total filament fraction in the cytoplasm should be taken into account when analysing the differences in mechanical properties of different cell types.

The changing inter pillar spacing plays a role in the different results shown in figure 5.4. However the functionalisation is surely a key difference as previously shown for the pancreas epithelial cells. By using silicon pillars it is straightforward to functionalise the gold capped pillar tops and let the fibroblasts adhere to the pillar tops (fig. 5.4 A). However, using epoxy pillars it is difficult to selectively functionalise the pillar tops, because the pillar top and the rest of the pillar are made of the same material. Fibroblasts plated on these pillars grow in between the pillars. Figure 5.4 B shows how the nucleus of a cell is deformed by the pillars.

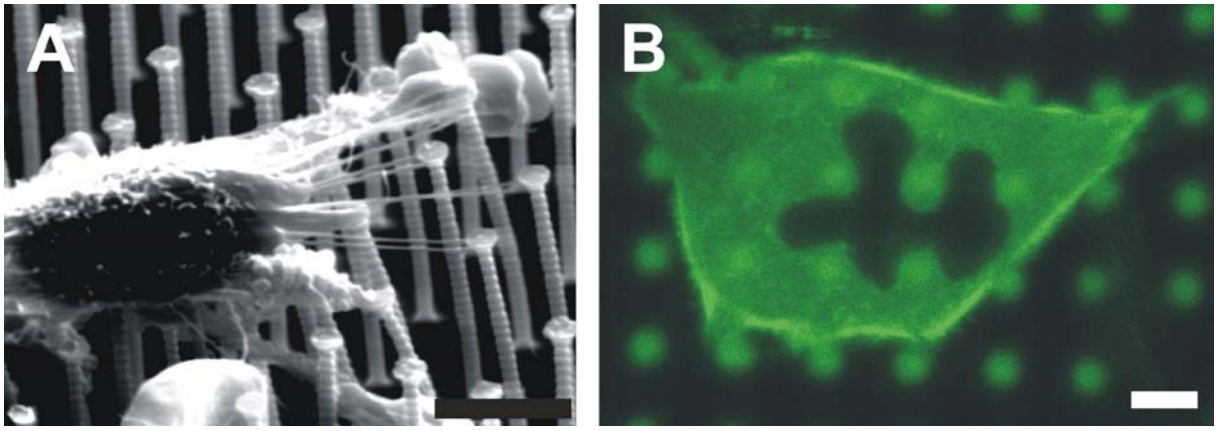

Fig. 5.4 Fibroblasts on different substrates. (A) Electron micrograph (viewing angle 45°) of fibroblast on top of silicon pillars. The gold disks on top of the pillars are functionalised with fibronectin. The cell grows on top of the pillars, even without passivating the silicon with PEG. Fixation is performed after 15 hours. Inter pillar gap is 2.5 μm, the pillar diameter is 0.7 μm and the aspect ratio of these pillars is 20 : 1. The force with which the pillars on the right of the image are bent is about 2 μN. Pillar stiffness is calculated as 1.4 ± 0.4 N/m. (B) Fibroblast in between epoxy pillars. The whole substrate is functionalised with fibronectin. Top view of living GFP-actin cell imaged with fluorescence confocal microscopy. The focus is on the pillar top. Inter pillar gap 5 μm and pillar diameter 2.5 μm. Scale bar 5 μm.

Because of the low compliance of the silicon pillars and the high fluorescence background of the epoxy pillars, further experiments are mainly conducted with PDMS pillars. These pillars can be functionalised by putting a droplet of fibronectin, or other extra cellular matrix molecules, on top of the pillars. Due to the hydrophobicity of PDMS pillar substrates such a droplet will not run in between the pillars and selective functionalisation can be obtained. A further advantage of PDMS is that it is transparent and non-fluorescent, which results in less background due to reflections during fluorescence microscopy. Cells plated on top of the PDMS pillar arrays do bend the pillars and the resuling displacement of the pillar heads can be followed by light microscopy. The following section discusses chicken heart muscle cells that are plated onto PDMS pillars and as a result from their periodic contraction the pillars are bent.

5.5 Heart muscle cells

There are three basic types of muscle cells found in vertebrates: skeletal, smooth and cardiac muscle [Lodish *et al*., 1999]. Skeletal muscle has a striated appearance and is capable of rapid, short-term contractions. These muscles connect the bones in arms and legs and they are used in complex activities like walking. Skeletal muscle is built up from myofibres, which are subdivided in myofibrils. The myofibrils consist of end-to-end packed sarcomeres and these sarcomeres consist of many parallel myosin fibres, alternated with parallel actin filaments oriented in the same direction as the myosin fibres. In the middle of the sarcomere, observed from a direction perpendicular to the fibres, the myosin fibres are present and a bit to the left and a bit to the right of the middle the actin filaments start. The actin filaments on both sides end in the z-disk, a fibre lattice that anchors the actin plus ends. The F-actin continues on the other side of the z-disk to form the next sarcomere, where there are again myosin fibres in the middle. Contraction takes place by the relative sliding of the myosin fibres compared to the actin filaments.

Smooth muscle cells are present around internal organs like intestines and large blood vessels. Smooth muscle is made up of loosely connected cells with a single nucleus. The cytoplasm of these cells is packed with bundles of actin and myosin filaments. Smooth muscle cells function in involuntary movements and / or autonomic responses. They contract and relax slowly compared to skeletal muscle and they are capable of sustained, long-term contraction.

Heart or cardiac muscle cells have a unicellular structure like smooth muscle cells and the striated structure of skeletal muscle. However, this is a branched striated structure, unlike the straight striated structure of skeletal muscle. The behaviour of cardiac muscle can be regarded as that of slow skeletal muscle. Cardiac cells are connected to each other by intercalating disks. As for smooth muscle the movement of heart muscle cells is normally involuntary.

Chicken heart muscle cells, isolated from 9 day old embryos, are directly plated onto PDMS pillar arrays. When the plating medium is exchanged for a medium without L-glutamin, these cells start to contract spontaneously with a frequency of 1 - 2 Hz. The forces these cells exert are relatively large and the contracting cells can easily bend the PDMS pillars on which they are plated. By imaging the cells via transmission light microscopy the bending of the pillars is recorded. The exerted forces can be easily calculated from the pillar top displacements. Figure 5.5 shows some images of the contracting cell. The force the cells exert

is depicted by arrows, which are drawn into the image. Cells supposedly exert forces to their environment only at focal adhesions and the focal adhesions do only make up for a certain amount of the contact area between cells and surfaces. Balaban *et al*. [2001] plated muscle cells on elastic substrates and analysed the forces the cell exerts in relation to their focal adhesions. Cells with fluorescently labelled vinculin were used. They found a stress of 2 - 5 $nN/\mu m^2$ for the focal adhesion sites, where the focal adhesion site was defined as vinculin rich areas. Vinculin is a protein mainly present in focal adhesions, so this is a reasonable assumption.

The pillar substrate forms a special surface for the cells. Because the cells can not adhere in between the pillars, there can only be forces exerted onto the pillar heads. It follows that there are only focal adhesions on the pillar heads. As the area where the cells can build focal adhesions is greatly reduced, it is a reasonable assumption that most or all of the pillar head surface is used as focal adhesion site. Assuming that a pillar has a top surface of 16 μm^2 and that the focal adhesions cover the whole pillar top surface, a maximum stress of 4 $nN/\mu m^2$ is found for the focal adhesion sites. This is in good agreement with the results of Balaban *et al*. In a different experiment Tan *et al*. [2003] cultured smooth muscle cells on top of pillar arrays and they also found stresses of about 5 $nN/\mu m^2$ exerted onto the pillar heads. Apparently the maximum exerted stresses are similar for heart muscle cells and for smooth muscle cells.

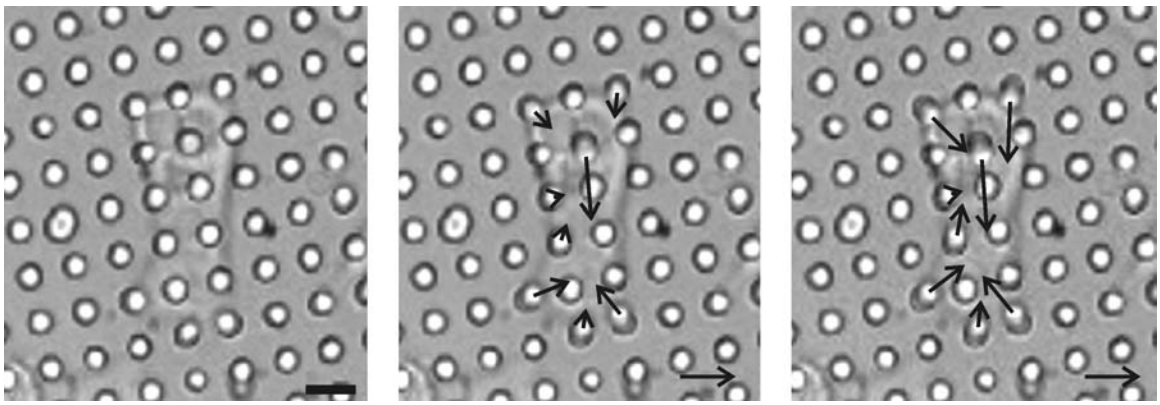

Fig. 5.5 Beating cardiac muscle cells on PDMS pillars. The beating frequency is about two Hz. The first image shows the relaxed cell on the pillars. The second image shows the onset of contraction. At the third image the cell is completely contracted. After the third image the cell relaxes and a situation as in the first image is obtained again. This cycle is periodically repeated. The arrows denote the force, which is exerted onto the pillars. An increase in exerted force can be seen from the second to the third image. The inter pillar gap is 5 µm and the pillar diameter is 4.5 µm. The pillar stiffness is calculated to be 0.018 ± 0.005 N/m. Transmission light microscopy images. The scale bar in the first image denotes 10 µm, the arrow in the lower right corner of the second and the last image denotes a force of 50 nN.

Acknowledgments:

Thanks to the group of P. Walther (Universität Ulm) for help with cell fixation, critical point drying and electron microscopy. R. Kemkemer and A. Micoulet (Universität Heidelberg) are thanked for introduction to cell culturing. C. Rutz (Universität Heidelberg) is

thanked for the heart muscle cell experiments. Thanks to T. Seufferlein (Universität Ulm) and B. Wehrle-Haller (Université de Genève) for providing the pancreas cells and the fibroblasts respectively. C. Kempendorf (Universität Heidelberg) is thanked for support with critical point drying.

Chapter 6

Discussion

Two dimensional arrays of pillars are microfabricated from (1) silicon by anisotropic etching, (2) optically transparent, fluorescent photo resists and (3) crosslinked PDMS. These micropillar force sensor arrays are used in a wide range of applications, on the subcellular and on the cellular level. For instance, from mechanical studies of single biofilaments to bundle dynamics, to the formation of two dimensional networks of actin, to whole cell mechanical studies. The production process of the pillar arrays is different for each type. However, for all these methods, the first step is photolithography-based. The silicon pillars are subsequently produced by Reactive Ion Etching (RIE), where the etch masks are 80 nm thick gold disks. The epoxy-based resist pillars are ready to use after photolithograpy. The polydimethylsiloxane (PDMS) pillars are formed by mixing the polymer with crosslinker and pouring this mixture into cylindrical holes, which are produced by photolithography.

The dimensions of the pillars can be easily tuned by changing the parameters of the photolithographical process. The following range in dimensions is used: diameter 0.5 - 5 µm, height 10 - 20 µm and inter pillar spacing 2.5 - 50 µm. The different pillars have different stiffnesses due to the variety in dimensions and in material they are made of. From a high to a low stiffness these pillars are respectively made of epoxy, silicon and PDMS. Where the former two are ideal to study fixation and drying forces of cells, the PDMS is ideal to study traction forces of living cells. Preliminary results with the production of pillars made from crosslinked polyethylene glycol (PEG) are promising. This material is flexible enough to study dynamic forces in motor protein crosslinked biofilament networks. Such type of experiments will be performed in the future. In the static configuration the silicon, epoxy and PDMS pillar substrates are used to study protein filament dynamics.

The two dimensional arrays of slender pillars open novel possibilities to assemble biofunctional filament systems on patterned surfaces. Such assemblies can be easily manipulated with biofunctional agents, like crosslinking proteins for biopolymers, since the access to the biofunctional system is not hindered by surfaces as for biomimetic systems deposited directly on solid surfaces. The persistence length of a single actin filament is determined by performing a Fourier analysis of the fluctuation modes of a freely suspended filament in between two pillars. The results show a good agreement with literature. Quasi two dimensional actin networks, crosslinked by the passive actin binding protein filamin, are constructed on top of pillar arrays. These systems can serve as a model for the cellular actin cortex, which is also a locally quasi two dimensional network. Whereas in cells it is difficult to separate all the contributions to the mechanical properties of the actin cortex, this is easily

controllable for an in vitro network. In the present work, it is shown that the pillar arrays enable the design of locally anchored networks of actin bundles, which are reminiscent of actin networks spanned between focal contact complexes in cells. The model system is expected to enable detailed studies of the mechanical properties of such networks under controlled boundary conditions. For instance, the bending modulus of actin bundles can be measured by fluctuation analysis.

Crosslinking of actin filaments is not only performed by the passive actin binding protein filamin. Actin crosslinking is also initiated by filaments of the motor protein myosin II. For this purpose the myosin is fluorescently labelled to determine the position of the myosin II in the actin network. The fluorescent marker attached to the myosin allows an accurate localisation of the motor on the actin filaments. It is observed that the myosin binds regularly all over the actin filaments. When ATP is added, the motors start producing force strokes and they subsequently detach from the actin filaments. In this way the crosslinks are removed and the bundles are dissociated into single filaments.

Next to crosslinking of actin filaments by myosin II also crosslinking with different divalent cations is performed. The threshold ion concentrations above which these divalent cations start to initiate actin bundling are determined. The following sequence lists the ions used, ordered by descending bundling threshold concentration: magnesium, calcium, barium, manganese, nickel, zinc and copper. Magnesium ions start to initiate the bundling of actin filaments at concentrations of about 14 mM, copper already turns actin filaments into bundles at a concentration of about 1.5 mM. By exchanging the buffer solution for a solution with low salt level, the crosslinks are removed again. Next to the bundling experiments the transport properties of myosin V motors, a processive motor protein, are quantified on networks. Until now these experiments have been hindered by the complex architecture of the cellular cytoskeleton. The pillar substrate approach offers excellent possibilities to study transport phenomena in two dimensional networks.

Microtubules gliding over kinesin coated pillar heads are shown to gap bridges of over 10 μm. This is not possible with actin, which will be due to the big difference in bending stiffness of actin filaments and microtubules. Actin filaments are much more flexible than microtubules, which explains why the stiff microtubules can glide from one pillar head to the other and the actin filaments are not able to do this. The high stiffness of microtubules is important in cells. For instance, to give rigidity to the axons of neurons and for positioning the spindle pole during cellular division.

The velocity of the gliding microtubules shows a wider distribution on PDMS pillars than on flat glass. An explanation for this is that the gliding microtubules experience less friction on the pillars, because there is less surface present which could hinder the movement. The result can be an increase in the velocity. On the other hand, it will happen that a gliding microtubule that reaches the next pillar will bump into this pillar when the microtubule fluctuates downwards due to random brownian motion. That will brake the moving microtubule and this will result in a reduced velocity. These two effects can explain the wider velocity distribution on pillars than on flat glass. It is shown that next to two dimensional networks of actin also comparable networks of microtubules can be formed. These microtubule networks are crosslinked by the kinesin motor Eg5.

Mouse fibroblasts, human pancreatic cancer cells and chicken heart muscle cells are shown to adhere to the pillar arrays. Depending on functionalisation of the pillar heads the cells either adhere to the top of the pillars or in between the pillars. Fibroblasts and epithelial cells are easy to cultivate on top of functionalised gold capped silicon pillars. The filopodial extensions of migrating fibroblasts can be seen on top of the pillar arrays. In between these

extensions the spread lamellipodia are present. The filopodia of the cells are shown to be able to gap distances of over 5 μm without any adhesion. This in contrast to gliding assays of single actin filaments over myosin coated pillars. That indicates that the actin filaments in the filopodia are somehow strengthened to obtain a bigger stiffness. During fixation and drying cells shrink as a result from a changing cellular structure and the loss of the intracellular water. The forces that play a role in these processes are determined by using silicon pillar arrays.

Epoxy pillars turn out to be suitable for studying single filament dynamics, but not for cultivating fibroblasts on top. Characteristic for epoxy pillars is that they are fluorescent over the whole visible wavelength regime. This is advantageous for localising the pillars during fluorescent imaging. However, the resulting high background due to these pillars, comes in as a disadvantage when recording high resolution images of fluorescent structures lying on the pillar tops.

Heart muscle cells are cultivated on top of flexible PDMS pillars. These muscle cells contract regularly on the pillar array, which can be imaged by live cell optical microscopy. The forces these living cells exert during contraction, results in a significant bending of the pillars. Analysing the bending gives the values for the force gradient pattern over the cell surface during contraction. The maximum exerted force per area of focal adhesion is estimated to be 4 $nN/\mu m^2$.

At the present state of the technique the smallest diameter of the pillars is 0.5 μm. Work is in progress to extend the technique to obtain pillars of nanometer diameter by epitaxial growth of ZnO on sapphire substrates [Haupt *et al.*, 2003]. Furthermore the production of pillars made from more elastic materials, like crosslinked polyethylene glycol, is in progress. Such pillars will allow for observing the bending of pillars under the tension of the two dimensional F-actin network including motor proteins. Analysing the force field of contracting motor-actin networks is not trivial. It is a mathematical underdetermined problem to evaluate the force field given the pillar displacements. Mohrdieck *et al.* [in preparation] show with a theoretical description that the pillar arrays are a force gradient sensor and not a force sensor. These considerations need to be taken into account when analysing the pillar displacements.

In summary it is shown that it is possible to fabricate micrometer sized pillar arrays by different techniques. The arrays are suitable for studying single filament dynamics and network formation of actin and microtubules interacting with passive and active filament binding proteins. Also transport properties of molecular motors and cation bundling of actin filaments is studied. Moving from the subcellular level to the cellular level, it is shown that whole cells are cultured on top of these pillars and that the exerted surface forces are evaluated.

Samenvatting

Dit werk beschrijft de fabricatie van zuilenmatrices, in micrometer grootte, die van verschillende materialen gemaakt zijn: siliciumzuilen met een bovenkant van goud, zuilen van fotolak op glas en zuilen van polydimethylsiloxaan, een polymeer. De eerste stap tot het maken van al deze zuilen is fotolithografisch. Daarna komen, in het geval van de siliciumzuilen, etsstappen. De fotolakzuilen zijn klaar voor gebruik na de fotolithografie. Voor de polydimethylsiloxaanzuilen wordt een mengsel van dit polymeer met een crosslinker in cilindrische gaten uit fotolak gegoten en daarna bij 65 ºC gebakken. Na vier uur kunnen de hard geworden zuilen uit de mal getrokken worden. De zuilen kunnen met verschillende dimensies gemaakt worden. Zo zijn er zuilen met diameters van 0,5 µm tot 5 µm, hoogtes van 10 tot 20 µm en zuilenafstanden van 2,5 µm tot 50 µm gebruikt. De zuilensubstraten kunnen als krachtsensor gebruikt worden door de verbuiging van de zuilen, onder het aanleggen van een kracht, te meten. In afnemende stijfheid zijn de zuilen gemaakt van fotolak, silicium en van polydimethylsiloxaan (PDMS). Naast het onderscheid in stijfheid hebben de verschillende substraten zo hun eigen specifieke voordelen. De fotolakzuilen zijn fluorescent en dus goed te lokaliseren tijdens fluorescentie lichtmicroscopische experimenten. Het voordeel van de siliciumzuilen is dat ze makkelijk selectief functioneel te maken zijn, doordat ze op de bovenkant een gouden schijf hebben en de rest van het substraat van silicium is. Deze twee verschillende materialen kunnen door specifieke oppervlakte-chemische processen verschillend behandeld worden. De PDMS substraten zijn erg flexibel en ook transparant, wat de lichtmicroscopische opnames vergemakkelijkt. De zuilenoppervlakken zijn gebruikt om mechanische eigenschappen van cellen en van intracellulaire componenten te bestuderen.

Veel menselijke en dierlijke cellen zijn in hun natuurlijke omgeving aan een oppervlak gebonden. Ook in vitro kunnen deze cellen aan oppervlakken hechten en daarover bewegen. Om zo'n beweging tot stand te brengen moet er een kracht op het oppervlak uitgeoefend worden. Hiervoor en ook om cellen een specifieke vorm te geven, moeten de cellen een skelet hebben, het zogenaamde cytoskelet. Dit bestaat uit de eiwitpolymeren actine, microtubuli en intermediaire filamenten. Deze polymeren, die verschillende stijfheden hebben, zijn aan elkaar en aan verschillende specifiek bindende eiwitten gebonden. Actine filamenten geven aan veel cellen vorm en stijfheid en doen dat onder meer door een quasi-tweedimensionaal netwerk onder het membraanoppervlak te vormen. Dit netwerk, dat de actine cortex genoemd wordt, wordt door passief en actief bindende eiwitten bij elkaar gehouden.

Om de mechanische eigenschappen van dit netwerk gecontroleerd te onderzoeken is een quasi-tweedimensionaal netwerk nagebootst op de bovenkant van de zuilenoppervlakken. Zo'n netwerk is een model voor de actine cortex in cellen. Het voordeel van in vitro experimenten aan deze netwerken is, dat alle parameters goed gecontroleerd kunnen worden. In vivo is het onmogelijk om de invloeden van alle eiwitten te controleren, maar in vitro is dat goed mogelijk. De hier besproken netwerken zitten alleen vast aan de bovenkant van de zuilen en hangen daartussen vrij als een brug. Dit is bewerkstelligd door de zuilenhoofden selectief

functioneel te maken en de rest van het substraat passief te maken. Doordat de totale oppervlakte van de zuilenhoofden kleiner is dan de oppervlakte van een vlak substraat met een vergelijkbare grootte als de zuilensubstraten, is de wisselwerking van de filamenten met oppervlakken geminimaliseerd. De tweedimensionale actine netwerken zijn gebruikt om de beweging van myosine V motoreiwitten te bestuderen. Dat zijn actief bindende eiwitten. De motoreiwitten familie van myosines bestaat uit grote eiwitten die zich gericht over filamenten kunnen bewegen, door het zetten van stappen, met als energiebron adenosinetrifosfaat (ATP). Deze beweging wordt bijvoorbeeld gebruikt voor intracellulair transport en voor het samentrekken van spieren. In cellen is het moeilijk om de bewegingen van deze motoren in netwerken te onderzoeken. Daarom is een aanpak met tweedimensionale netwerken op zuilen ideaal om dit transport te onderzoeken.

Naast het onderzoek aan eiwitmotoren zijn er Fourier analyses uitgevoerd van fluctuerende actinefilamenten die tussen twee zuilen opgehangen zijn. Hieruit kan de buigstijfheid van dit polymeer bepaald worden. De gevonden waarde stemt overeen met de waardes die in de literatuur beschreven zijn. Zulke metingen kunnen in de toekomst waarschijnlijk ook met bundels van actinefilamenten gemaakt worden. Actinebundels zijn belangrijk in cellen, omdat ze zogenaamde "stress fibers" vormen waardoor cellen krachten op oppervlakken kunnen uitoefenen. Dit soort bundels wordt in vitro gemaakt door enkele actinefilamenten aan elkaar te binden met behulp van passief en actief actine bindende eiwitten. Deze eiwitten, zoals filamine en myosine II, hebben twee bindingsplekken voor actine en kunnen zo twee filamenten met elkaar verknopen. Hiernaast is het ook mogelijk om filamenten met behulp van tweewaardig positieve ionen aan elkaar te binden. Actine filamenten hebben een hoge negatieve lading en stoten elkaar normaal gesproken af. Indien er een hoge concentratie aan tweewaardig positieve ionen aanwezig is, bezetten die de actinefilamenten in een zó hoge dichtheid dat ze voor andere actinefilamenten aantrekkelijk worden. Zo kunnen dus ook bundels gevormd worden.

De binding van eiwitten, zoals filamine aan actine, kan niet zo makkelijk opgeheven worden. Dit betekent dat netwerken of bundels van actine-filamine niet makkelijk op te lossen zijn. Dit is anders voor de binding van motoreiwitten, zoals myosine II, aan actine. Zonder ATP in de bufferoplossing gedragen deze eiwitten zich als passief bindende eiwitten, zoals filamine. Als er echter energie in de vorm van ATP toegevoegd wordt, beginnen de motoren te lopen. Dit betekent dat ze, na het zetten van een stap, loskomen van de actinefilamenten. Nu is de binding dus opgelost en de actinefilamenten zijn weer alleen en ongebonden. Dit effect is geobserveerd voor actinefilamenten die door myosine II verbonden zijn op de bovenkant van de zuilensubstraten. Het is ook eenvoudig de binding van actinefilamenten die door tweewaardig positieve ionen verbonden zijn, ongedaan te maken. Dit kan eenvoudig bewerkstelligd worden door de bundels in een oplossing met een veel lagere concentratie van ionen te brengen. De bundels lossen zich dan vanzelf op en men heeft de enkele filamenten weer terug.

Eén van de andere eiwitfilamenten in cellen, de microtubuli, zijn veel stijver dan actine. Ze zijn onder andere belangrijk voor intracellulair transport van membraanblaasjes, voor de stijfheid van axonen van zenuwcellen en voor het uit elkaar trekken van de chromosomen tijdens de celdeling. Ook microtubuli hebben geassocieerde eiwitten die gericht over deze filamenten kunnen lopen. Deze zogenaamde kinesine motoren zijn aan de zuilenhoofden vastgemaakt via biotine-streptavidine bindingen. Wanneer microtubuli met ATP toegevoegd worden in de stromingscel, ziet men dat de microtubuli door de kinesine motoren van de ene zuil naar de andere zuil doorgeschoven worden. De microtubuli kunnen zonder problemen afstanden van meer dan 10 μm overbruggen. Met actine filamenten zijn

zulke experimenten niet gelukt. Dit heeft waarschijnlijk te maken met het feit dat microtubuli veel stijver zijn dan actine filamenten.

Fibroblasten, pancreaskankercellen en hartspiercellen zijn bovenop de zuilensubstraten gecultiveerd. Dit is gedaan door de bovenkant van de zuilen selectief met fibronectine functioneel te maken. Fibronectine is een extracellulair matrixeiwit waar cellen zich aan vastbinden via het transmembraan eiwit integrine. Deze integrines clusteren samen en vormen de focale kontakten van cellen. Dit zijn de kontakten van cellen met de buitenwereld en de kontakten waardoor ze kracht kunnen uitoefenen op de omgeving. De cellen die bovenop de zuilen zitten en zich bewegen oefenen een kracht uit op de zuilen. Dit betekent dat de zuilen zullen verbuigen. Als de stijfheid van de zuilen bekend is en de verbuiging gemeten wordt, kunnen de uitgeoefende krachten bepaald worden. Zo zijn bijvoorbeeld de krachten gemeten van hartspiercellen op PDMS zuilen die zich periodiek, met een frequentie van 1 - 2 Hz, samentrekken. Deze experimenten zijn mogelijk op PDMS zuilen, omdat die zeer flexibel zijn. Siliciumzuilen, daarentegen, zijn te stijf om door levende cellen verbogen te worden.

Als de zuilenhoofden niet specifiek met fibronectine worden behandeld, zakken de cellen tussen de zuilen in. Dit soort experimenten zijn met siliciumzuilen uitgevoerd. Levend kunnen de cellen deze zuilen niet verbuigen. Als de cellen echter gefixeerd en gedroogd worden om ze onder de elektronenmicroscoop te bekijken, buigen de zuilen zich wel om. Blijkbaar zijn de krachten die een rol spelen bij fixeren en drogen van cellen veel groter dan de krachten die levende cellen uit kunnen oefenen. Levende cellen oefenen krachten op de omgeving uit in de grootte van 1 - 100 nN. Het fixeren en drogen van cellen levert krachten op van 1 - 100 μN.

Samengevat heeft deze studie laten zien dat substraten met regelmatig geplaatste zuilen van verschillende materialen gemaakt kunnen worden. Deze zuilensubstraten zijn succesvol ingezet om de mechanische eigenschappen van cellen te onderzoeken. Daarnaast zijn de substraten gebruikt om eigenschappen van tweedimensionale actine netwerken te onderzoeken. Deze netwerken kunnen met behulp van verschillende actine bindende eiwitten en ionen gemaakt worden. Tenslotte is nog aangetoond dat microtubuli stijf genoeg zijn om ze over zuilenhoofden te laten glijden met behulp van motoreiwitten.

Danksagung

Viele Leute haben dazu beigetragen, dass diese Arbeit zustande gekommen ist. Einigen von ihnen möchte ich meinen besondere Dank aussprechen.

Zuerst möchte ich mich bei meinem Betreuer Joachim Spatz bedanken, der mir die Möglichkeit gegeben hat, in vielen interessanten Themengebieten tätig zu werden. Auch unterstützte er mich dabei, meine Kenntnisse außerhalb unseres Institutes durch Zusammenarbeit mit anderen Forschungsgruppen und durch Tagungsbesuche zu erweitern.

Meine Promotion habe ich in Ulm begonnen, erst nach einigen Monaten zog ich mit Joachim nach Heidelberg. Für die angenehme Zeit an der Universität Ulm möchte ich den Leuten aus der Arbeitsgruppe von Prof. Möller, "der OC III", danken. Ich danke auch den ersten Arbeitsgruppenmitgliedern Alexandre, Marcell, Ralf, Simon, Roman und Fabiola für die nette Momente während und nach der Arbeit. Die Einladungen zum Abendessen von Alexandre, die Nächte mit Roman in der “Pufferbar” und mit Simon in vagen Kneipen werden noch lange in meiner Erinnerung bleiben. Die Squashspiele mit unter anderen Mark, Vanessa und Alexandre waren eine willkommene Ablenkung vom Mikroskopieren. Vor allem der Letztgenannte hat mich immer wieder die Lungen aus meinem Leib laufen lassen. Paul danke ich für seine Gastfreundlichkeit während der Jahre, die er in Ulm wohnte und für die Abende im “Kornhäusle”, wo wir immer so lecker aßen. Alfred Plettl möchte ich Dank sagen für die Hilfe bei den Arbeiten im Reinraum, Dieter Kaufmann dafür, dass er seine Zellkultur zur Verfügung stellte und der Gruppe von Prof. Walther für die Hilfe rundum das REM. Für das Ionenätzen bedanke ich mich herzlich bei Johannes Konle.

Der Aufbau der Labore in Heidelberg hat mehr Zeit in Anspruch genommen als erwartet, aber die Fürsorglichkeit unserer Sekretärin Frau Boczek - auch schon vor unserer Ankunft - hat “ihren Burschen” vieles erleichtert. Vertragsverlängerungen, Reisekostenabrechnungen, leckere Kuchen und vieles mehr hat sie effektiv und manchmal, bevor man selbst daran gedacht hatte, durchgeführt oder bereitet. In diesem Zusammenhang danke ich auch Herrn Hasslinger.

Für meinen einmonatigen Forschungsaufenthalt an der technischen Universität München danke ich Herrn Prof. Sackmann herzlich, es ist eine sehr lehrreiche Zeit gewesen. Hier begann auch die langjährige Zusammenarbeit mit Alexander Roth. Alex hat mich unter anderem in die Geheimnisse der Aktine eingeführt. Neben den bayerischen bleiben mir auch die außereuropäischen Arbeitstreffen mit ihm in angenehmer Erinnerung. Über die Jahre hinweg habe ich mich immer wieder mit den Münchnern zum Arbeiten zusammengefunden. Die Tage im Münchner Labor waren lang, aber ausserhalb des Arbeitsplatzes wurden sie meistens noch länger. Alex, der kleine und der große Laurent, Kheya und Nikita haben mich so gut in das Münchner Nachtleben eingeführt, dass daraus “zeitungsreife” Abende wurden.

Zudem möchte ich mich auch herzlich bei Monika Rusp, Frau Kirpal, Herrn Bärmann und Junshan Zhang für die Eiweißvorbereitungen bedanken, die mir während der Jahre gute Experimente ermöglichten.

Ich danke auch Frank Thiele und Camilla Mohrdieck aus der Gruppe von Herrn Prof. Arzt am Max-Planck-Institut für Metallforschung in Stuttgart für die spannende Diskussionen. Zusammen mit Frank führte ich interessante Experimente durch.

Bei Thomas Surrey vom Europäischen Molekular-Biologischen Labor (EMBL) in Heidelberg möchte ich mich für die erfolgreiche Zusammenarbeit an den Microtubuli bedanken. Auch den anderen Mitarbeitern danke ich für ihre Hilfe. Es hat Spass gemacht, am EMBL zu experimentieren. Die “Beer sessions” am Freitagnachmittag und das exzellente Mittagessen sind mir noch gut in Erinnerung. Außerdem traf ich viele sympathische Forscher beim “Runtertrampen” in die Stadt.

Die meiste Zeit meiner Doktorarbeit habe ich aber an der Ruprecht-Karls-Universität Heidelberg verbracht. Den Kollegen dort möchte ich herzlich für die Zusammenarbeit danken, insbesondere der “Säulenfraktion” Jens, Stefan G., Moyu und Christoph und der “Aktinfraktion” Christian, Jennifer, Simon, Albert und Stefan Q.. Der vorher schon erwähnte Franzose Alexandre M. hat mich immer wieder mit etwas zum Lachen und auch manchmal mit leckerem Essen versorgt. Das war sehr nett. Den “South-end-Brüdern” Roman und Marco danke ich für viele unvergessliche Momente: Roundabout bleibt in Erinnerung! Ada hat mir immer bei biologischen Fragen weiter helfen können. Jacques danke ich für die PEG-Herstellung und für die swingenden Konzerte. Anna war eine lustige Nachbarin und Tamas immer bereit, etwas zu erklären - zwar manchmal etwas unverständlich, aber meistens gut. Richard danke ich für die kleinen Sachen rund um die Arbeit, auch wünsche ich ihm viel Erfolg bei der nächsten Neuinstallation. Christian danke ich für mehrere erfolgreiche Ausflüge in die Pfalz und Roman dafür, dass sie unvergesslich geworden sind. Allen neuen Mitarbeitern in unserer Gruppe danke ich für die geselligen Grillabende und für den Wissenschafts- und Laberrababer-Austausch.

Zudem möchte ich Herrn Prof. Cremer als Gutachter dieser Arbeit danken und aus seiner Gruppe Roman Amberger für die nette Zusammenarbeit. Frau Prof. Pollerberg und ihr Arbeitskreis haben mir hilfreiche Einblicke in die Untersuchungen an der Fakultät für Biowissenschaften gegeben. Karsten, Chris und Blanka danke ich in diesem Zusammenhang besonders herzlich. Auch Frau Kempendorf darf nicht unerwähnt bleiben. Sie leistete mir Hilfe beim “Kritisch-Punkt-Trocknen”.

Neben meinen unmittelbaren Kollegen gibt es noch weitere Mitarbeiter am Institut der Physikalischen Chemie, denen ich Dank schulde. Die Werkstatt von Herrn Weiss hat stets gute Arbeit geleistet. Herr Jeschka und Herr Meinusch hatten immer ein offenes Ohr für Fragen rund um das Themenfeld Elektrotechnik. Hausmeister, Glasbläser und Putzfrauen haben mich immer freundlich angelächelt am frühen Morgen, um den Tagesanfang zu erleichtern. Matthias danke ich dafür, dass wir uns gegenseitig Mut zusprachen, Vergangenheitsdiskussionen führten, oder einfach "ouwehoerden". Das konnte dann meistens entweder im Labor oder an der Theke des “Storchennest(s)” stattfinden. Dem "chothu raja" Abbas danke ich für die netten Plaudermomente und die Schwimmstunden. Ein herzliches Extra-Danke für das kritisch Durchlesen und Korrigieren von Teilen dieser Arbeit geht an Ada, Jennifer, Eilif, Beri, Matthias, Abbas, Patrick, Tamas und Roman. Der Volkswagen-

Stiftung und der Alfried Krupp von Bohlen und Halbach - Stiftung danke ich für finanzielle Unterstützung.

Den DJs von “Radio Sunshine live” bin ich sehr verbunden für das Spielen von zahlreichen, guten Platten. Ob im Labor oder am Schreibtisch, die Nummern haben mich immer in gute Laune versetzt.

Außerdem möchte ich Wiebke dafür danken, dass sie mich durch eine Mischung von aufmunternden Worten und Kritik aus Phasen geringer Motivation oder sogar Verzweiflung herausgeholt hat. Wie man sieht, mit Erfolg. Zuletzt möchte ich meinen Eltern, meinem Bruder und meiner Schwester danken für die jahrelange Unterstützung und Geduld, die sie mir entgegen gebracht haben.

References

Alberts, B., A. Johnson, J. Lewis, M. Raff, K. Roberts, P. Walter (2002) *Molecular biology of the cell*, 4th ed., Garland Science, New York, USA

Ali, M. Y., S. Uemura, K. Adachi, H. Itoh, K. Kinosita Jr., S. Ishiwata (2002) *Nature structural biology*, Vol. **9**, p464-467

Arnold, M., E. A. Cavalcanti-Adam, R. Glass, J. Blümmel, W. Eck, M. Kantlehner, H. Kessler, J. P. Spatz (2004) *ChemPhysChem*, Vol. **5**, p383-388

Ayon, A. A., R. Braff, C. C. Lin, H. H. Sawin, M. A. Schmidt (1999) *J. electrochemical society*, Vol. **146**, p339 - 349

Balaban, N. Q., U. S. Schwarz, D. Riveline, P. Goichberg, G. Tzur, I. Sabanay, D. Mahalu, S. Safran, A. Bershadsky, L. Addadi, B. Geiger (2001) *Nature cell biology*, Vol. **3**, p466-472

Barlow, R. J. (1989) *Statistics*, John Wiley & Sons, Chichester, UK

Bausch, A. R., F. Ziemann, A. A. Boulbitch, K. Jacobson, E. Sackmann (1998) *Biophysical J.*, Vol. **75**, p2038-2049

Bausch, A. R., W. Moller, E. Sackmann (1999) *Biophysical J.*, Vol. **76**, p573-579

Bausch, A. R., U. Hellerer, M. Essler, M. Aepfelbacher, E. Sackmann (2001) *Biophysical J.*, Vol. **80**, p2649-2657

Bear, J. E., T. M. Svitkina, M. Krause, D. A. Schafer, J. J. Loureiro, G. A. Strasser, I. V. Maly, O. Y. Chaga, J. A. Cooper, G. G. Borisy, F. B. Gertler (2002) *Cell*, Vol. **109**, p509-521

Beil, M., A. Micoulet, G. v. Wichert, S. Paschke, P. Walther, M. B. Omary, P. P. v. Veldhoven, U. Gern, E. Wolff-Hieber, J. Eggermann, J. Waltenberger, G. Adler, J. Spatz, T. Seufferlein (2003) *Nature cell biology*, Vol. **5**, p803-811

Bell, E., B. Ivarsson, C. Merril (1979) *Proc. Natl. Acad. Sci. U.S.A.*, Vol. **76**, p1274-1278

Borukhov, I., R. F. Bruinsma, W. M. Gelbart, A. J. Liu (2001) *Phys. Rev. Lett.*, Vol. **86**, p2182-2185

Bowick, M., A. Cacciuto, G. Thorleifsson, A. Travesset (2001) *Phys. Rev. Lett.*, Vol. **87**, p148103_1-4

Braet, F., C. Seynaeve, R. de Zanger, E. Wisse (1998) *J. of Microscopy*, Vol. **190**, p328-338

Burton, K., D. L. Taylor (1997) *Nature*, Vol. **385**, p450-454

Cande, W. Z. (1986) *Methods Enzymology*, Vol. **134**, p473-477

Campbell, D. J., K. J. Beckman, C. E. Calderon, P. W. Doolan, R. M. Ottosen, A. B. Ellis, G. C. Lisensky (1999) *J. of chemical education*, Vol. **75**, p537-541

Chen, C. S., M. Mrkisch, S. Huang, G. M. Whitesides, D. E. Ingber (1997) *Science,* Vol. **276**, p1425-1428

Cheney, R. E. (1998) *Methods in Enzymol*ogy, Vol. **298**, p3-18

Craighead, H. G., C. D. James, A. M. P. Turner (2001) *Current opinion in solid state and materials science*, Vol. **5**, p177-184

Cunningham, C. C., R. Vegners, R. Bucki, M. Funaki, N. Korde, J. H. Hartwig, T. P. Stossel, P. A. Janmey (2001) *J. biological chemistry*, Vol. **276**, p43390-43399
DeBiasio, R. L., L. Wang, G. W. Fisher, D. L. Taylor (1988) *J. of cell biology*, Vol. **107**, p2631-2645
Dembo, M., T. Oliver, A. Ishihara, K. Jacobsen (1996) *Biophysical J.*, Vol. **70**, p2008-2022
Dichtl, M. A., E. Sackmann (1999) *New J. Physics*, Vol. **1**, p18
Dickson, B. J. (2002) *Science*, Vol. **298**, p1959-1964
Doi, M., S. F. Edwards (1986) *The theory of polymer dynamics*, Clarendon Press, Oxford, UK, p317
Dogterom, M., B. Yurke (1997) *Science*, Vol. **278**, p856-860
Dupuis, D. E., W. H. Guildford, J. Wu, D. M Warshaw (1997) *Journal of muscle research and cell motility*, Vol. **18**, p17-30
Eichenlaub-Ritter, U., J. B. Tucker (1984) *Nature*, Vol. **307**, p60-62
Elbaum, M., D. K. Fygenson, A. Libchaber (1996) *Phys. Rev. Lett.*, Vol. **76**, p4078-4092
Engel, J., H. Fasold, F.W. Hulla, F. Waechter, A. Wegner (1977) *Mol. Cell. Biochem.*, Vol. **18**, p3-13
Evans, E. (1993) *Biophysical J.*, Vol. **64**, p1306-1322
Faivre-Moskalenko, C., M. Dogterom (2002) *Proc. Natl. Acad. Sci. U.S.A.*, Vol. **99**, p16788-16793
Fenteany, G., P. A. Janmey, T. P. Stossel (2000) *Current biology*, Vol. **10**, p831-838
Frey, E. (2002) *ChemPhysChem*, Vol. **3**, p270-275
Fujime, S. (1970) *J. of the physical society of Japan*, Vol. **29**, p751-759
Fung, Y. C. (1993) *Biomechanics: mechanical properties of living tissues*, ed. 2, Springer, Heidelberg, Germany
Galbraith, C. G., M. P. Sheetz (1997) *Proc. Natl. Acad. Sci. U.S.A.*, Vol. **94**, p9114-9118
Galbraith, C. G., M. P. Sheetz (1998) *Current opinion in cell biology*, Vol. **10**, p566-571
Garcia, J. G., K. L. Schaphorst (1995) *J. investigative medicine*, Vol. **43**, p117-126
Gardel, M. L., M. T. Valentine, J. C. Crocker, A. R. Bausch, D. A. Weitz (2003) *Phys. Rev. Lett.,*, Vol. **91**, p158302_1-4
Geiger, B., A. Bershadsky (2002) *Cell*, Vol. **110**, p139-142
Gerbal, F., V. Laurent, A. Ott, M-F. Carlier, P. Chaikin, J. Prost (2000) *European biophysical J.*, Vol. **29**, p134-140
Gittes, F., B. Mickey, J. Nettleton, J. Howard (1993) *J. cell biology*, Vol. **120**, p923-934
Gittes, F., E. Meyhöfer, S. Baek, J. Howard (1996) *Biophysical J.*, Vol. **70**, p418-429
Golestanian, R., M. Kardar, T. B. Liverpool (1999) *Phys. Rev. Lett.*, Vol. **82**, p4456-4459
Götter, R., K. Kroy, E. Frey, M. Bärmann, E. Sackmann (1996) *Macromolecules*, Vol. **29**, p30-36
Grabar, K. C., K. J. Allison, B. E. Baker, R. M. Bright, K. R. Brown, R. G. Freeman, A. P. Fox, C. D. Keating, M. D. Musick, M. J. Natan (1996) *Langmuir*, Vol. **12**, p2353-2361
Harris, A. K., P. Wild, D. Stopak (1980) *Science*, Vol. **208**, p177-179
Haupt, M., A. Ladenburger, R. Sauer, K. Thonke, R. Glass, W. Roos, J. P. Spatz, H. Rauscher, S. Riethmüller, M. Möller (2003) *J. applied physics*, Vol. **93**, p6252-6257
Harris, R. A., J. E. Hearst (1966) *J. of chemical physics*, Vol. **44**, p2595-2602
Heald, R., R. Tournebize, A. Habermann, E. Karsenti, A. Hyman (1997) *The journal of cell biology*, Vol. **138**, p615-628
Helfer, E., S. Harlepp, L. Bourdieu, J. Robert, F. C. MacKintosh, D. Chatenay (2001) *Phys. Rev. Lett.*, Vol. **87**, p088103_1-4

Hess, H., J. Clemmens, J. Howard, V. Vogel (2002a) *Nano letters*, Vol. **2**, p113-116
Hess, H., J. Clemmens, C. M. Matzke, G. D. Bachand, B. C. Bunker, V. Vogel (2002b) *Applied Physics A*, Vol. **75**, p309-313
Hinner, B., M. Tempel, E. Sackmann, K. Kroy, E. Frey (1998) *Phys. Rev. Lett.*, Vol. **81**, p2614-2617
Hoh, J. H., C. Schoenenberger (1994) *J. of cell science*, Vol. **107**, p1105-1114
Horwitz, A. R., J. T. Parsons (1999) *Science*, Vol. **286**, p1102-1103
Howard, J. (2001) *Mechanics of Motor Proteins and the Cytoskeleton,* Sinauer Assoc., Sunderland MA, USA
Humphrey, D., C. Duggan, D. Saha, D. Smith, J. Kas (2002) *Nature*, Vol. **416**, p413-416
Hyman, A., D. Drechsel, D. Kellogg, S. Salser, K. Sawin, P. Steffen, L. Wordeman, T. Mitchison (1991) *Methods in enzymology*, Vol. **196**, p478-485
Hynes, T. R., S. M. Block, B. T. White, J. A. Spudich (1987) *Cell*, Vol. **48**, p953-963
Ingber, D. E. (2004) *Mechanics and chemistry of biosystems*, Vol. **1**, p53-68
Ishijima A., T. Doi, K. Sakurada, T. Yanagida (1991) *Nature*, Vol. **352**, p301-306
Janmey, P. A., S. Hvidt, J. Kas, D. Lerche, A. Maggs, E. Sackmann, M. Schliwa, T. P. Stossel (1994) *J. biological chemistry*, Vol. **269**, p32503-32513
Janmey, P. A. (2001a) *Proc. Natl. Acad. Sci. U.S.A.*, Vol. **98**, p14745-14747
Janmey, P. A., J. V. Shah, J. X. Tang, T. P. Stossel (2001b) in *Molecular Interactions of actin: actin structure and actin binding proteins (Results and Problems in Cell Differentiation, 32),* Eds.: C. G. dos Remedios, D. D. Thomas, Springer, Heidelberg, p181-199
Janson, M. (2002) *Force generation by growing microtubules*, PhD. thesis, Leiden, Netherlands
Jungbauer, S., R. Kemkemer, H. Gruler, D. Kaufmann, J. P. Spatz (2004) *ChemPhysChem*, Vol. **5**, p85-92
Käs, J., H. Strey, E. Sackmann (1994) *Nature*, Vol. **368**, p226-229
Kapoor, T. M., T. J. Mitchison (2001) *J. cell biology*, Vol. **154**, p1125-1133
Kawamura, M., K. Maruyama (1970) *J. of biochemistry*, Vol. **68**, p885-899
Kojima, H., A. Ishijima, T. Yanagida (1994) *Proc. Natl. Acad. Sci. U.S.A.*, Vol. **91**, p12962-12966
Kovacs, G. T. A., N. I. Maluf, K. E. Petersen (1998) *Proceedings of the IEEE*, Vol. **86**, p1536-1551
Lakes R. (2001) *Nature*, Vol. **414**, p503-504
Landau, L. D., E. M. Lifschitz (1987) *Lehrbuch der theoretischen Physik, V Statistische Physik Teil 1*, ed. 3, Akademie-Verlag, Berlin, Germany
Landau, L. D., E. M. Lifschitz (1991) *Lehrbuch der Theoretischen Physik, VII Elastizitäts-theorie*, ed. 7, Akademie Verlag, Berlin, Germany
Le Goff, L., O. Hallatschek, E. Frey, F. Amblard (2002) *Phys. Rev. Lett.*, Vol. **89**, p258101_1-4
Limozin, L., E. Sackmann (2002) *Phys. Rev. Lett*, Vol. **89**, p168103_1-4
Lo, C-M., H-B Wang, M. Dembo, Y-L Wang (2000) *Biophysical J.*, Vol. **79**, p144-152
Lodish, H., A. Berk, S. L. Zipursky, P. Matsudaira, D. Baltimore, J. Darnell (1999) *Molecular cell biology*, 4th ed., Freeman, Basingstoke, UK
Lorenz, H., M. Despont, N. Fahrni, N. LaBianca, P. Renaud, P. Vettiger (1997) *J. of micromechanics and microengineering*, Vol. **7**, p121-124
MacLean-Fletcher, S., T. D. Pollard (1980) *Biochemical and biophysical research communications*, Vol. **96**, 18-27
Maly, I. V., G. G. Borisy (2001) *Proc. Natl. Acad. Sci. U.S.A.*, Vol. **98**, p11324-11324
Margossian, S. S., S. Lowey (1982) *Methods in Enzymology*, Vol. **85**, p55-71

Mehta, A. D., R. S. Rock, M. Rief, J. A. Spudich, M. S. Mooseker, R. E. Cheney (1999) *Nature*, Vol. **400**, p590-593
Meltzer, S., R. Resch, B. E. Koel, M. E. Thompson, A. Madhukar, A. A. G. Requicha, P. Will (2001) *Langmuir*, Vol. **17**, p1713-1718
Mitchison, T., M. Kirschner (1984) *Nature*, Vol. **312**, p232-237
Mohrdieck, C. *et al.* in preparation
Mrkisch, M., L. E. Dike, J. Tien, D. E. Ingber, G. M. Whitesides (1997) *Experimental cell research*, Vol. **235**, p. 305-313
Müller, O., H.E. Gaub, M. Bärmann, E. Sackmann (1991) *Macromolecules*, Vol. **24**, p3111-3120
Munevar, S., Y-L Wang, M. Dembo (2001) *Biophysical J.*, Vol. **80**, p1744-1757
Nakamura, F., E. Osborn, P. A. Janmey, T. P. Stossel (2002) *J. biological chemistry*, Vol. **277**, p9148-9154
Ott, A., M. Magnasco, A. Simon, A. Libchaber (1993) *Physical review E*, Vol. **48**, pR1642-R1645
Patankar, N. A., (2004) *Langmuir*, Vol. **20**, p8209-8213
Pardee, J. D., J. A. Spudich (1982) *Methods in enzymology*, Vol. **85**, p164-181
Pelham, R. J., Y. Wang (1997) *Proc. Natl. Acad. Sci. U.S.A.*, Vol. **94**, p13661-13665
Pollard, T. D., J. A. Cooper (1982) *Methods in enzymology*, Vol. **85**, p211-233
Pollard, T. D. (1987) *Cell*, Vol. **48**, p909-910
Riveline, D., C. H. Wiggins, R. E. Goldstein, A. Ott (1997) *Physical review E*, Vol. **56**, pR1330-1333
Roos, W. H., A. Roth, J. Konle, H. Presting, E. Sackmann, J. P. Spatz (2003) *Chemphyschem*, Vol. **4**, p872-877
Roure, du, O., C. Dequidt, A. Richert, R. H. Austin, A. Buguin, P. Chavrier, P. Silberzan, B. Ladoux (2003) *Proceedings of SPIE*, Vol. **5345**, p26-34
Rouzina, I., V. A. Bloomfield (1998) *Biophysical J.*, Vol. **74**, p3152-3164
Rovensky, Y. A., A. D. Bershadsky, E. I. Givargizov, L. N. Obolenskaya, J. M. Vasiliev (1991) *Experimental Cell Research*, Vol. **197**, p107-112
Ruddies, R., W.H. Goldmann, G. Isenberg, E. Sackmann (1993) *European biophysical J.*, Vol. **22**, p309-321
Rutz, C. (2003) *Bestimmung der Kontraktionskraft adhärierter Zellen auf selektiv funktionalisierten Kraftsensoren*, Diplomarbeit, Universität Heidelberg, Germany
Schmidt, C., M. Bärmann, G. Isenberg, E. Sackmann (1989) *Macromolecules*, Vol. **22**, p3638-3649
Schweitz, J. (1992) *MRS Bulletin*, Vol. **17** (july 1992), p34-45
Shaw, J. M., J. D. Gelorme, N. C. LaBianca, W. E. Conley, S. J. Holmes (1997) *IBM J. of research and development*, Vol. **41**, p81-94
Shizuta, Y., H. Shizuta, M. Gallo, P. Davies, I. Pastan, M. S. Lewis (1976) *J. biological Chemistry*, Vol. **251**, p6562-6567
Spatz, J. P., S. Gräter, W. Roos, J. Ulmer (2004) *Oberfläche mit einer Anordnung einer Vielzahl säulenförmiger Erhebungen und deren Anwendungen*, German patent pending
Stossel, T. P. (1993) *Science*, Vol. **260**,p1086-1094.
Stossel, T. P., J. Condeelis, L. Cooley, J. H. Hartwig, A. Noegel, M. Schleicher, S. S. Shapiro (2001) *Nat. Rev. Mol. Cell Biol.* Vol. **2**, p138-147
Surrey, T., M. B. Elowitz, P. Wolf, F. Yang, F. Nédélec, K. Shokat, S. Leibler (1998) *Proc. Natl. Acad. Sci. U.S.A.*, Vol. **95**, p4293-4298
Surrey, T., F. Nédélec, S. Leibler, E. Karsenti (2001) *Science*, Vol. **291**, p1167-1171

Svitkina, T. M., A. B. Verkhovsky, G. G. Borisy (1995) *J. of structural biology*, Vol. **115**, p290-303
Svitkina, T. M., G. G. Borisy (1999) *Trends biochemical sciences*, Vol. **24**, p432-436
Svoboda K., C. F. Schmidt, B. J. Schnapp, S. M. Block (1993) *Nature*, Vol. **365**, p721-727
Svoboda K., S. M. Block (1994) *Cell*, Vol. **77**, p773-784
Takebayashi, T., Y. Morita, F. Oosawa (1977) *Biochimica et Biophysica Acta*, Vol. **492**, p357-363
Tan, J. L., J. Tien, D. M. Pirone, D. S. Gray, K. Bhadriraju, C. S. Chen (2003) *Proc. Natl. Acad. Sci. U.S.A.*, Vol. **100**, p1484-1489;
Tang, J. X., P. A. Janmey (1996) *J .of biological chemistry*, Vol. **271**, p8556-8563
Tempel, M., G. Isenberg, E. Sackmann (1996) *Physical review E*, Vol. **54**, p1802- 1810
Turner, A. M. P., N. Dowell, S. W. P. Turner, L. Kam, M. Isaacson, J. N. Turner, H. G. Craighead, W. Shain (2000) *J. biomedical material research*, Vol. **51**, p430-441
Uhde, J., M. Keller, E. Sackmann, A. Parmeggiani, E. Frey (2003) *ArXiv* physics/0307014
Vale, R. D., R. A. Milligan (2000) *Science*, Vol. **288**, p88-95
Verde, F., M. Dogterom, E. Stelzer, E. Karsenti, S. Leibler (1992) *J. of cell biology*, Vol. **118**, p1097-1108
Watari, M. (2003) *Application of an array of point-like shear forces on living cells*, Diploma thesis, Universität Heidelberg, Germany
Wiggins, C. H., D. Riveline, A. Ott, R. E. Goldstein (1998) *Biophysical J.*, Vol. **74**, p1043-1060
Wilhelm, J., E. Frey (1996) *Phys. Rev. Lett.*, Vol. **77**, p2581-2584
Williams, K. R., R. S. Muller (1996) *J. of microelectromechanical systems*, Vol. **5**, p256-269
Wong, G. C. L., A. Lin, J. X. Tang, Y. Li, P. A. Janmey, C. R. Safinya (2003) *Phys. Rev. Lett.*, Vol. **91**, p018103_1-4
Yanagida, T., M. Nakase, K. Nishiyama, F. Oosawa (1984) *Nature*, Vol. **307**, p58-60
Yildiz, A., J. N. Forkey, S. A. McKinney, T. Ha, Y. E. Goldman, P. R. Selvin (2003) *Science*, Vol. **300**, p2061-2065
Young, E. C., H. K. Mahtani, J. Gelles (1998) *Biochemistry*, Vol. **37**, p3467-3479
Zhang, J., 2004, *New model systems for the study of myosin V mediated transport on biofunctionalized surfaces*, PhD thesis, TU München, Germany